

POLITECNICO DI TORINO

Collegio di Ingegneria Chimica e dei Materiali

**Master of Science Course
in Materials Engineering**

Master of Science Thesis

Synthesis and characterization of sulfonated polysulfone membranes for forward osmosis applications



Tutors

prof. Alberto Tiraferri
prof. Marco Sangermano
dott.ssa Daria Grinic

Signature of the tutors

.....
.....
.....

Candidate

Andrea Cosola

Signature of the candidate

.....

December 2017

In loving memory of my father

Abstract

Due to its potential advantages over the well-established membrane processes, Forward Osmosis (FO) has gained increasing attention as a promising system to produce high quality water. However, the industrial implementation of this process is still restricted due to the lack of high performance membranes. During the last years, several studies have been carried out with the aim of developing new thin-film composite membranes (TFC) characterized by hydrophilic substrates.

The purpose of this thesis is the design of tailored sulfonated polysulfone membranes for FO application in water purification. The primary objectives of this work are to: 1) prepare sulfonated polysulfones (SPSU) with different degree of sulfonation; 2) fabricate SPSU membranes and evaluate their potential application as substrates for thin film composite membranes (TFC); 3) prepare TFC membranes *via* interfacial polymerization and 4) evaluate membrane performance.

In this work, a series of sulfonated polysulfones with different degree of sulfonation (SPSU_0.10, SPSU_0.25 and SPSU_0.50) were prepared by introducing hydrophilic sodium sulfonate groups *via* an electrophilic substitution reaction. The sulfonation was investigated by means of DSC, TGA, and ATR-FTIR analysis, thus validating the synthesis protocol. Then, sulfonated membranes were prepared by a two-step method involving UV-curing, followed by the traditional non-solvent induced phase separation (NIPS). It was necessary to blend sulfonated polysulfone with the pristine polysulfone to achieve phase separation; UV-curing was used to induce cross-linking and to further increase the mechanical resistance of the substrates. The enhanced hydrophilicity was confirmed by both contact angle and cloud point measurements. These membrane substrates have shown a pure water permeability that varies in the range 200 – 400 L m⁻² h⁻¹ bar⁻¹, and an average surface pore size of around 30 – 40 nm. These results have met the expectation for the realization of membrane substrates for TFC in FO. Finally, TFC membranes were prepared onto the sulfonated substrates *via* interfacial polymerization. Filtration studies are still in progress.

TABLE OF CONTENTS

1. Introduction	1
2. Literature review	3
2.1. Classification of membranes	3
2.1.1. Chemical classification	3
2.1.2. Structural classification	4
2.1.3. Morphological classification	5
2.2. Membrane filtration processes	6
2.2.1. Flow configuration of membrane processes	7
2.2.2. Transport models	9
2.3. Forward Osmosis (FO)	11
2.3.1. FO basic principles	12
2.3.2. Draw Solutions (DS)	14
2.3.3. Reverse diffusion	15
2.3.4. Membrane Fouling	16
2.3.5. Concentration polarization	18
2.3.6. Development of FO membranes	20
2.3.7. Fabrication of TFC-FO membranes	23
2.3.8. Recent applications of forward osmosis	26
2.4. Aim of the thesis and study objectives	28
3. Materials and methods	29
3.1. Polysulfone (PSU) and sulfonated polysulfone (SPSU) properties	29
3.2. Synthesis of SPSU	31
3.3. Fabrication of the SPSU-based membrane substrates	33
3.3.1. Casting solutions preparation	34
3.3.2. Casting plate preparation	34
3.3.3. Casting solution deposition	37
3.3.4. UV-curing	38
3.3.5. NIPS	39
3.4. Polyamide active layer formation <i>via</i> interfacial polymerization	41
3.5. Characterization of sulfonated polymers	44
3.5.1. Differential Scanning Calorimetry (DSC)	45
3.5.2. Thermal Gravimetric Analysis (TGA)	46
3.5.3. Attenuated total reflection Fourier transform infrared (ATR-FTIR) spectroscopy	47
3.6. Characterization of the membrane substrates	47
3.6.1. Static contact angle measurements	48
3.6.2. Cloud point measurements	50
3.6.3. Mass transport tests	52
3.6.3.1. UV-vis spectroscopy	55
3.7. FO performances of TFC membranes	56
4. Results and discussion	61
4.1. Characterization of sulfonated polymers	61
4.1.1. Effect of sulfonation on glass transition temperature	62
4.1.2. Effect of sulfonation on thermal stability	63
4.1.3. Confirmation of sulfonation by ATR-FTIR spectroscopy	64

4.2. Characterization of the membrane substrates	66
4.2.1. Casting solution composition	66
4.2.2. Substrates wettability	68
4.2.3. Interaction between polymer, solvent and non-solvent	69
4.2.4. Pure water permeance of sulfonated substrates	70
4.2.5. Selectivity of sulfonated substrates	72
4.3. TFC membranes	73
4.3.1. FO performances	74
5. Concluding remarks	75
References	77
Acknowledgments	85

LIST OF FIGURES

Figure 1.1: Increase of FO publications in the period 1994-2016 [3].	2
Figure 2.1: Chemical structure of the most widely used polymeric materials for membrane preparation [10].	4
Figure 2.2: Schematic representation of isotropic and anisotropic membranes [11].	5
Figure 2.3: Classification of membrane processes in terms of membrane pore diameter.	6
Figure 2.4: a) schematic representation of dead-end filtration; b) influence of the cake layer on membrane performance.	8
Figure 2.5: Schematic representation of stirred dead-end filtration.	8
Figure 2.6: a) schematic representation of cross-flow filtration; b) influence of the cake layer on membrane performance.	9
Figure 2.7: Mass transport across porous (on the left) and dense (on the right) membranes [11].	9
Figure 2.8: Schematic representation of FO process.	12
Figure 2.9: Schematic classification of osmotically driven membrane processes.	13
Figure 2.10: Schematic illustration of reverse solute diffusion across a semipermeable membrane.	15
Figure 2.11: Fouling reversibility in FO membranes [36].	17
Figure 2.12: Schematic representation of concentration polarization at the membrane boundary layer [1].	18
Figure 2.13: Schematic representation of concentration polarization in FO membranes.	19
Figure 2.14: Schematic illustration of typical thin film composite membranes for RO [1].	20
Figure 2.15: The ideal structure of a TFC-FO membrane.	22
Figure 2.16: Principles of non-solvent induced phase separation (NIPS) process.	23
Figure 2.17: Three-component phase diagram used to explain phase separation processes.	24
Figure 2.18: Steps of polymer precipitation.	25
Figure 2.19: Schematic representation of phase separation as a line through the three-component phase diagram.	25
Figure 2.20: Interfacial polymerization between meta-phenylenediamine and trimesoyl Chloride.	26
Figure 2.21: Schematic diagram of interfacial polymerization procedure.	26
Figure 2.22: FO operation modes: osmotic dilution and pre-treatment modes.	27
Figure 3.1: Schematic representation of a TFC membrane structure.	29
Figure 3.2: Chemical structure of PSU.	30
Figure 3.3: Chemical structure of sulfonated polysulfone.	31
Figure 3.4: Schematic representation of the sulfonation procedure of a PSU unit using trimethylsilyl chlorosulfonate as sulfonating agent (Me indicates a methyl group).	31

Figure 3.5: Synthesis set-up consisting of a three-neck round bottom flask equipped with mechanical stirrer, reflux condenser and nitrogen inlet.	32
Figure 3.6: Complete fabrication protocol of the fabrication of the sulfonated support layer.	33
Figure 3.7: Casting support consisting of a glass plate covered by a PET fabric fixed onto its surface by means of a water-resistant adhesive tape.	36
Figure 3.8: Schematic representation of the casting solution deposition by means of a hand-held film casting knife.	37
Figure 3.9: Gardco Microm II film casting knife.	37
Figure 3.10: Formation of PEGDA cross-linked network.	38
Figure 3.11: Representation of the experimental protocol selected for the realization of the support layer. After the deposition of the casting solution (a), the polymer is subjected to a photo-curing process (b) followed by NIPS (c).	39
Figure 3.12: Laboratory-scale NIPS set-up.	40
Figure 3.13: Membranes immersed in the coagulation bath.	40
Figure 3.14: Removal of the corner areas of the membrane.	41
Figure 3.15: Schematic illustration of the complete fabrication process of TFC membranes including the final IP step.	41
Figure 3.16: Schematic representation of the IP process. The microporous support layer is first immersed into MPD solution and then into a TMC solution to form cross-linked polyamide layer at the interface between the two components.	42
Figure 3.17: Schematic representation of the interfacial polymerization fabrication process.	43
Figure 3.18: Preparation to the membrane sample to be subjected to IP.	43
Figure 3.19: Immersion of the glass covered by the membrane sample into a sloping bath containing the polyamine solution.	44
Figure 3.20: Schematic illustration of a Differential Scanning Calorimeter.	45
Figure 3.21: Working principle of a TGA analyzer.	46
Figure 3.22: Schematic representation of an ATR system.	47
Figure 3.23: Schematic diagram of DSA working principle.	48
Figure 3.24: Contact angle determination.	49
Figure 3.25: Experimental set-up of the contact angle drop shape analysis. The final value of contact angle is taken as an average of six DSA measurements.	49
Figure 3.26: Phase diagram of a three components system (Polymer/Solvent/Non-solvent).	50
Figure 3.27: Turbidity occurrence during a Cloud Point measurement as compared to the clear starting solution (on the left).	51
Figure 3.28: Experimental set-up of the Cloud point measures.	51
Figure 3.29: Schematic diagram of the lab-scale dead-end ultrafiltration system used for the evaluation of the support layer permeance.	52
Figure 3.30: Expanded view of the Amicon Cell 8010 produced by Millipore Corporation.	53
Figure 3.31: Schematic diagram of the experimental set-up used for the determination of membrane support selectivity.	54
Figure 3.32: Schematic diagram of UV-visible Spectrometer working principle.	55

Figure 3.33: Protocol followed for the determination of the intrinsic parameters.	56
Figure 3.34: Schematic diagram of the lab-scale FO system used experimentally for the characterization of the composite membranes.	57
Figure 3.35: Lab-scale FO system.	58
Figure 3.36: FO membrane cell.	58
Figure 4.1: Comparative DSC curves of polysulfone and sulfonated-polysulfone samples, reported in the range of 140-160 °C.	62
Figure 4.2: Comparative TGA thermograms of polysulfone and sulfonated-polysulfone samples, reported from 50 to 620 °C.	64
Figure 4.3: Transmittance spectra of pristine polysulfone and sulfonated-polysulfone samples (SPSU 0.25 and SPSU 0.50), reported from 650 to 1650 cm^{-1}	65
Figure 4.4: Influence of sulfonation degree on phase separation process: a) polymer detachment during phase inversion; b) formation of a gel phase.	66
Figure 4.5: Schematic representation of the fabrication protocol used for membrane substrates preparation.	67
Figure 4.6: Contact angles of PSU, SPSU_0.10, SPSU_0.25/PSU 50:50 and SPSU_0.50/PSU 30:70. The error bars represent the standard deviations of each measurements from the average value.	68
Figure 4.7: Images of droplets deposited onto PSU, SPSU_0.10 and blended thin films (SPSU_0.25/PSU 50:50 and SPSU_0.50/PSU 30:70).	69
Figure 4.8: Ternary phase diagram of PSU, SPSU 0.10, SPSU_0.25/PSU 50:50 and SPSU_0.50/PSU 50:50.	70
Figure 4.9: Pure water permeability of SPSU 0.10, SPSU_0.25/PSU 50:50 and SPSU_0.50/PSU 30:70 membrane substrates. Results are taken as the average of three tests for each membrane sample. The error bars represent the standard deviations of each measurement from the average value.	71
Figure 4.10: Rejection percentage of SPSU 0.10, SPSU_0.25/PSU 50:50 and SPSU_0.50/PSU 30:70 membrane substrates. Results are taken as the average of three spectroscopic measurements for each membrane sample. The error bars represent the standard deviations of each measurement from the average value.	73

LIST OF TABLES

Table 2.1: Driving forces, membrane structure and transport mechanism of the different membrane processes.	10
Table 3.1: Key properties of polysulfone.	30
Table 3.2: List of the synthesized sulfonated polysulfone samples. The name have been assigned according to the theoretical degree of sulfonation.	33
Table 3.3: Composition of the membrane support layers casting solutions.	34
Table 3.4: Concentration of the NaCl draw solution used for each of the five stages of the test. The second column of the table represents the volume (mL) of draw solution, which has to be added to the draw solution reservoir for each stage. Before starting with the first stage, the DS-reservoir was filled with 1 L of DI-water.	59
Table 4.1: Sulfonated polysulfone samples characterized through DSC, TGA and ATR-FTIR.	61
Table 4.2: Glass transition temperature of PSU and SPSU samples.	63
Table 4.3: Onset of degradation of PSU and SPSU samples.	63
Table 4.4: IR bands of polysulfones and sulfonated derivatives.	65
Table 4.5: Properties of SPSU membrane substrates.	73

Sommario

Per introdurre il lavoro svolto in questa tesi, si può osservare come la crescente domanda di acqua potabile sia ad oggi uno dei più grandi problemi con i quali bisogna misurarsi. Questo spiega il motivo di una sempre rinnovata attenzione rivolta ai metodi di purificazione delle acque ed in particolare ai processi a membrana che, andando a sostituire gradualmente le tradizionali tecniche di separazione, hanno suscitato negli anni un vivo interesse.

Sebbene le tecnologie a membrana abbiano già registrato notevoli progressi, va rilevato come nell'ultimo decennio siano stati messi a punto processi alternativi alle tradizionali tecniche di filtrazione a membrana. Uno di questi processi è l'osmosi diretta, noto anche come *Forward Osmosis* (FO), che si affianca ai tradizionali processi a membrana quali l'osmosi inversa (RO), la nanofiltrazione (NF), l'ultrafiltrazione (UF) e la microfiltrazione (MF). La commercializzazione dell'FO su larga scala in ambito industriale è tuttavia ad oggi limitata dalla mancanza di membrane ad alto rendimento.

Il secondo capitolo di questa ricerca descrive l'attuale stato dell'arte, analizzando brevemente le tipologie di membrane ed i relativi processi utilizzati nelle applicazioni industriali per poi trattare nel dettaglio l'osmosi diretta.

In particolare, per quanto riguarda la classificazione, le membrane possono essere suddivise secondo tre differenti criteri: 1) natura chimica, 2) struttura e 3) morfologia.

Quanto alla natura chimica, si distinguono le membrane organiche da quelle inorganiche. Le membrane organiche sono quelle maggiormente impiegate nei processi di purificazione delle acque grazie alla grande disponibilità di polimeri, quali il polisulfone, uno dei più utilizzati. Le membrane possono poi essere suddivise, in base alla struttura, in non porose o porose. Le prime, utilizzate in osmosi inversa e diretta, sono costituite da un film denso, di composizione e spessore uniforme, attraverso il quale le specie possono permeare seguendo un meccanismo di trasporto di tipo diffusivo. Le seconde, maggiormente diffuse, presentano una struttura sostanzialmente simile a quella dei filtri convenzionali, caratterizzata da pori interconnessi distribuiti in tutto lo spessore. Ciò che le contraddistingue è la dimensione delle porosità che può variare da qualche nanometro a qualche micrometro. La dimensione di tali pori assume rilevanza anche ai fini di identificare i diversi processi di filtrazione. Andando a diminuire progressivamente la dimensione delle porosità, si ottengono membrane utilizzabili in microfiltrazione, ultrafiltrazione e nanofiltrazione. Dal punto di vista morfologico, infine, le membrane si presentano simmetriche o asimmetriche. Tra le asimmetriche, quelle composite sono costituite da una struttura multistrato formata da un sottile e denso *layer* superficiale che sovrasta un substrato poroso, con dimensioni dei pori via via crescenti nello spessore o costanti. Esse sono ampiamente utilizzate nei processi ad osmosi inversa e sono considerate le membrane più promettenti per ottimizzare i processi ad osmosi diretta.

Nelle sezioni successive sono descritti i meccanismi di trasporto posti alla base dei processi di permeazione attraverso membrane semipermeabili. In particolare, a seconda della struttura della membrana, vengono utilizzati due modelli. Il primo, noto con il nome di *pore flow model* e basato sulla legge di Darcy (Equazione 2.1), viene impiegato per descrivere i fenomeni di trasporto attraverso membrane porose da microfiltrazione o ultrafiltrazione. In questo caso il processo di filtrazione è strettamente correlato alla relazione che intercorre tra la dimensione dei pori della membrana e quella delle specie chimiche in soluzione. Il secondo

modello, che prende il nome di *solution diffusion model*, si rifà alla legge di Fick (Equazione 2.2), prevedendo un meccanismo diffusivo generato da gradienti di concentrazione che si instaurano ai lati della membrana. Esso viene impiegato per descrivere i fenomeni di trasporto attraverso membrane che presentano uno strato superficiale denso e sono impiegate nel campo della nanofiltrazione e dell'osmosi inversa o diretta.

Viene poi fornita una breve descrizione delle diverse configurazioni dei processi a membrana in modo tale da comprendere le modalità operative dei test sperimentali di filtrazione eseguiti, che sono descritti nel Capitolo 3. In sintesi, si distinguono la configurazione *dead-end*, in cui il flusso di alimentazione scorre perpendicolarmente rispetto alla membrana e la configurazione *cross-flow*, in cui il flusso scorre invece tangenzialmente.

Come premesso, la seconda parte del Capitolo 2 tratta nel dettaglio il processo FO. L'osmosi diretta è un processo osmotico che guida la permeazione dell'acqua attraverso una membrana, facendola passare da una soluzione di alimentazione (nota come *feed solution*, FS) ad una soluzione molto concentrata (detta *draw solution*, DS). La forza spingente, non è più la pressione idraulica applicata all'alimentazione, come avviene nei tradizionali processi a membrana, bensì il gradiente di pressione osmotica che si genera tra la *feed solution* e la *draw solution*. Non richiedendo l'utilizzo di pressioni idrauliche elevate, tale processo presenta alcuni sostanziali vantaggi, relativi soprattutto ad un inferiore consumo energetico ed ad un ridotto e reversibile "sporcamento" delle membrane, comunemente definito *fouling*. Tuttavia esistono anche problematiche che ne limitano l'efficienza, quali la diffusione inversa dei soluti della *draw solution* e la polarizzazione di concentrazione.

Negli ultimi anni la ricerca si è concentrata su diverse tipologie di *draw solution*, con particolare attenzione alle soluzioni contenenti sali organici, inorganici o materiali sintetici innovativi. L'obiettivo è di utilizzare un soluto che generi un elevato gradiente osmotico e che sia altamente solubile in soluzione acquosa, non tossico, facilmente rigenerabile nel post-trattamento, economico e che limiti il più possibile la polarizzazione di concentrazione. Tra tutte le ipotesi prospettate, si è riscontrato in letteratura come le soluzioni a base di NaCl siano le più utilizzate.

Un aspetto che sicuramente va a influire sulle *performance* del processo è la diffusione inversa dei soluti che compongono la *draw solution*. I soluti tendono, infatti, a retrodiffondere verso la *feed solution* causando una diminuzione del gradiente osmotico e, conseguentemente, del flusso di permeato. Data l'importanza di tale fenomeno, è stato introdotto un parametro caratteristico definito come il rapporto tra il flusso di acqua attraverso la membrana ed il flusso inverso dei soluti.

Come premesso, un'altra problematica nei processi di osmosi diretta è la polarizzazione di concentrazione. Nei processi FO, si manifesta sia la polarizzazione esterna sia quella interna. La polarizzazione esterna è dovuta all'accumulo del soluto della soluzione concentrata sulla superficie dello strato attivo della membrana. La polarizzazione interna, che è considerata quale fattore maggiormente limitante, è invece dovuta alla diluizione del soluto all'interno dei pori dello strato di supporto. Data la struttura tortuosa derivante dalle porosità interconnesse, si genera un gradiente di concentrazione all'interno del substrato e, di conseguenza, una diminuzione della pressione osmotica effettiva. Complessivamente, gli effetti della polarizzazione di concentrazione influiscono negativamente provocando una diminuzione del flusso.

Va osservato, peraltro, che la fabbricazione di membrane con struttura e proprietà specifiche può portare a una rilevante diminuzione di tali problematiche. I primi studi riguardanti l'osmosi diretta sono stati condotti con membrane composite tipicamente utilizzate per processi di osmosi inversa (RO), costituite da uno strato denso di poliammide realizzato sopra

un substrato poroso in polisulfone. L'idrofobicità, la morfologia e lo spessore del substrato di tali membrane comportavano scarse *performance* in FO, dovute soprattutto a un'intensa polarizzazione di concentrazione. Queste caratteristiche rispecchiavano la necessità di mantenere l'integrità della membrana in condizioni di alte pressioni tipiche dell'RO. Pressioni che invece sono estremamente più basse in FO, rendendo quindi inutili tali prerogative.

Le membrane asimmetriche in triacetato di cellulosa (CTA) prodotte e commercializzate dall'Hydration Technology Inc. (HTI) all'inizio degli anni duemila, sono state le prime ad essere realizzate appositamente per FO. Tali membrane, caratterizzate da un'ottima resistenza meccanica, garantiscono buoni flussi in virtù di un'elevata idrofilia che consente anche di ridurre il *fouling*. Tuttavia, non permettono di ottenere un'adeguata efficienza di rimozione e possono essere utilizzate solo in un limitato intervallo di pH.

Al fine di migliorare le *performance*, oggi la ricerca è focalizzata sulla realizzazione di membrane composite strutturate appositamente per processi FO. Queste membrane sono infatti le più promettenti, in quanto è possibile andare ad ottimizzare i vari *layer* separatamente. La membrana ideale per un processo FO dovrà pertanto avere una struttura anisotropa, caratterizzata da un denso strato superficiale - che garantisca un buon flusso, un'elevata efficienza di rimozione dei contaminanti ed una limitata retrodiffusione di soluti - e da uno strato di supporto poroso, idrofilo e di spessore limitato per minimizzare la polarizzazione di concentrazione. Inoltre, il substrato dovrà presentare una struttura porosa con morfologia cilindrica e bassa tortuosità. I dati riscontrati in letteratura mostrano come il polisulfone (PSU) ed i suoi derivati, continuino ad essere i materiali più utilizzati per la preparazione di substrati di membrane composite. Ciononostante, data la loro idrofobicità, sono state studiate valide soluzioni volte ad aumentarne la bagnabilità. A tal fine sono stati messi a punto diversi processi di modifica della catena polimerica del PSU per massimizzarne l'idrofilia, tra i quali la solfonazione sembra essere la soluzione più promettente.

Il capitolo si conclude con la descrizione delle tecniche di fabbricazione delle membrane composite. Queste ultime sono ottenute seguendo due diversi *step* relativi rispettivamente alla realizzazione dello strato di supporto e di quello attivo. Il substrato poroso viene realizzato tramite separazione di fase indotta da un non-solvente (NIPS), ovvero la soluzione polimerica viene immersa in un bagno di acqua che causa la precipitazione del polimero. Il processo è dovuto a fenomeni di scambio tra il solvente e il non-solvente che permettono di generare una membrana porosa ed anisotropa. Complessivamente, il processo dipende da 6 fattori fondamentali: 1) proprietà chimiche del polimero in soluzione; 2) composizione della soluzione; 3) composizione del bagno di coagulazione contenente il non-solvente; 4) tempo di reazione; 5) umidità e 6) temperatura.

Passando ora al sottile e denso strato attivo, esso è realizzato sul substrato tramite polimerizzazione interfacciale. Il processo si basa su una reazione di poliamidazione secondo il meccanismo Shotten-Bauman e consiste nella formazione di uno strato polimerico di poliammide (PA).

E' proprio nell'ambito della ricerca riguardante la fabbricazione di membrane performanti per FO, che si contestualizza questo lavoro di tesi. Lo scopo, infatti, è quello di realizzare membrane TFC appositamente strutturate per processi FO. Sulla base dell'attuale stato dell'arte, si è deciso di realizzare i substrati in polisulfone solfonato. Come è già stato sottolineato, l'idrofobicità del polimero PSU impedirebbe l'ottenimento di supporti idrofili. Conseguentemente, si è deciso di migliorarne la bagnabilità andando a inserire, lungo la sua catena, gruppi funzionali idrofili. Gli obiettivi primari della ricerca sono, pertanto, i seguenti: 1) sintesi di polisolfoni solfonati a diverso grado di solfonazione; 2) fabbricazione di substrati solfonati; 3) realizzazione di membrane TFC tramite polimerizzazione interfacciale di uno

strato denso di poliammide sulla superficie dei substrati sulfonati e 4) analisi delle *performance* delle membrane.

Il Capitolo 3 descrive i materiali ed i metodi utilizzati. Nella prima parte sono presentati proprietà e processo di sintesi del polisulfone sulfonato, per poi entrare nel merito della vera e propria fabbricazione delle membrane. La seconda parte del capitolo descrive invece le metodiche di caratterizzazione dei polimeri sintetizzati (DSC, TGA e ATR-FTIR) e delle membrane fabbricate (angolo di contatto, *cloud point*, permeanza, e selettività dei substrati; test preliminari su membrane TFC).

In conformità ai metodi reperibili in letteratura, il polisulfone sulfonato è stato sintetizzato facendo reagire il polisulfone con un agente sulfonante (Figura 1).

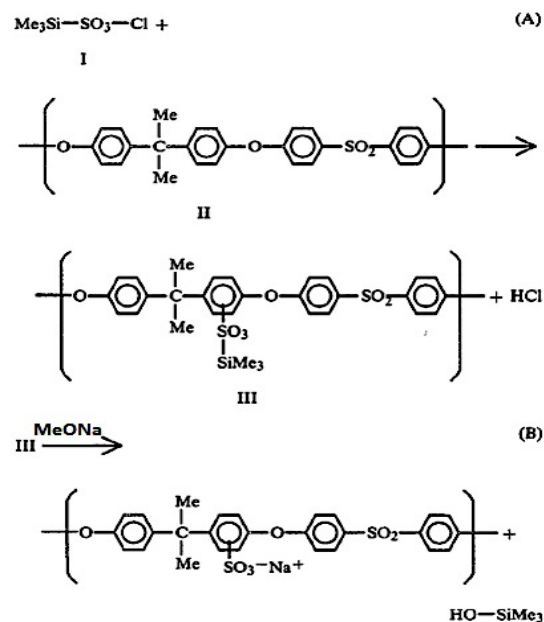


Figura 1: Rappresentazione schematica del processo di solfonazione di un'unità ripetitiva di PSU, utilizzando trimetilsilil clorosulfonato come agente sulfonante. (Me indica il gruppo metile)

Il primo stadio della reazione consiste nella sostituzione elettrofila aromatica tra il polisulfone e il trimetilsilil clorosulfonato (TMSCS), che comporta la formazione di un prodotto intermedio con eliminazione di HCl. In seguito, il prodotto intermedio viene fatto reagire con metossido di sodio (MeONa), ottenendo così un polisulfone sulfonato in forma salificata. Il rapporto tra le unità ripetitive di PSU e il TMSCS è stato regolato in modo tale da ottenere polimeri a diverso grado di solfonazione: SPSU_0.10, SPSU_0.25 e SPSU_0.50, dove 0.10, 0.25 e 0.50 rappresentano il grado di solfonazione teorico.

I polimeri così preparati sono stati utilizzati per fabbricare membrane porose e asimmetriche. Il processo di fabbricazione si articola in 5 diverse fasi: 1) preparazione della soluzione polimerica; 2) preparazione del supporto di polimerizzazione; 3) deposizione della soluzione polimerica e successivo *hand casting*; 4) foto-reticolazione e 5) separazione di fase indotta da non-solvente.

I polisolfoni sulfonati sono stati disciolti, in concentrazione pari al 12% in peso, in N-metil-2-pirrolidone. Tuttavia, per i due polimeri più sulfonati è stato necessario realizzare dei *blend* con il polisulfone per garantire la separazione di fase e la formazione della membrana. Le soluzioni sono state poste in agitazione per 4 ore per garantire la completa solubilizzazione

del polimero. Sono stati inoltre aggiunti in tutte le formulazioni, un agente reticolante (polietilenglicole diacrilato, PEGDA) ed un fotoiniziatore, in modo tale da poter procedere con la reticolazione indotta da UV. La concentrazione di PEGDA è relativa al peso totale della soluzione, mentre quella di fotoiniziatore è calcolata rispetto alla quantità di agente reticolante. Le formulazioni finali sono riportate in Tabella 1.

Tabella 1: Composizioni delle soluzioni polimeriche

Membrane	% p/p	SPSU (%)	PSU (%)	PEGDA (%)	Fotoiniziatore (%)
SPSU_0,10	12	100	0	15	3
SPSU_0,25/PSU	12	50	50	10	3
SPSU_0,50/PSU	12	30	70	10	3

Preparate le soluzioni, è stato realizzato il supporto di vetro ricoperto di polietilentereftalato (PET) necessario per la fabbricazione delle membrane (Figura 2).

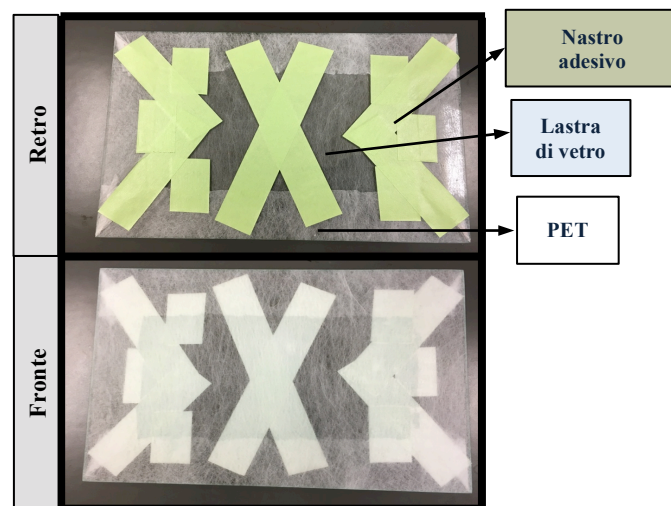


Figura 2: Supporto di fabbricazione realizzato fissando, con un nastro adesivo resistente all'acqua, un sottile tessuto di PET su una lastra di vetro

Il sottile tessuto di polietilentereftalato (PET), che sarà lo strato rinforzante della futura membrana, è stato fissato sul vetro con un nastro adesivo resistente all'acqua. E' stata quindi stesa la soluzione polimerica sulla superficie del PET utilizzando un *casting blade* settato manualmente per ottenere un film polimerico di spessore nominale pari a 150 μm .

Terminata l'operazione di *casting*, il film polimerico è stato sottoposto a foto-reticolazione per 1 minuto sotto una lampada UV (Dymax ECE 5000-UV). L'irraggiamento causa la scissione del fotoiniziatore e, conseguentemente, la formazione di un radicale che reagisce con il PEGDA, provocando una polimerizzazione a catena. Tale polimerizzazione induce la formazione di un reticolo di PEGDA in cui il polisulfone sulfonato rimane intrappolato.

Conclusasi la foto-reticolazione, le membrane sono state ottenute tramite separazione di fase indotta da un non-solvente (NIPS). Le lastre sono state immerse in una prima vasca di acqua deionizzata per 10 minuti ed in seguito trasferite in una seconda vasca di acqua deionizzata per 24 ore, in modo tale da poter completare la separazione di fase.

Sui substrati sulfonati così ottenuti è stato realizzato uno strato attivo di poliammide tramite polimerizzazione interfacciale *in-situ*. La formazione di tale strato è dovuta alla reazione che

avviene all'interfaccia liquido-liquido tra una soluzione di un'ammina polifunzionale solubile in acqua (m-fenilendiammina, MPD) e una soluzione contenente un cloruro acilico (cloruro di trimesoile, TMC) (Figura 3).

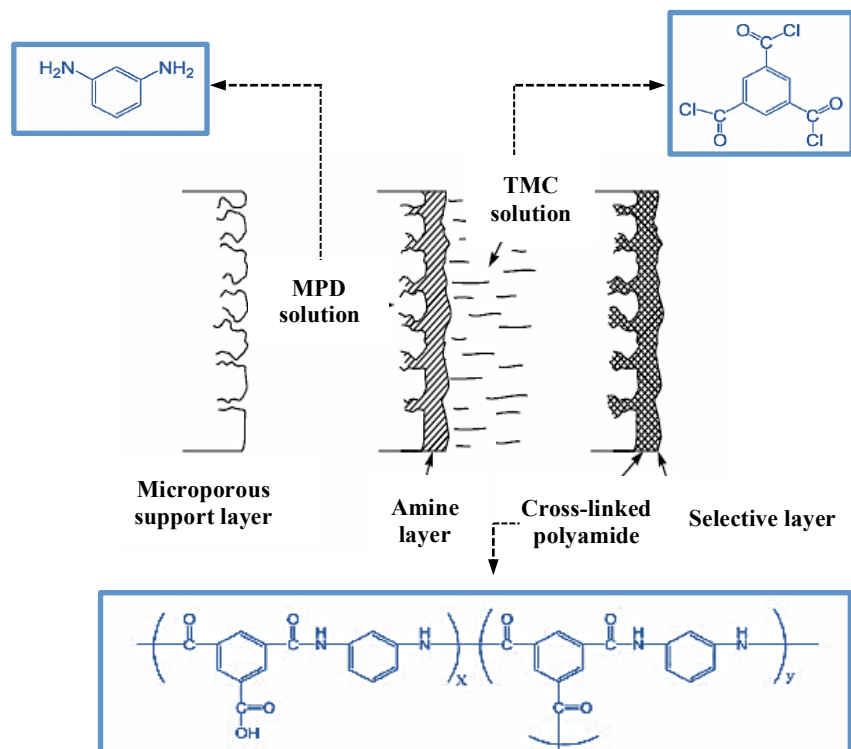


Figura 3: Rappresentazione schematica del processo di polimerizzazione interfacciale. Il substrato microporoso è prima immerso nella soluzione di MPD e poi in quella di TMC. Lo strato poliammidico si genera all'interfaccia tra le due soluzioni immiscibili.

Il processo si articola in diverse fasi. Per iniziare, un campione del substrato sulfonato viene ritagliato e fissato con un nastro adesivo su un supporto di vetro, rivolgendo il lato attivo della membrana verso l'alto. Il vetro è poi immerso per 2 minuti in una soluzione di MPD in modo tale che solo lo strato attivo del substrato sia in contatto con la soluzione amminica. In seguito, il substrato è asciugato dalla soluzione in eccesso e immerso nella soluzione di TMC. E' in questo *step* che si genera il sottile strato di poliammide per reazioni all'interfaccia tra le due soluzioni immiscibili MPD-TMC. Il vetro è poi rimosso dalla soluzione di TMC ed è lasciato riposare per due minuti a temperatura ambiente prima di essere immerso per altri due minuti in acqua deionizzata a 95 °C. Terminato questo *step*, la membrana così formata viene immersa prima in una soluzione di NaOCl per 2 minuti e poi in una soluzione di metabisolfito di sodio per 30 secondi. Infine, la membrana è trattata in acqua deionizzata a 95 °C per un processo finale di *curing*, volto ad ottimizzare l'adesione tra il substrato sulfonato e lo strato superficiale poliammidico.

La seconda parte del capitolo è suddivisa in sezioni dedicate alle tecniche di caratterizzazione dei polimeri sintetizzati, nonché all'analisi della bagnabilità e del comportamento durante la separazione di fase dei substrati sulfonati. Infine, sono presentate le metodiche di filtrazione utilizzate per investigare le *performance* dei substrati e delle membrane TFC.

I polimeri sintetizzati sono stati esaminati tramite analisi termiche (DSC e TGA) e spettroscopiche (ATR-FTIR), eseguite sui seguenti campioni: PSU, SPSU_0.10, SPSU_0.25 e SPSU_0.50.

La calorimetria differenziale a scansione (DSC) è stata utilizzata per studiare la variazione della temperatura di transizione vetrosa (T_g) dei polisolfoni dovuta alla solfonazione. Per eseguire le misure, è stato impiegato lo strumento DSC1 Mettler Toledo. Le analisi calorimetriche sono state effettuate su campioni di 10-12 mg sotto un flusso costante di N_2 (50 ml/min), impostando una rampa termica di 10 °C/min fino a 280 °C. I dati ottenuti sono stati rielaborati utilizzando il software STARe.

L'analisi termogravimetrica (TGA) è stata usata per valutare e confrontare la stabilità termica dei polisolfoni a diverso grado di solfonazione con quella del polisolfone non modificato. In particolare, si è cercato di analizzare la degradazione termica dei polimeri solfonati tra 270 e 400 °C, tipico *range* di desolfonazione. Per eseguire le misure, è stata utilizzata la macchina TGA/SDTA851° Mettler Toledo. Le analisi termogravimetriche sono state effettuate su campioni di 10-12 mg sotto un flusso costante di N_2 (60 ml/min), impostando tre rampe termiche: 1) isoterma a 40 °C per 10 minuti; 2) rampa termica di 20 °C/min da 40 a 140 °C e 3) rampa termica di 10 °C/min da 140 a 650 °C. Prima di ogni misura è stato eseguito un bianco, successivamente sottratto dal software STARe durante la rielaborazione dei dati.

La spettrofotometria infrarossa in riflettanza totale attenuata (ATR-FTIR) è stata attuata con lo scopo di confermare la presenza dei gruppi solfonati nel *backbone* del polisolfone. Per eseguire le misure, è stato utilizzato uno spettrometro Nicolet iS50 FT-IR equipaggiato con un cristallo di diamante (Thermo Scientific, Madison, WI). Le analisi spettroscopiche sono state effettuate in trasmittanza nel range di lunghezze d'onda comprese tra 4000 e 650 cm^{-1} (16 scansioni, risoluzione di 4 cm^{-1}). Prima di ogni misura è stato eseguito un bianco, successivamente sottratto dal software OMNIC durante la rielaborazione dei dati.

Le sezioni successive del capitolo sono invece dedicate alle metodiche di caratterizzazione delle membrane prodotte: misure di angoli di contatto e di *cloud point*, prove di filtrazione e di selettività dei substrati ed infine test preliminari effettuati sulle membrane TFC.

L'analisi degli angoli di contatto è stata utilizzata per valutare e confrontare la bagnabilità dei substrati in polisolfone solfonato con quella di membrane di PSU. Le misure non sono state effettuate sulle membrane prodotte ma su appositi film sottili realizzati in modo tale da evitare la presenza delle porosità che potrebbero andare ad influenzare il reale valore dell'angolo di contatto. Tali film sono stati ottenuti per deposizione su vetrini da microscopio di soluzioni di PSU, SPSU_0.10, SPSU_0.25/PSU 50:50 e SPSU_0.50/PSU 30:70 in NMP al 12% in peso e successivo trattamento termico in forno per 3 ore a 105 °C per indurre l'evaporazione del solvente. Le misure dell'angolo di contatto sono state eseguite utilizzando il misuratore DSA100 della Kruss nella modalità goccia sessile ed i risultati sono stati rielaborati dal software integrato Advance Drop Shaper. Ogni campione è stato sottoposto a sei diverse misure in posizioni casuali per minimizzare il più possibile l'eventuale errore sperimentale.

Le misure dei *cloud point* delle diverse soluzioni polimeriche sono state impiegate per investigare il processo di separazione di fase del sistema tri-componente polimero/solvente/non-solvente. Il comportamento termodinamico di un sistema tri-componente è convenzionalmente descritto attraverso un diagramma di fase ternario (Figura 4). Con il termine *cloud point* si fa riferimento al momento esatto in cui avviene la transizione dalla regione stabile e monofasica del diagramma a quella instabile dove si verifica separazione di fase. Tale transizione è visibile chiaramente in quanto la soluzione diventa torbida assumendo una colorazione biancastra. Poiché il *cloud point* è unico per un dato sistema tri-componente, tali prove sono state effettuate al fine di valutare l'influenza della

solfoazione sull'equilibrio termodinamico tra solvente, non-solvente e polimero. In altre parole, l'obiettivo di tali prove è di determinare la quantità di non-solvente necessaria per indurre l'inversione di fase.

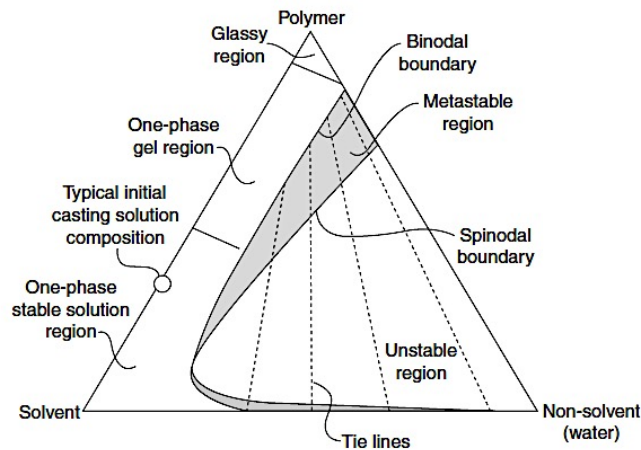


Figura 4: Diagramma di fase di un sistema tri-componente (polimero/solvente/non-solvente).

Le posizioni dei *cloud points* sono state determinate tramite misure di titolazione. Il processo consiste nell'aggiungere volumi di una miscela solvente/non-solvente alla soluzione polimerica fino a che non se ne riscontra la torbidità. La composizione del sistema al raggiungimento della torbidità rappresenta la composizione critica che comporta la transizione dalla regione monofasica del diagramma a quella bifasica. Pertanto, sono state preparate soluzioni al 15-20-25% in peso di PSU, SPSU_0.10, SPSU_0.25/PSU 50:50 e SPSU_0.50/PSU 50:50 in NMP ed una miscela di NMP e acqua deionizzata in rapporto 4:1 in peso. Volumi della miscela NMP/H₂O sono stati aggiunti goccia a goccia alle soluzioni polimeriche fino al raggiungimento della torbidità. Questa prima parte dell'esperimento viene effettuata a temperatura ambiente (T_{amb}). Tuttavia, una volta raggiunta la torbidità, le soluzioni sono state prima riscaldate per 15 minuti fino a 70 °C e poi raffreddate per tornare a T_{amb} . Se la torbidità si rimanifesta una volta ritornati a T_{amb} , allora significa che il *cloud point* è stato davvero raggiunto. Altrimenti, il protocollo è ripetuto fino a che ciò non accade. L'esatta composizione in peso della soluzione finale è stata calcolata tramite un bilancio di massa.

Per quanto riguarda invece le *performance* dei substrati sulfonati, le membrane realizzate sono state sottoposte a test di filtrazione per determinarne la permeanza e la selettività. Sono stati testati campioni dei seguenti substrati: SPSU_0.10, SPSU_0.25/PSU 50:50 e SPSU_0.50/PSU 30:70.

I test di permeabilità sono stati effettuati su campioni di membrana circolari (diametro 25 mm e area effettiva di 4,1 cm²) utilizzando un impianto di filtrazione *dead end* (Figura 5) composto da una cella da ultrafiltrazione (Amicon 8010, capacità 10 ml, Millipore Corporation), un vessel contenente acqua deionizzata ed una bombola di azoto che agisce da compressore facendo fluire l'acqua dal vessel alla cella. I test sono stati eseguiti alla pressione di 10 psi, dopo aver compattato i campioni nella cella per 10 minuti a 12 psi. Il permeato è stato raccolto in un beaker posto su una bilancia elettronica che valuta ogni minuto la variazione di peso. I dati sono stati raccolti e rielaborati dal software Winwedge che

permette di ottenere la permeanza della membrana. I test sono stati ripetuti tre volte per ogni tipologia di membrana.

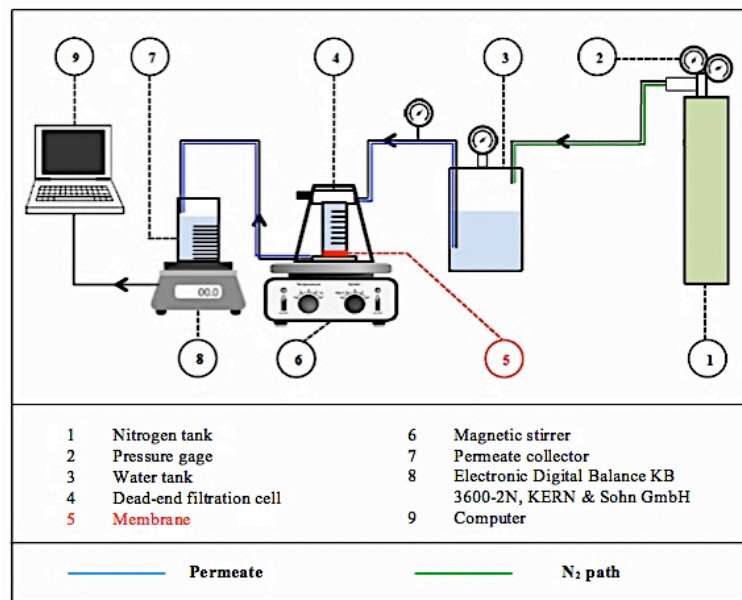


Figura 5: Diagramma di fase di un sistema tri-componente (polimero/solvente/non-solvente).

Le prove di selettività sono state effettuate tramite test di filtrazione seguiti da analisi spettroscopiche al fine di valutare la dimensione dei pori delle membrane. Le prove di filtrazione sono state eseguite con un sistema *dead-end* molto simile a quello presentato in Figura 5, eccetto per il vessel che in questo caso non è più necessario. E' stata utilizzata, quale soluzione di alimentazione, una soluzione in concentrazione pari a 7 g/l di silice colloidale (LUDOX® HS-40), le cui particelle presentano una dimensione media di 32 nm. Le prove sono state condotte alla pressione di 10 psi, dopo aver compattato il campione nella cella per 10 minuti a 12 psi e, per ogni test, sono stati raccolti 6 ml di permeato da sottoporre ad una misura spettroscopica. Tale analisi, effettuate con lo spettrofotometro Specord S600, permettono di valutare la concentrazione di LUDOX® HS-40 presente nel permeato sfruttando la legge di Lambert-Beer che correla l'assorbanza alla concentrazione della specie presente nella soluzione. Dai valori di assorbanza ricavati sono state determinate le concentrazioni di silice colloidale mediante una retta di calibrazione (Equazione 3.7) ottenuta tramite misure spettroscopiche realizzate su una serie di soluzioni di silice a concentrazione nota. Il valore di selettività è stato infine calcolato utilizzando l'Equazione 3.4.

La parte conclusiva del capitolo descrive le metodiche dei test preliminari eseguiti sulle membrane TFC per valutare le *performance* in FO. Le prove sono state realizzate con un sistema *cross-flow* su campioni di membrana di area pari a 19,8 cm², utilizzando acqua deionizzata come *feed solution* e una soluzione di NaCl come *draw solution*. La cella che ospita la membrana da testare è collegata a due recipienti contenenti rispettivamente la *feed* e la *draw solution*. Le soluzioni, che sono entrambe termostatate a 25 °C, iniziano a fluire all'interno della cella attivando due pompe peristaltiche. Tenendo conto dei principi dell'osmosi diretta descritti nel capitolo 2.3, l'acqua permea la membrana verso la *draw solution* per effetto del gradiente di pressione osmotica. Contemporaneamente, il soluto della *draw solution* tende a seguire il percorso inverso. Il valore del flusso di acqua viene valutato tramite un bilancio di massa in quanto il recipiente della *feed solution* è collocato su una bilancia elettronica che analizza minuto per minuto le variazioni di peso. La diffusione

inversa del soluto viene invece analizzata immergendo nel recipiente della *feed-solution* un conduttivimetro che misura minuto per minuto le variazioni di conducibilità.

Il Capitolo 4 presenta i risultati delle prove descritte nel capitolo precedente ed è diviso in tre parti: 1) caratterizzazione del polisulfone sulfonato; 2) caratteristiche e *performance* dei substrati sulfonati e 3) test preliminari sulle membrane TFC.

Le analisi termiche e spettroscopiche hanno confermato l'avvenuta solfonazione del polimero. L'analisi calorimetrica (DSC) ha rivelato un progressivo aumento della temperatura di transizione vetrosa (T_g) con il crescere del grado di solfonazione (Figura 6a). Le T_g dei polisulfoni sulfonati sono state individuate tra 190 e 220 °C (190 °C per SPSU_0.10, 200°C per SPSU_0.25 e 220 °C per SPSU_0.50) mentre i risultati ottenuti con il PSU (185 °C) sono in buon accordo con i valori reperibili in letteratura. L'aumento della T_g è dovuto alla sostituzione di un atomo di -H dell'anello aromatico con un gruppo sulfonato. L'introduzione del gruppo $-SO_3Na$ nel *backbone* polimerico del PSU causa un aumento di ingombro sterico e lo sviluppo di interazioni tra gruppi sulfonati pendenti. Entrambi questi effetti comportano una ridotta mobilità della catena polimerica e, pertanto, un aumento della temperatura di transizione vetrosa.

Tali risultati hanno avuto una seconda conferma dagli esiti delle analisi termogravimetriche (TGA) Figura 6b. La curva relativa al polisulfone mostra un'unica perdita di peso intorno ai 500 °C dovuta alla degradazione termica del *backbone* polimerico. I termogrammi che si riferiscono ai campioni sulfonati mostrano invece due degradazioni distinte. In tutti i casi si osserva un primo *step* tra 270 e 400 °C che è riconducibile alla degradazione termica dei gruppi sulfonati con conseguente generazione di SO e SO₂. Il secondo *step* avviene invece intorno ai 450 °C e corrisponde alla degradazione della catena principale del polimero, analogamente a quanto ottenuto nel caso del PSU.

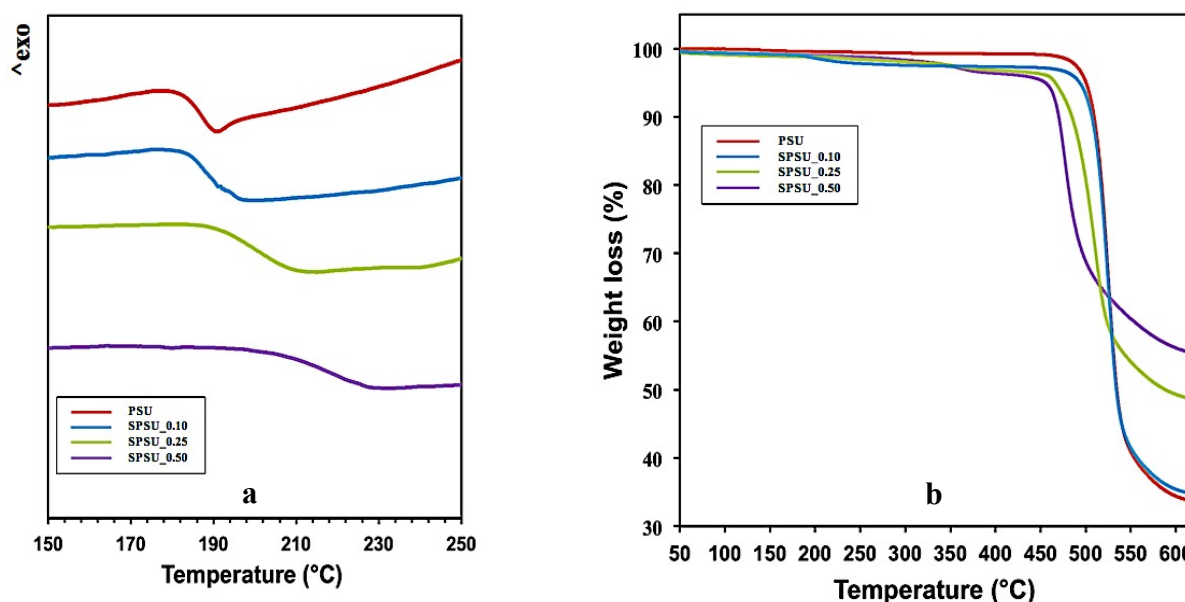


Figura 6: Risultati delle analisi termiche effettuate: a) curve DSC riportate nel *range* di temperature 150-250°C e b) curve TGA riportate nel *range* di temperature 50-650 °C

La definitiva conferma dell'effettiva solfonazione è stata ottenuta dai risultati della spettroscopia IR (Figura 7). Tutte le analisi effettuate sui campioni sulfonati mostrano il picco caratteristico a 1040 cm⁻¹ relativo allo stretching simmetrico del gruppo SO₃. Si sottolinea

inoltre come all'aumentare del grado di solfonazione aumenti anche l'intensità del picco caratteristico a 1040 cm^{-1} .

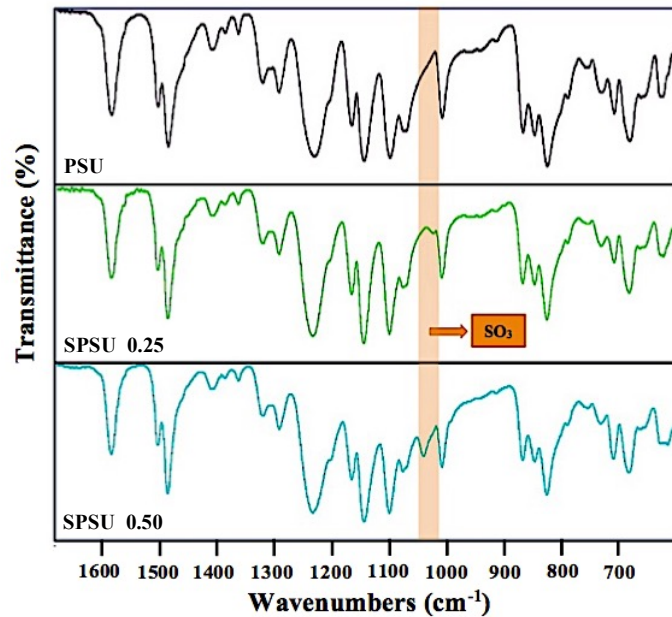


Figura 7: Spettri in trasmittanza relativi a PSU, SPSU_0.25 e SPSU_0.50, riportati nel *range* di lunghezze d'onda $650\text{-}1650\text{ cm}^{-1}$.

La seconda sezione del capitolo presenta le caratteristiche e le *performance* dei substrati solfonati realizzati seguendo il protocollo di fabbricazione descritto in materiali e metodi (Capitolo 3.3).

La prima parte illustra le motivazioni che hanno portato alla scelta delle soluzioni polimeriche da utilizzare per la fabbricazione dei substrati. Le formulazioni, riportate in Tabella 3.3, sono il risultato di studi preliminari eseguiti su polimeri con vari gradi di solfonazione. Le membrane fabbricate con polisolfoni altamente solfonati hanno evidenziato tre problematiche: 1) limitata stabilità e scarsa adesione al supporto in PET; 2) mancata separazione di fase quando il grado di solfonazione è troppo alto e 3) basse velocità di inversione di fase dovute all'idrofilia del SPSU. La scelta è infine ricaduta su tre polisolfoni con più basso livello di solfonazione: SPSU_0.10, SPSU_0.25 e SPSU_0.50. Tuttavia, sia l'utilizzo di SPSU_0.25, sia di SPSU_0.50 comportava la realizzazione di membrane meccanicamente instabili. Per risolvere tale problema, si è deciso di realizzare dei blend con polisulfone. Per quanto riguarda SPSU_0.10, non si è riscontrato tale inconveniente. Inoltre, a causa dell'elevato *swelling*, ovvero il rigonfiamento in acqua, si è deciso di implementare il processo di fabbricazione aggiungendo lo step di fotoreticolazione in modo da migliorare la stabilità e la resistenza del substrato. Questo è il motivo dell'aggiunta in tutte le formulazioni del polietilenglicole diacrilato (PEGDA) e del fotoiniziatore.

Per quanto riguarda la bagnabilità dei substrati realizzati, le misure dell'angolo di contatto hanno confermato l'aumento di idrofilia dovuto alla presenza dei gruppi solfonati che tendono a formare legami idrogeno con l'acqua. I campioni di PSU hanno mostrato un angolo di contatto di 75° mentre i campioni solfonati presentano angoli di contatto molto più bassi (49° per SPSU_0.10, 43° per SPSU_0.25/PSU 50/50 e 39° per SPSU_0.50/PSU 30:70).

Questi risultati hanno trovato un'ulteriore conferma con le misure di *cloud point* (Figura 8).

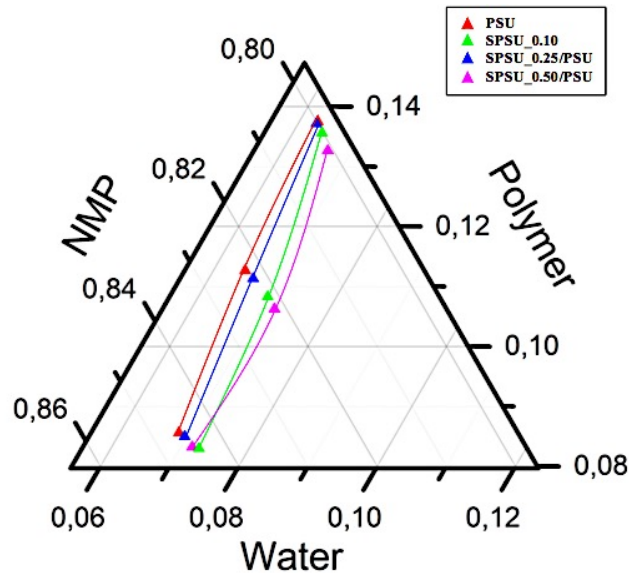


Figura 8: Diagramma di fase ternario relativo a soluzioni polimeriche contenenti PSU, SPSU_0.10, SPSU_0.25/PSU 50:50 p/p e SPSU_0.50/PSU 50:50 p/p.

Come si può osservare dal diagramma ternario riportato in figura, nel caso dei polisolfoni sulfonati l'area relativa alla regione monofasica aumenta se confrontata con quella del polisulfone. Ciò significa che le soluzioni polimeriche che contengono i polisolfoni sulfonati richiedono una maggiore quantità di acqua per essere sottoposti a separazione di fase. Il cambiamento di fase è ritardato rispetto ai sistemi non sulfonati. Questo comportamento è dovuto alla maggiore affinità con l'acqua.

Per quanto riguarda le *performance* delle membrane sulfonate, sia le prove di permeabilità che quelle di selettività hanno confermato il potenziale utilizzo di tali membrane quali possibili substrati per membrane composite in FO.

I risultati dei test di permeabilità sono presentati in Figura 9.

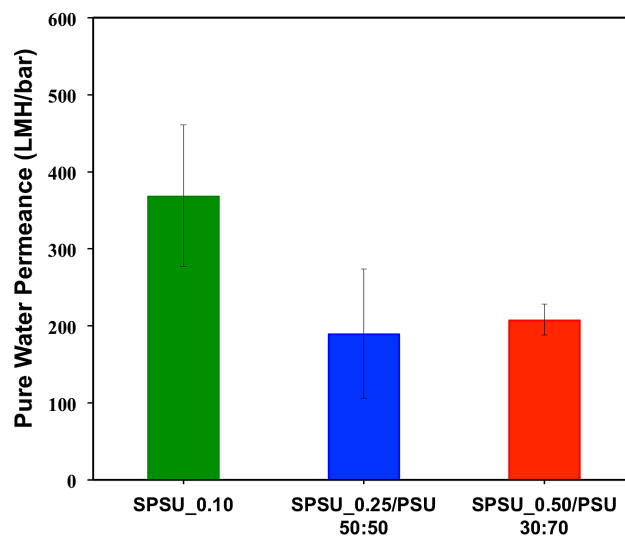


Figura 4.9: Valori di permeanza relativi ai test effettuati sui seguenti campioni: SPSU_0.10, SPSU_0.25/PSU 50:50 e SPSU_0.50/PSU 50:50. I valori riportati sono la media di tre misurazioni effettuate su ogni lotto di membrane e le barre di errore rappresentano le deviazioni standard.

Complessivamente, i substrati SPSU_0.10, SPSU_0.25/PSU 50:50 e SPSU_0.50/PSU 30:70 hanno mostrato permeanze di 369, 190 e 209 LMH/bar. Valori, questi, che collocano tali membrane nel tipico *range* di ultrafiltrazione che era l'obiettivo prefissato. Non si nota tuttavia un trend dovuto all'aumento del grado di solfonazione. Le deviazioni standard osservabili sono da considerare accettabili dal momento che le prove sono state effettuate su membrane *lab made*. Sono infatti molteplici i fattori che possono influenzare il valore finale di permeanza, tra i quali vanno sottolineati la presenza di macropori generati da bolle d'aria nella soluzione e la disomogeneità dello spessore delle membrane.

I risultati delle prove di selettività sono illustrati in Figura 10.

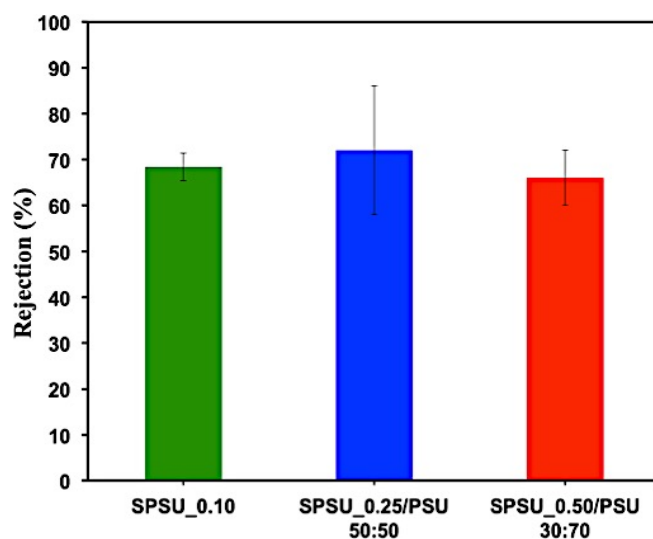


Figura 10: Valori di selettività relativi ai test effettuati sui seguenti campioni: SPSU_0.10, SPSU_0.25/PSU 50:50 e SPSU_0.50/PSU 50:50. I valori riportati sono la media di tre misurazioni effettuate su ogni lotto di membrane e le barre di errore rappresentano le deviazioni standard.

I valori di rimozione di particelle di silice ottenuti variano nel range 66-72% per tutti i campioni testati. Alla luce di tali risultati e, considerando che le particelle di silice hanno una dimensione media di 32 nm, si può ragionevolmente affermare che la dimensione media dei pori delle membrane possa collocarsi tra 30 e 40 nm.

L'ultima sezione del capitolo presenta i risultati dei test preliminari effettuati sulle membrane TFC. I primi risultati non sono stati del tutto soddisfacenti. Si è ipotizzato che ciò possa essere dovuto alla presenza di macroporosità nello strato superficiale dei substrati ed anche alla loro idrofilia che può portare alla formazione di uno strato di poliammide non solo superficiale ma disomogeneamente distribuito all'interno dei pori. Tuttavia, le analisi delle *performance* di tali membrane sono ancora in corso così come lo studio dell'adesione dello strato attivo in PA sui substrati solfonati.

In conclusione, sono stati sintetizzati diversi polisolfoni solfonati tramite una reazione di sostituzione elettrofila aromatica tra il polisulfone ed un agente solfonante (trimetilsilil clorosulfonato). Le analisi termiche (DSC e TGA) hanno confermato l'avvenuta solfonazione e quindi validato il protocollo di sintesi. Successivamente, i polimeri solfonati sono stati utilizzati per preparare membrane idrofile. Le prove di bagnabilità e le misure di *cloud point* hanno dimostrato l'aumento di idrofilia delle membrane se paragonate a membrane di PSU non modificato. Infine, i test di permeabilità e selettività hanno confermato il potenziale

utilizzo delle membrane fabbricate nel campo dell'ultrafiltrazione o come substrati di membrane TFC nei processi FO.

1 Introduction

Nowadays, the demand of freshwater is rapidly increasing due to the continuous growth of the world population. Even if there is a lot of water on our planet, freshwater represents only the 2.5%, as the remainder 97.5% is mainly contained in the oceans or consists minimally of brackish water (0.5%) [1-2-3]. Furthermore, freshwater is often inaccessible since only 0.3% is easily available from lakes and rivers, whereas the 68.9% is locked in polar icecaps, glaciers or permanent mountain snow and 30.8% is groundwater [3]. Therefore, freshwater shortage is considered, along with the depletion of the traditional energy sources, one of the major concerns for our society. It has been estimated that freshwater demand will increase by 53% within 2030 [3] leaving almost 3.2 billion people under water stress. Freshwater demand will increase especially for developing countries, such as Africa, India and in the Middle East but also in those countries (i.e. Australia, China and Mexico), where freshwater resources do not allow to cover their demand. Furthermore, the great development of coastal regions in the last century led to a great challenge in terms of water supply, due to the lack of directly available freshwater sources.

In the light of the above, new strategies have to be found to solve the problem of water scarcity, such as seawater desalination and wastewater treatment. Membrane filtration processes seems to be the most interesting and advanced technology for water purification.

Membrane technologies have gained a growing interest in the last century and have gradually replaced the traditional separation techniques, such as distillation, which dominated the desalination scene until the seventies. Compared to these traditional systems, membrane processes have a number of important advantages, namely: 1) possibility to separate particles from the molecular scale to larger sizes so that a wide range separation processes can be performed (microfiltration, ultrafiltration, nanofiltration, reverse osmosis and forward osmosis); 2) lower energy requirement; 3) higher selectivity; 4) wide chemistry availability: many polymeric and inorganic materials can be used for membrane fabrication so that membrane properties can be easily varied, especially in terms of selectivity; 5) possibility of operating continuously or on demand; 6) modular and compact equipment, and 7) potentially lower environmental contamination.

These are the reasons why, nowadays, membranes play a fundamental role in chemical technology. Along with water purification processes, i.e. desalination and wastewater treatments, they find application in a wide range of other industrial fields, such as ultrapure water production for the semiconductor industry, metal recovery as colloidal oxides or hydroxides, condensed water purification at nuclear plants and oil-water emulsions separation, cold beverages sterilization and medical applications (transfusion filter set, purification of surgical water).

With regard to desalination processes, reverse osmosis is nowadays the most used technique. This membrane process separates salts from water using high hydraulic pressure as the driving force. However, high applied pressures mean also high energy request and thus high costs of operations. This issue, along with fouling propensity, led researchers to find innovative technological solutions. It is in this context that, since the early 2000s, forward osmosis (FO) started to gain increasing attention (Figure 1.1) as a potential system to produce high quality water [4-5-6].

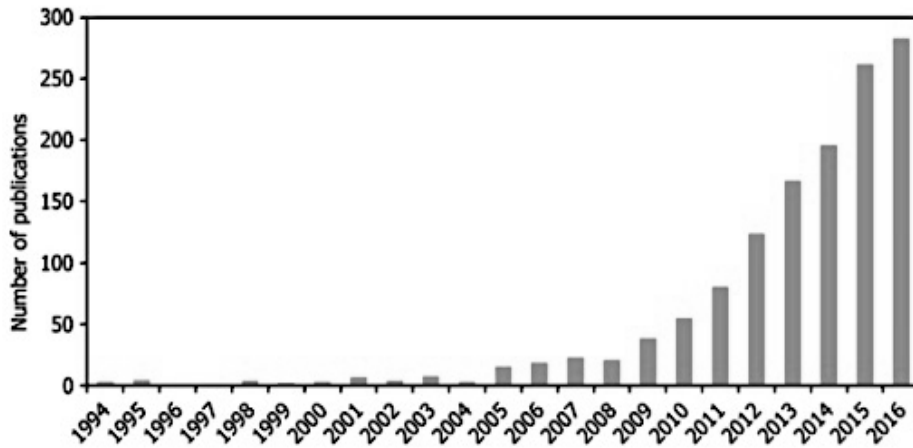


Figure 1.1: Increase of FO publications in the period 1994-2016 [3]

This emerging membrane process is considered a promising technique due to its great advantages over the well established pressure driven membrane processes (MF, UF, NF, RO); namely [8-9]: 1) no hydraulic pressure is needed, thus FO requires lower energy consumption; 2) lower and more reversible fouling, 3) potentially higher water recovery if compared to RO; 3) lower costs. Accordingly, researchers have identified FO as a potential system to produce high quality water, reducing energy requirements, capital costs and fouling propensity in water purification processes [3].

In the last decade, lots of studies have been carried out in order to demonstrate the advantages of this process and its potential industrialization. Nevertheless, the industrial implementation is still restricted due to the lack of high performance membranes [8]. Therefore, further research and developments are required to allow a successful commercialization [3].

2 Literature review

This chapter will first introduce a membrane classification according to different criteria, such as chemical nature, structure, and physical morphology. Then, a brief overview of membrane processes will be given, highlighting flow configurations and transport models. The rest of the chapter will focus specifically on forward osmosis by discussing its principles and recent developments.

2.1 Classification of membranes

Membranes can be seen as selective barriers that moderate the permeation of chemical species, i.e., the separation is achieved by permeating one or more species of a stream through the membrane while hindering the diffusion of others. Membranes can be categorized according to three different criteria [10]: 1) chemical nature (organic or inorganic), 2) structure (dense or porous) and 3) morphology (symmetric/asymmetric or isotropic/anisotropic).

2.1.1 Chemical classification

Membranes can be classified according to their material into two categories: organic and inorganic membranes.

Organic membranes are based either on cellulose and cellulose derivatives or on synthetic polymers. They are currently leaders in industrial applications, such as wastewater treatments, due to their commercial availability. Potentially, many polymers can be used, but due to the processing requests and membrane lifetime, only a limited number of polymers is used nowadays (Figure 2.1) [10]. Nevertheless, these membranes are typically employed in a limited pH range that varies from 2 to 12, showing a maximum operating temperature of 50 °C.

Polyamide membranes are used for desalination processes because of their better thermo-chemical and hydrolytical stability than cellulose esters. Polysulfones, unlike the other polymers mentioned above, are hydrophobic and are thus more subjected to adsorption and fouling phenomena. This is the reason why they are generally blended with hydrophilic segments that increase the fouling resistance. Despite their hydrophobic nature, polysulfones are widely used because of their excellent chemical and thermo-mechanical stability.

Another popular class of hydrophobic polymer includes polytetrafluoroethylene (Teflon) and isotactic polypropylene (PP), which find application in those water treatments procedures where high thermal and chemical stability are requested.

Inorganic membranes are usually divided into five categories, namely: 1) glass; 2) ceramic; 3) metallic and 4) carbon membranes [10-11]. These membranes can resist higher pressure, are usually more durable and more resistant to a wider variety of chemicals (acids, alkali, solvents) if compared to the organic ones. Also, they can be treated more easily with cleaning agents and have a theoretically unlimited lifetime. Furthermore, they can be used in a broad

range of pH (2-12) and at higher operating and cleaning temperature (105 °C) and have better antifouling properties.

Nevertheless, they have higher replacement costs and are very sensitive to embrittlement phenomena. Nowadays, inorganic membranes are used for ultrafiltration and microfiltration processes and find application in chemical industry for aggressive fluids treatments.

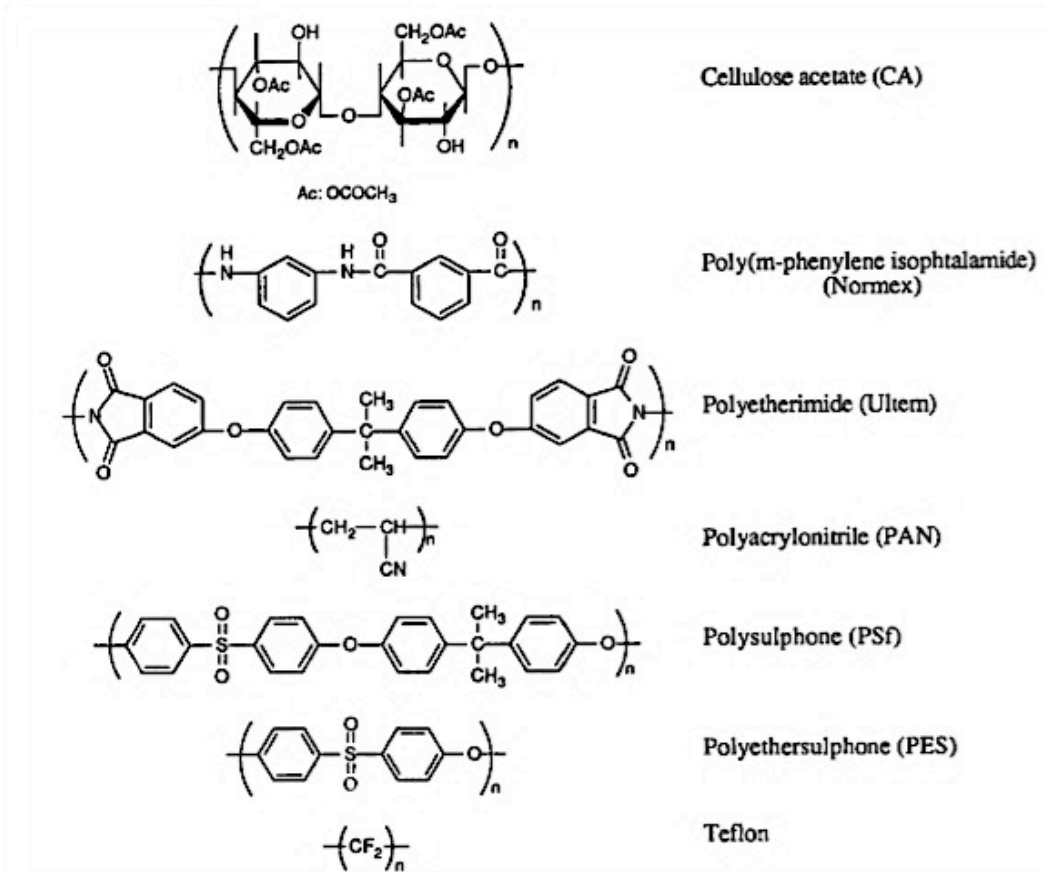


Figure 2.1: Chemical structure of the most widely used polymeric materials for membrane preparation [10].

2.1.2 Structural classification

Membranes can be classified based on their structure into dense or porous membranes [1-10-11].

Dense membranes show a homogeneous and symmetric structure, usually with a variable thickness of 30-500 μm. They consist of a dense layer that controls the separation process by diffusion mechanisms under a specific driving force (pressure, concentration or electric potential) [11]. The transport of the various species through the membrane depends on the diffusivity and solubility of each species and occurs in the free-volume generated between the macromolecular chains. This type of membrane can therefore separate species with different solubility and diffusivity coefficients. In general, they show very low flux because, along with their dense structure, a discrete thickness is needed to reach the mechanical strength requested. Accordingly, their thickness limits the obtainment of high fluxes. Most reverse and forward osmosis membranes use a dense top layer to perform the separation process.

Nowadays, however, the vast majority of membranes are porous. These membranes, similar to conventional filters, consist of highly porous and rigid structure. They can be further divided according to their pore diameter into:

1. Microporous membranes ($d_p < 2 \text{ nm}$)
2. Mesoporous membranes ($2 \text{ nm} < d_p < 50 \text{ nm}$)
3. Macroporous membranes ($d_p > 50 \text{ nm}$)

They show a symmetric structure and generally present a variable thickness of 30-500 μm . The separation process is governed by the porosity, meaning that a chemical species larger than the greatest pore are rejected, whereas those species that are smaller than the smallest pore can freely permeate across the membrane. It is clearly evident that the most important parameter in this process is the pore size distribution of the membrane.

Furthermore, porous membranes are characterised by two additional parameters: percentage of porosity (ϵ) and membrane tortuosity (τ), which is the average pore length compared to the membrane thickness. Typically, ϵ varies in the range 0.3-0.8 but can also decrease to 0.05, whereas τ values are usually between 1.5 and 2.5 [11].

There is another particular category of microporous membranes: electrically charged membranes [11]. These membranes can be also dense but generally show a very fine microporous structure characterized by the presence of fixed positively or negatively charged ions within the pore walls. The separation process with charged membranes consists in the exclusion of ions of the same charge of the ions fixed in the pore walls.

2.1.3 Morphological classification

Membranes can be further classified into isotropic and anisotropic membranes according to their morphology [10-11]. As illustrated in Figure 2.2, porous membranes can be symmetrical or anisotropic, whereas dense membranes are generally considered isotropic. Since in membrane processes the transport rate of a species is inversely proportional to membrane thickness, the development of anisotropic membranes consisting of an ultrathin top layer supported by a porous layer led to a breakthrough in industrial fields.

A brief description of anisotropic membranes is given below.

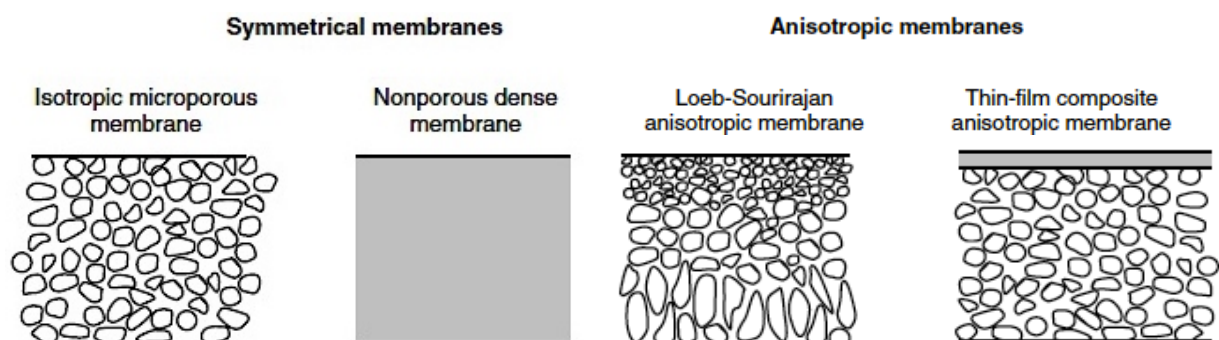


Figure 2.2: Schematic representation of isotropic and anisotropic membranes [11].

Anisotropic porous membranes are prepared from the same material and characterized by a particular gradient morphology. This asymmetric structure consist of a 0.1-5 μm thick superficial layer with small pores supported by a highly porous layer that gives mechanical

strength and has almost negligible resistance to mass transfer [10-11]. The advantage in terms of higher flux makes these membranes the most widely used in a variety of commercial applications.

Composite membranes, commonly known as thin-film composite (TFC) membranes, currently dominate the market for desalination applications, wastewater treatments and purification of biological products. These membrane consist of two or three layers prepared from different polymeric materials: a top ultrathin and dense layer made of aromatic polyamide (PA) on top of a much thicker microporous support layer typically made of polysulfone (PSU), which is itself an anisotropic membrane [1-10-11], and a reinforcing fabric on the bottom.

The great advantage of TFC membranes is that each layer of the composite structure is custom-tailored in order to reach the required selectivity and permeability, while ensuring appropriate mechanical to resist at the operating conditions.

2.2 Membrane filtration processes

There are four well established membrane separation processes commonly used in industrial applications, which are classified according to the membrane pore size (Figure 2.3) [1-11-12]: microfiltration (MF), ultrafiltration (UF), nanofiltration (NF) and reverse osmosis (RO).

These processes are rarely spontaneous and are usually governed by the appropriate driving force. MF, UF, NF and RO are pressure-driven processes [1-10-11], because the separation process is achieved by applying an external hydraulic pressure, which needs to increase with decreasing pore diameter.

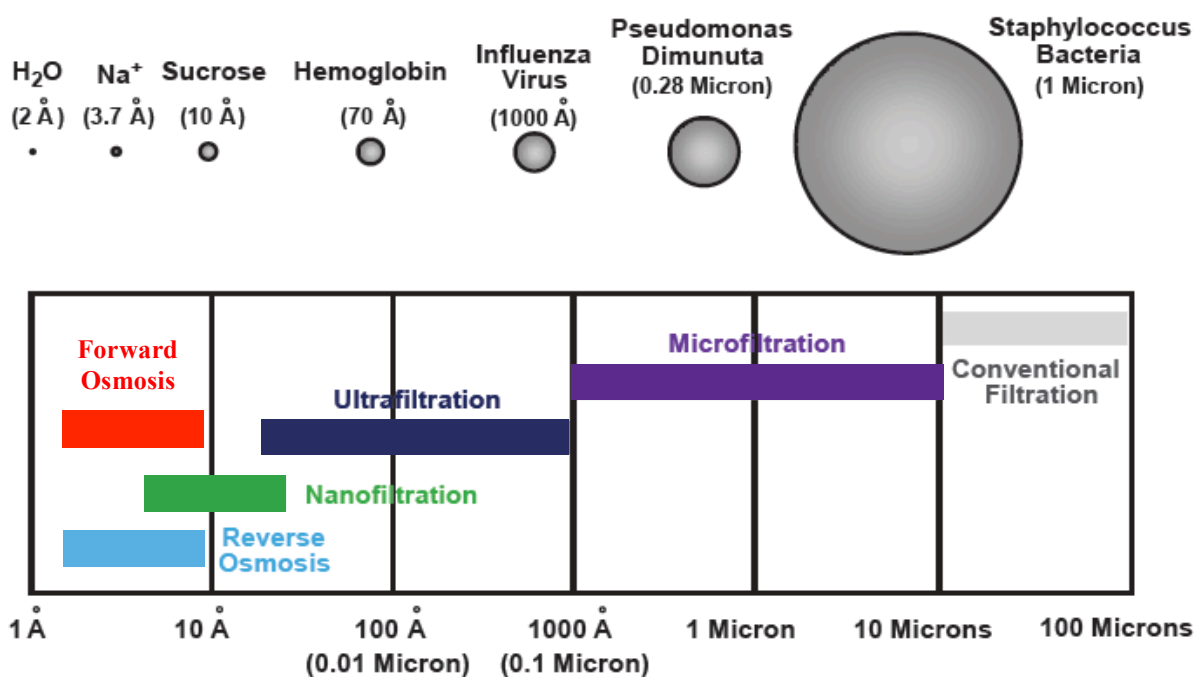


Figure 2.3: Classification of membrane processes in terms of membrane pore diameter.

Microfiltration is used to remove colloidal particles, bacteria and other chemical species whose dimensions are higher than the maximum pore size of the membrane [10-11]. MF membranes are synthetic polymeric membranes, which are usually symmetrical and show pores with a dimension that can vary from 0.1 to 10 μm . Most of these membranes are depth filters, i.e. the rejection of particles is obtained by capturing them inside the internal wall of the porous structure.

Ultrafiltration is very similar to microfiltration, the main difference being the membrane pore size (smaller in UF). UF process separates small solid solutes, colloids, emulsions and macromolecules whereas it allows the permeation of sugars, salts and low molecular weight organic particles. As far as their morphological structure is concerned [11], UF membranes are considered as screen-filters and not depth-filters. Acting as screen-filters, they perform the rejection by capturing and accumulating species larger than the pore size directly on the surface, thus leaving smaller particles to permeate easily. Ultrafiltration membranes have a porosity with a dimension that varies in the range 10-1000 \AA .

For what concerns nanofiltration, NF membranes show pores with a dimension inferior to 0.01 μm , present high rejection values to most organic solutes and also good salt rejection at salt concentration below 1000-2000 ppm. The process operates at higher pressure if compared to MF and UF [11].

Reverse osmosis membranes separate water from water-solutes mixtures at a pressure that can overcome the osmotic pressure of the solution. This process is typically used in desalination plants. RO membranes have porosity with dimension inferior to 0.001 μm and are usually made of cellulose acetate, polysulfone, polyethersulfone and/or polyamide. Thin-film composite membranes represent the best solution because of the tradeoff between selectivity and permeability.

In addition to these well-established processes there is also forward osmosis (FO), a recently developed technique, which is attracting increasing attention. Contrary to the pressure-driven processes, the separation in FO is attained as a consequence of an osmotic gradient without applying any external hydraulic pressure [4-5]. The typical rejection ranges of FO are comparable to tight nanofiltration and reverse osmosis. FO requires asymmetric or composite membranes with tailored properties. These membranes are generally made of cellulose, polyamide, polysulfone and derivatives. This technique will be described in details in the following sections.

Microfiltration, ultrafiltration, nanofiltration, reverse and forward osmosis differ not only according to pore dimensions and membrane morphology (generally symmetrical in MF whereas asymmetrical or composite for UF, NF, RO and FO) but also in terms of separation mechanism and transport model. In MF and UF the transport phenomena occur via pore flow mode, thus removing particles having sizes comparable to their membrane pores, whereas NF, RO and FO operate via solution-diffusion mechanisms because of the non-porous morphology of their membrane top layer.

2.2.1 Flow configurations of membrane processes

There are two main configurations of membrane processes: dead-end and cross-flow filtration modes [12-13]. Dead-end systems are simpler and cost-effective, but performance is usually poor if compared to cross-flow units due to the high flow resistance, which develops in dead-end filtration.

In dead-end filtration, the feed flow is perpendicular (Figure 2.4A) to the membrane surface. The fluid that diffuses across the membrane is known as *filtrate*, whereas the rejected particles form a *retentate*. In time, the latter starts generating a static cake layer in proximity to the porous surface of the membrane. This phenomenon is known as *fouling*.

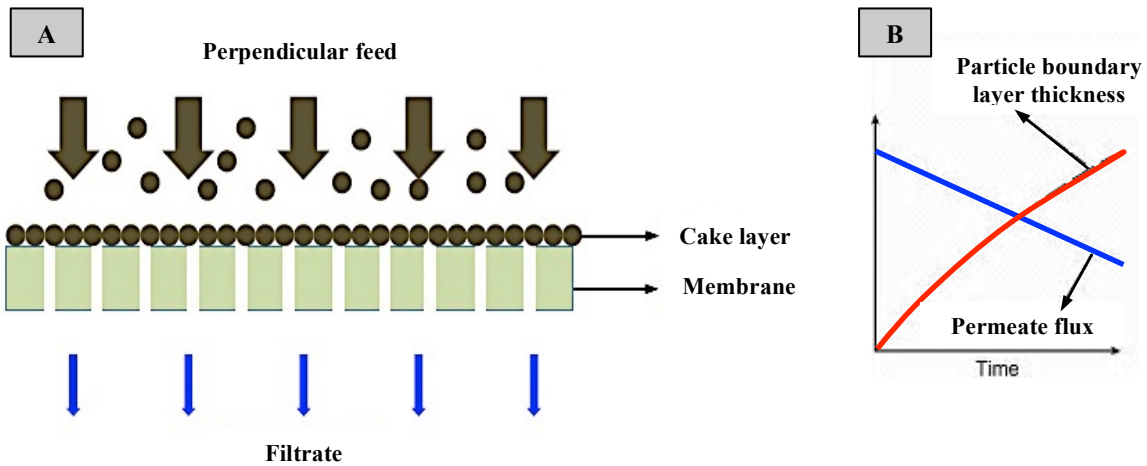


Figure 2.4: a) schematic representation of dead-end filtration; b) influence of the cake layer on membrane performance.

As the separation process goes on, this cake layer increases its thickness. This decreases the system's efficiency because it affects negatively the permeate flux (Figure 2.4B) until the clogging cake is removed by washing cycles. This is the reason why dead-end system is used preferably when the amount of particles in the feed stream is low. A variant of this process is the stirred-dead end filtration that is typically employed for lab-scale filtration. The only difference consists on the continuous stirring of the feed solution in order to reduce the cake layer formation, thus preserving the efficiency of the membrane for as long as possible (Figure 2.5). Thanks to stirring, the particles remain suspended in the fluid without generating the cake layer.

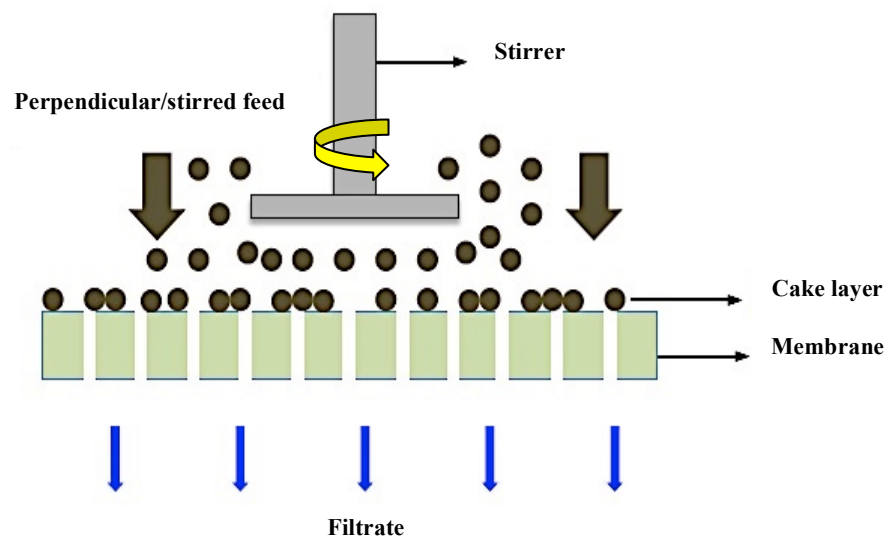


Figure 2.5: Schematic representation of stirred dead-end filtration.

Unlike the previous configurations, in cross-flow mode a turbulent feed-stream flows parallel to the membrane surface with a high pressure driving force (Figure 2.6A). This process produces both a permeate and a retentate that flow tangentially to the membrane surface.

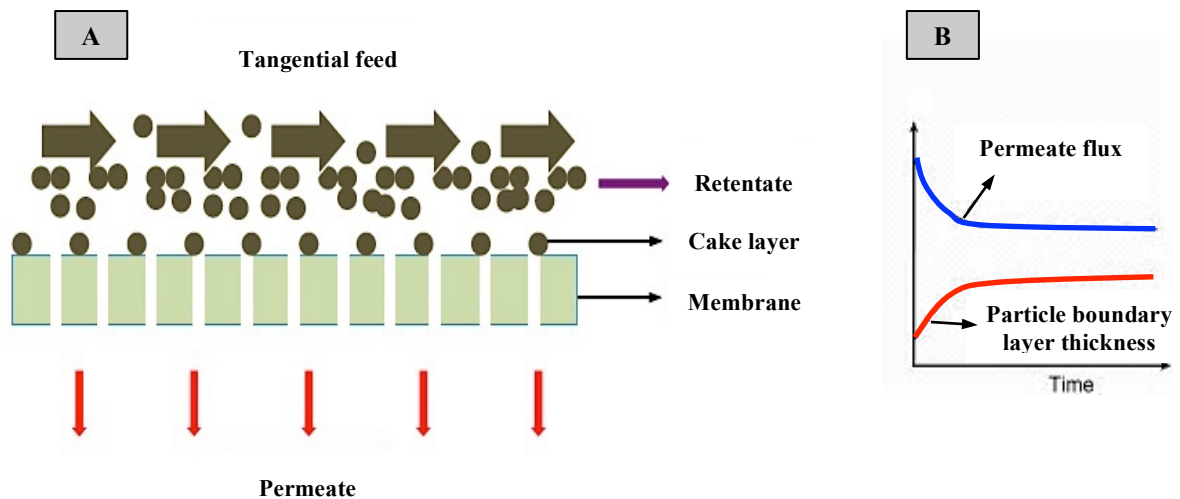


Figure 2.6: a) schematic representation of cross-flow filtration; b) influence of the cake layer on membrane performance.

This operating configuration allows the formation of a dynamic cake layer, which is easy to control, leading to lower flow resistance. Actually, it is possible to regulate the cake layer formation by varying the speed of the feed-stream in order to keep the clogging under an optimum thickness over a certain period. Therefore there is no great reduction in the permeate flux (Figure 2.6B).

2.2.2 Transport models

Two different models describe the mechanism of permeation through membranes: solution-diffusion and pore-flow [1-11]. Porous membranes separate particles by molecular filtration according to pore flow model, whereas dense membrane separation consists on diffusion mechanisms according to solution-diffusion model (Figure 2.7).

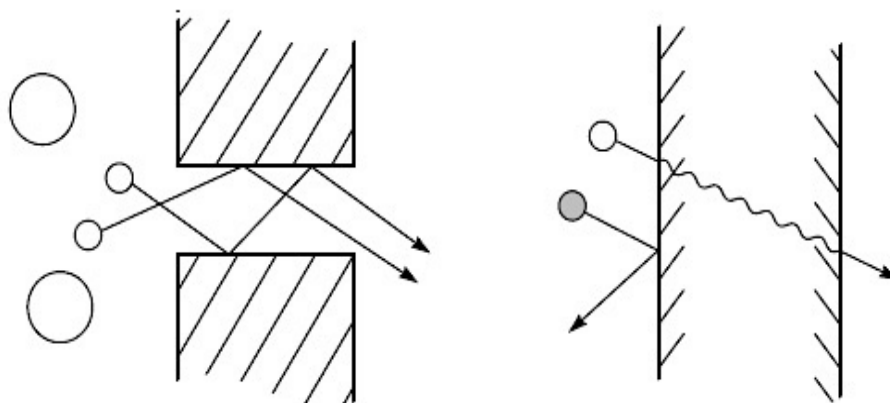


Figure 2.7: Mass transport across porous (on the left) and dense (on the right) membranes [11].

Solution-diffusion occurs when pores are very small and are generated by the free-volume regions between the polymer chains [11]. Furthermore, these pores are not fixed, but transient, so they can fluctuate due to thermal motion of the macromolecules. On the other hand, pore-flow model is associated to the presence of permanent pores, which are not only bigger but also fixed in specific positions, and the permeation rate is much higher. In first approximation, it is possible to distinguish transport mechanisms by simply considering membrane pore size. The transition from solution-diffusion to pore-flow model can be appreciated in the specific pore size range of 0.5-5 nm, which is the common range of nanofiltration.

Therefore, as discussed in chapter 2.2, microfiltration and ultrafiltration membranes are porous and the transport phenomena can be described with pore-flow model, whereas solution-diffusion is used to evaluate mass transport in reverse and forward osmosis processes, where membranes show a superficial dense layer with no defined pores [1-10-11]. A comparison between the different membrane processes in terms of transport model, driving force and membranes structure is presented in Table 2.1.

Table 2.1: Driving forces, membrane structure and transport mechanism of the different membrane processes.

Process	Driving force	Membrane structure	Transport model
Microfiltration	Hydraulic pressure	Macropore	Pore flow
Ultrafiltration	Hydraulic pressure	Mesopore	Pore flow
Nanofiltration	Hydraulic pressure	Micropore/dense	Pore flow/ Solution-diffusion
Reverse Osmosis	Hydraulic pressure	Dense	Solution diffusion
Forward Osmosis	Osmotic gradient	Dense	Solution diffusion

According to the solution-diffusion model, permeation consists of 1) the dissolution of chemicals in the membrane, followed by 2) the diffusion of these species through the membrane. The separation process occurs because of the difference in the solubility coefficients between the permeate and the membrane material. Instead, the pore flow model describes permeation as a flux of species through fine pores induced by a pressure drop [11].

Both models can be described by thermodynamics [11]. As mentioned before, membrane separation processes are rarely spontaneous since they are usually governed by a driving force. These driving forces can be expressed in terms of chemical potential. Thus, the permeation flux can be evaluate as follows (Equation 2.1):

$$J_i = -L_i \frac{d\mu_i}{dx} \quad (2.1)$$

where L_i is a specific coefficient that correlates the chemical potential to the flux and $d\mu/dx$ is the chemical potential gradient of component i .

In the solution diffusion model, two assumptions are made to describe mass transfer in terms of diffusion mechanisms:

- The chemical potential across the membrane is continuous
- The pressure throughout membrane is constant at the highest value

According to these considerations, we assume that the pressure is constant within the active layer of the membrane and the chemical potential is expressed only in terms of concentration gradient. As a result, Equation 2.1 can be adapted to solution-diffusion model as follows:

$$J_i = -\frac{RTL_i}{c_i} \frac{dc_i}{dx} \quad (2.2)$$

This expression has the same form as Fick's law if we consider the first term as the diffusion coefficient.

Starting from the thermodynamic approach to the solution diffusion model, it is possible to derive the water and salt membrane permeability constants:

$$J_i = A(\Delta P - \Delta \pi) \quad (2.3)$$

$$J_i = B(c_{j0} - c_{j1}) \quad (2.4)$$

where A and B are respectively the water and salt permeability constants, ΔP the hydrostatic pressures difference across the membrane, $\Delta \pi$ is the osmotic gradient between the solution facing the membrane whereas c_{j0} and c_{j1} refer to the concentration gradient across the membrane.

It is also possible to evaluate the rejection coefficient considering the concentration differences between the feed and the permeate solutions:

$$R = \left(1 - \frac{c_P}{c_F}\right) \times 100\% \quad (2.5)$$

where c_P and c_F are respectively the concentration of solute in feed and permeate, whereas the R is the rejection coefficient, which represents the membrane's capacity to reject particles from the feed stream.

While solution-diffusion model is described by diffusion equations, pore-flow model can be evaluated starting from the pressure-driven convective flow [11]. As mentioned before, this model describes the permeation of species through fine pores due to a pressure drop. The latter forces the chemical components of the feed stream in contact with the membrane, so as particles small enough can pass through pores and permeate.

Therefore, the pore-flow model can be described by Darcy's law:

$$J_i = K'c_i \frac{dp}{dx} \quad (2.6)$$

where dp/dx is the pressure gradient in the membrane, c_i is the concentration of component i, K' is a specific coefficient closely related to the material of the membrane and J_i is the permeation flux. Typically, pore-flow model fluxes are higher than solution-diffusion fluxes.

2.3 Forward Osmosis (FO)

Forward osmosis (FO), also known as direct osmosis, is an osmotic process in which water flux across a semipermeable membrane (Figure 2.8) is governed by the osmotic pressure gradient between the feed solution (FS) and a highly concentrated solution known as draw solution (DS) [17-18-19].

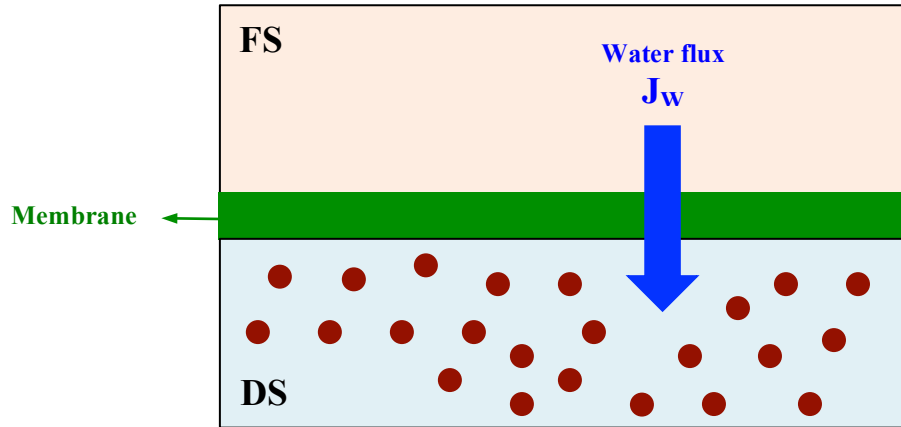


Figure 2.8: Schematic representation of FO process.

2.3.1 FO basic principles

Osmosis is a chemical/physical phenomenon defined as a net movement of a solvent across a semipermeable membrane toward a higher solute concentration region driven by an osmotic gradient.

The osmotic pressure (π), related to the concentration of dissolved ions in solutions, can be calculated using the Van't Hoff equation:

$$\pi = RT\Sigma iM \quad (2.7)$$

where R is the ideal gas constant ($0,08206 \text{ L atm mol}^{-1} \text{ K}^{-1}$), i is the Van't Hoff factor, M is the molarity of the specific ion, and T is the temperature.

Lee et al. [20] described water permeation in osmotic processes across a semipermeable membrane using the following equation derived from the solution-diffusion model (Chapter 2.2.2):

$$J_w = A(\sigma\Delta\pi - \Delta P) \quad (2.8)$$

where J_w is the water flux, A the water permeability of the membrane, $\Delta\pi$ the osmotic gradient, σ the reflection coefficient, and ΔP is the applied hydraulic pressure.

According to equation 2.8, osmotic membrane processes can be classified as follows (Figure 2.9):

1. Reverse Osmosis: $\Delta P > \Delta\pi$
2. Pressure Retarded Osmosis: $\Delta P < \Delta\pi$
3. Forward Osmosis: $\Delta P = 0$

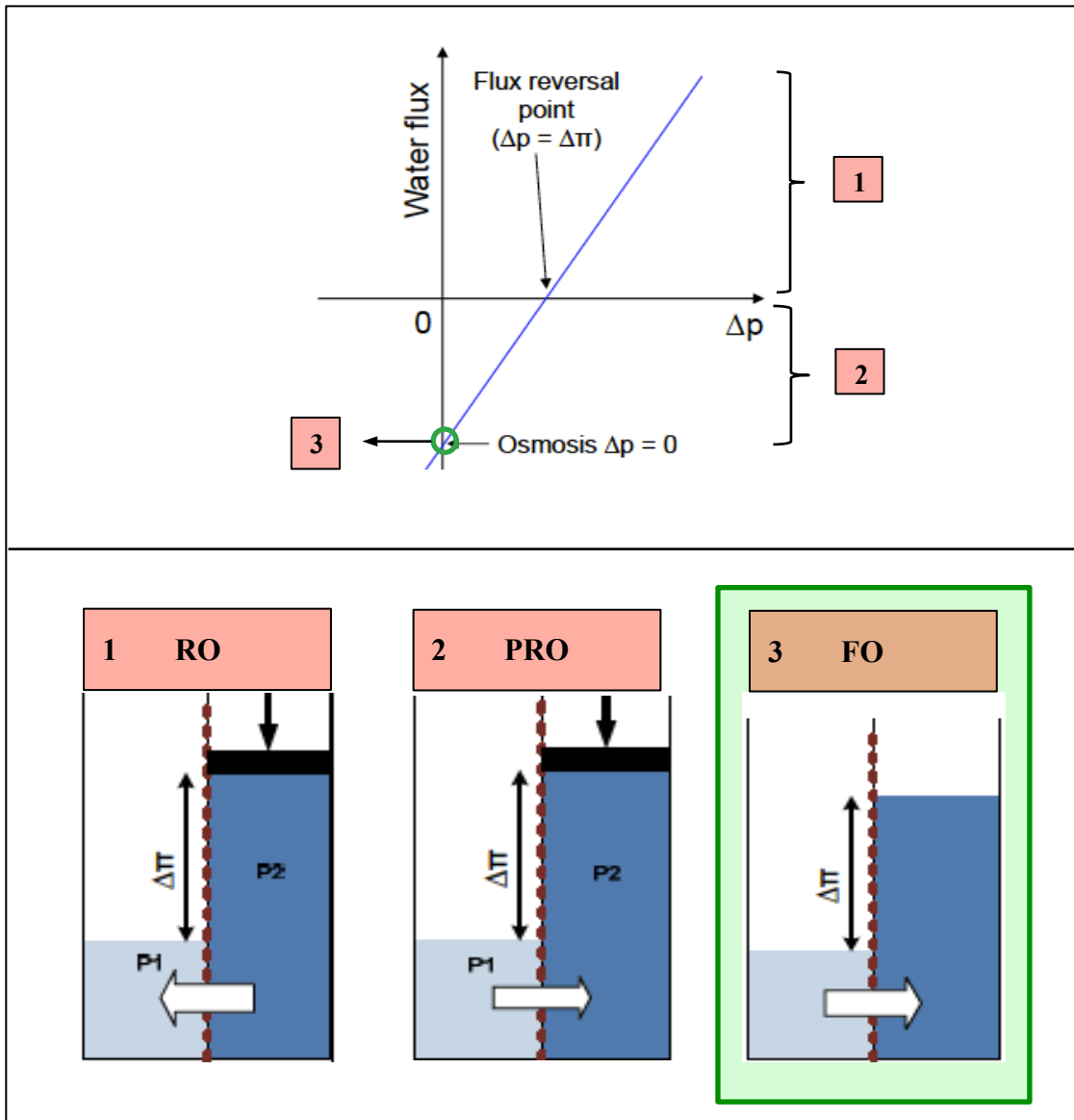


Figure 2.9: Schematic classification of osmotically driven membrane processes.

Since in FO no hydraulic pressure is applied, the permeation flux can be rewritten considering as driving force only the difference between the osmotic pressure of the feed and the draw solution:

$$J_w = A(\Delta\pi) \quad (2.9)$$

However, Equation 2.1 is not suitable for forward osmosis. In this case it is necessary to refer to the Lee's equation for low concentration solutions [20]:

$$\frac{J_1}{A\pi_{Hi}} = \frac{1 - \left(\frac{C_{low}}{C_{Hi}}\right) \exp(J_1 K)}{1 + \frac{B}{J_1} (\exp(J_1 K) - 1)} \quad (2.10)$$

where π_{Hi} is the osmotic pressure of the draw solution, A and B respectively the water and the salt permeation constant, J_1 the flux measured during the experiment, C_{low} and C_{Hi} the solutions concentrations and K is the solute resistivity of the membrane.

Furthermore, Loeb et al. [21] derived an equation that can be applied to FO process:

$$K = \frac{1}{J} \ln \left(\frac{\pi_{Hi}}{\pi_{low}} \right) \quad (2.11)$$

where K is the solute resistivity of the membrane, π_{Hi}/π_{low} the ratio between the osmotic pressure of the solutions, which is considered equal to C_{Hi}/C_{low} ratio, and J is the flux.

As far as the solute transport across the semipermeable membrane is concerned, the driving force is the diffusion due to concentration gradients.

$$J_s = B(\Delta C) \quad (2.12)$$

where J_s is the salt flux, B the solute permeability and ΔC is the solute concentration difference between the draw and feed solutions.

In forward osmosis there are two potential solute fluxes: 1) feed solute diffusion towards the draw solution and 2) draw solute flux towards the feed solution, called *reverse solute diffusion*. The choice of the draw solution is fundamental in order to optimize FO process, because the reverse solute diffusion across the membrane decreases FO efficiency. This concern will be analysed in the following sections.

Since FO process requires no external pressure, it has several benefits with respect to the traditional pressure-driven membrane processes (MF, UF, NF and RO), namely: 1) lower energy requirements [17] and thus lower capital costs; 2) lower propensity to membrane fouling; 3) lower internal concentration polarization (ICP) [22-23-24]; 4) high rejection of almost all solutes [22]; 5) high water recovery and 6) easy membrane cleaning.

However, in spite of all these advantages, there are still some critical challenges preventing the large scale commercialization of FO [25], such as limited choice of easily recoverable draw solutions, reverse solute diffusion, concentration polarization, membrane design and also membrane fouling, even if FO fouling is less pronounced than in other membrane processes, as discussed above. To overcome these concerns, the research has been focused on the development of new custom-tailored membranes. All these challenges will be analysed in the following sections.

2.3.2 Draw solutions (DS)

The efficiency of a FO process is closely related to the selection of the most suitable draw solution (DS), where DS or just brine, is defined as a concentrated solution used to generate high osmotic pressure.

Regarding the dissolved draw solutes, they must be highly soluble and have very low effect on internal concentration polarization (ICP). Further, they also must be non-toxic, resistant to biofouling and stable at natural pH, inexpensive and easily available. They should be easy to recover/regenerate through conventional techniques such as reverse osmosis, distillation, precipitation etc. and they must not damage the membrane surface [5]. It is clearly very challenging to find an ideal draw solute having all these characteristics, thus a compromise has to be found.

In the last 50 years, a great number of draw solutes for FO has been investigated with a particular attention to inorganic salts, organic salts, and synthetic materials. Before 2000s, volatile gases have been widely tested as draw solutes because they can be easily regenerated through distillation [5]. In those years, Elimelech et al. [26-27] proposed a new draw solution based on $\text{NH}_3\text{-CO}_2$ water-soluble mixture, which is characterized by high osmotic pressure leading to high water flux across the membrane.

More recently, new synthetic materials have been tested as potential draw solute, like magnetic or hydrophilic nanoparticles (NPs) [28-29], or stimuli-responsive hydrogel polymer [30]. Ge et al. [31] provided a list of a wide range of draw solutions that have been reported in literature.

Achilli et al. [32] reported that, in terms of performances and costs, inorganic based draw solutions, such as NaCl , KHCO_3 , MgSO_4 and NaHCO_3 , seemed to be the most suitable solutions for commercial applications. However, the final selection criterion is closely related to the specific FO process and to the interaction with the feed solution. Among the criteria for the most suitable DS introduced above, the most important are the selection of a solution easily recoverable along with its high osmotic pressure and low cost. This is the reason why NaCl is the most widely employed draw solution (40% of experiments reported in literature).

2.3.3 Reverse diffusion

Another important parameter that influences the choice of the most suitable draw solution is the reverse diffusion of the draw solutes through the membrane. Reverse diffusion is an inevitable phenomenon in all the osmotically driven membrane processes. It is characterized by the diffusion of draw solutes across the membrane from the draw solution towards the feed-stream [33], as a result of the concentration gradient between the two sides (Figure 2.10).

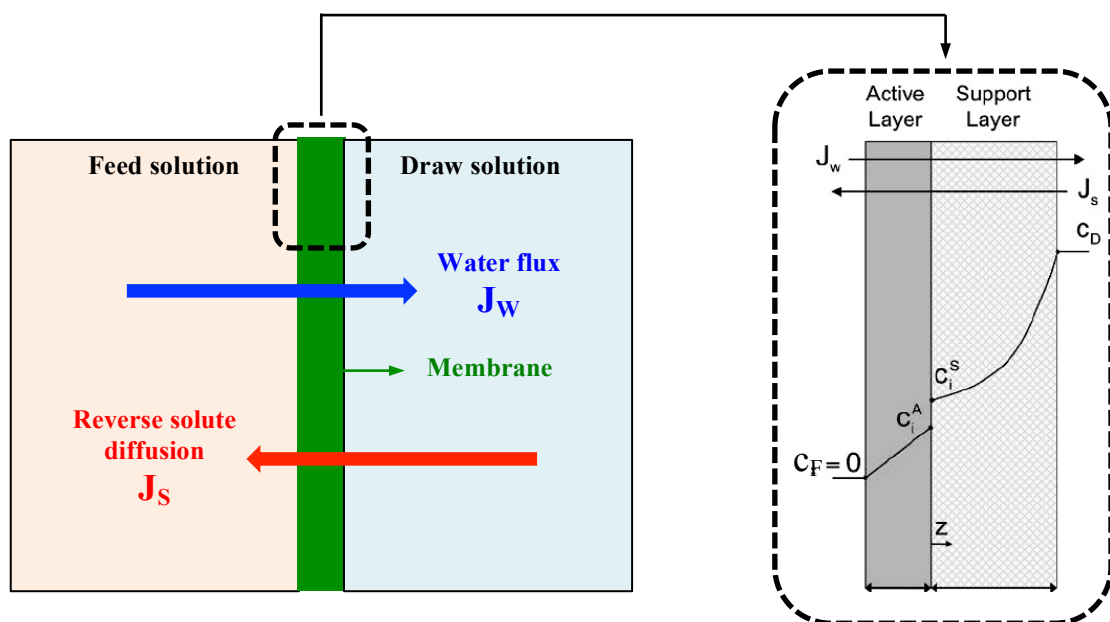


Figure 2.10: Schematic illustration of reverse solute diffusion across a semipermeable membrane.

This process depends on the diffusivity coefficient of the draw solute and on the operating temperature.

Reverse diffusion decreases both the effective driving force as well as the water flux. Therefore, when a high value of rejection is required, multivalent-ion solutions with low diffusion coefficient seem to be the best option in order to reduce the reverse solute diffusion. However, multivalent ions characterized by low diffusion coefficient and large size may cause an increase of the internal concentration polarization.

Furthermore, it was observed that the accumulation of solutes onto the active layer due to reverse diffusion could also enhance the aggregation of foulants [5].

Overall, the reverse diffusion should be carefully considered and minimized in the fabrication of high performances FO membrane. This is the reason why *Reverse Solute Flux Selectivity* (RSFS) was introduced as an additional parameter to water permeability and salt rejection for evaluating forward osmosis process [34]. RSFS is defined as ratio of FO water flux to reverse salt flux and can be calculated with the following equation:

$$\text{RSFS} = \frac{J_w}{J_s} \quad (2.13)$$

where J_s and J_w are respectively salt flux and water flux. A higher value of the reverse diffusion indicates lower membrane selectivity and a decrease in FO performances. Therefore, the goal is maximizing RSFS.

2.3.4 Membrane Fouling

Fouling is the principle cause of performance decrease for membrane processes in terms of flux and permeability. It can be seen as a progressive deposition of retained inorganic particles, organic macromolecules, salts, biomolecules etc. onto the active surface of the membrane, inducing a severe decline of the membrane permeability. Fouling is generally classified into four different categories [11]:

1. scaling
2. deposition of particulates/silt
3. biofouling
4. organic fouling

Scaling is generated by the deposition of salts in the stream feed or other suspended solids onto the active layer of the membrane. These particles are progressively removed during the permeation of the feed across the membrane until the solubility limit is reached causing the precipitation. These precipitated solid material influences negatively the performance of the membrane by reducing the permeate flux. Typical salts that generate scaling are: calcium carbonate (is the most common source of scaling), calcium sulphate, silica complexes, barium sulphate, strontium sulphate and calcium fluoride. This kind of fouling is very difficult to control, although calcium carbonate can be easily removed by acidifying the feed or by adding chemical antiscalants. As far as the other sources of scaling are concerned, silica is definitely the most difficult to control because no efficient antiscalants are available [11].

The formation of silt is due to the precipitation of organic colloids, corrosion products and other particulates onto the membrane surface. This phenomenon is commonly described by using the Silt Density Index, a specific index that describes the propensity of the feed to generate fouling [11].

Biofouling is generated by bacterial proliferation on the membrane surface and is closely related to the material of the membrane. Generally, TFC membranes are characterized by good resistance to biofouling. Nevertheless, they are periodically treated with bactericides.

Alternatively, these membranes can also be subjected to a chlorination treatment [11], but due to their sensibility to chlorine the residual solution must be carefully removed.

Finally, organic fouling is due to the adsorption of organic materials on the membrane.

Membrane fouling in FO is different from the typical fouling of the pressure driven membrane processes because forward osmosis requires no external pressure to perform the separation process. Several researchers [36] have investigated FO membrane propensity to fouling, stating that FO processes are less sensitive to fouling and that fouling is almost completely reversible. FO fouling was studied for the first time by Cath's group [35] that reported no strong flux reduction.

Recently, Elimelech and co-workers [36] have investigated the effect of both organic and inorganic fouling on FO efficiency and found a relationship between the organic fouling and intermolecular adhesion. According to their study, FO fouling is a complex process governed by both chemical and hydrodynamic effects and is related to the membrane material. However, they also reported that FO fouling is reversible and can be removed through water rinsing (Figure 2.11).

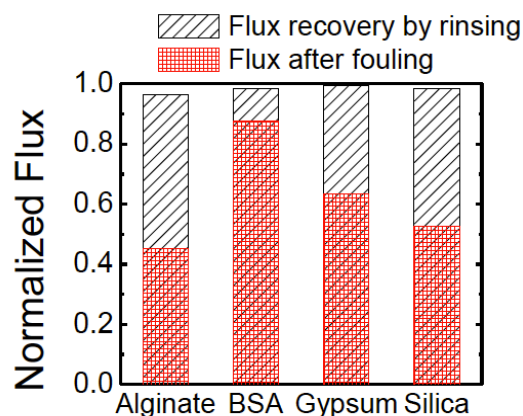


Figure 2.11: Fouling reversibility in FO membranes [36].

Lee et al. [37] analysed FO fouling in terms of reverse draw salt diffusion. They reported that draw solutes reverse diffusion is the principle cause of both the reduction of the osmotic driving force and the increase of the concentration polarization. Furthermore, they compared FO to RO in terms of organic fouling, concluding that fouling in forward osmosis can be controlled by increasing the cross-flow velocity of the feed-stream.

Other studies [38] reported that there is a correlation between high working temperature and FO scale formation during desalination processes. They observed that the generation of inorganic fouling is principally due to silica particles that can also promote the formation of organic fouling. They also showed that FO membrane rejection is closely related to the nature of fouling.

More recently, new studies of FO fouling were carried on by investigating foulants using microscopic techniques [39]. This method has the limit that only foulants with high dimension can be directly observed. Nevertheless, it was used for the determination of the so-called “critical flux”, defined as the lowest permeate flux above which fouling occurs. However, further studies in this field are required.

2.3.5 Concentration Polarization

Concentration polarization (CP) is a typical phenomenon generated by concentration gradients that occurs in both pressure-driven and osmotic membrane processes, influencing negatively the membrane efficiency. CP occurs when the flux of solutes back to the bulk-feed solution is lower than the water flux across the membrane.

Accordingly, the solute concentration in the boundary layer increases reaching a maximum value at the membrane surface [1]. When this condition is reached, both the osmotic and the solute concentration gradient across the membrane increase dramatically, leading to water flux decrease and salt flux increase through the membrane. A schematic representation of CP is illustrated in Figure 2.12.

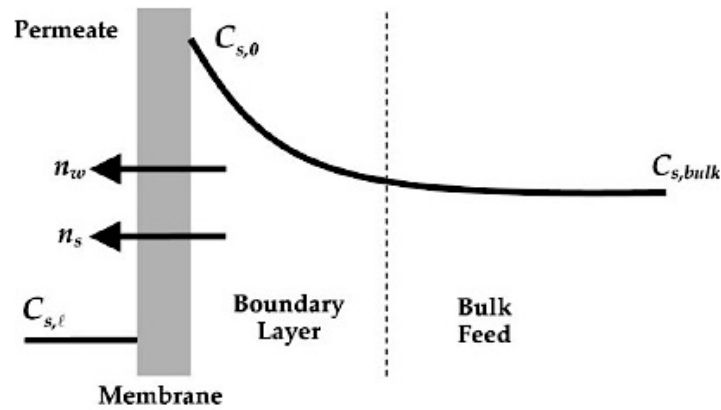


Figure 2.12: Schematic representation of concentration polarization at the membrane boundary layer [1].

There are two different types of CP [4]: external concentration polarization (ECP) and internal concentration polarization (ICP). Furthermore, depending on the membrane orientation, ECP and ICP can occur in both concentrative and dilutive configurations.

Regarding FO processes used for desalination and wastewater treatments, both concentrative external concentration polarization (CECP) and dilutive internal concentration polarization (DICP) can occur during the process, both decreasing the driving force and thus the permeate flux. Considering CECP (Figure 2.13), draw solutes build up on the top of the active layer reducing the water flux across the membrane due to the decrease of the osmotic driving force [40]. ECP in osmotic process can be described using the boundary layer theory. Concentrative ECP can be expressed as follows [5]:

$$\frac{\pi_{m-feed}}{\pi_{b-feed}} = \exp\left(\frac{J_w}{k_{feed}}\right) \quad (2.14)$$

where π_{m-feed} is the osmotic pressure of the feed that is in contact with the surface of the membrane, π_{b-feed} is the osmotic pressure of the feed solution in the bulk, whereas k is the mass transfer constant. The limit of this ECP model for FO is that it is not suitable for composite asymmetric membranes. However, ECP influence is less evident if compared to ICP and can be reduced by increasing both the cross-flow velocity and turbulence effects on both the feed and the draw sides.

Dilutive internal concentration polarization (DICP) is considered as the most limiting factor and the greatest challenge in FO process [4-5]. DICP derives from the dilution of the draw

solutes within the porous support layer (Figure 2.13). This dilution reduces the net osmotic driving force to the final effective available value.

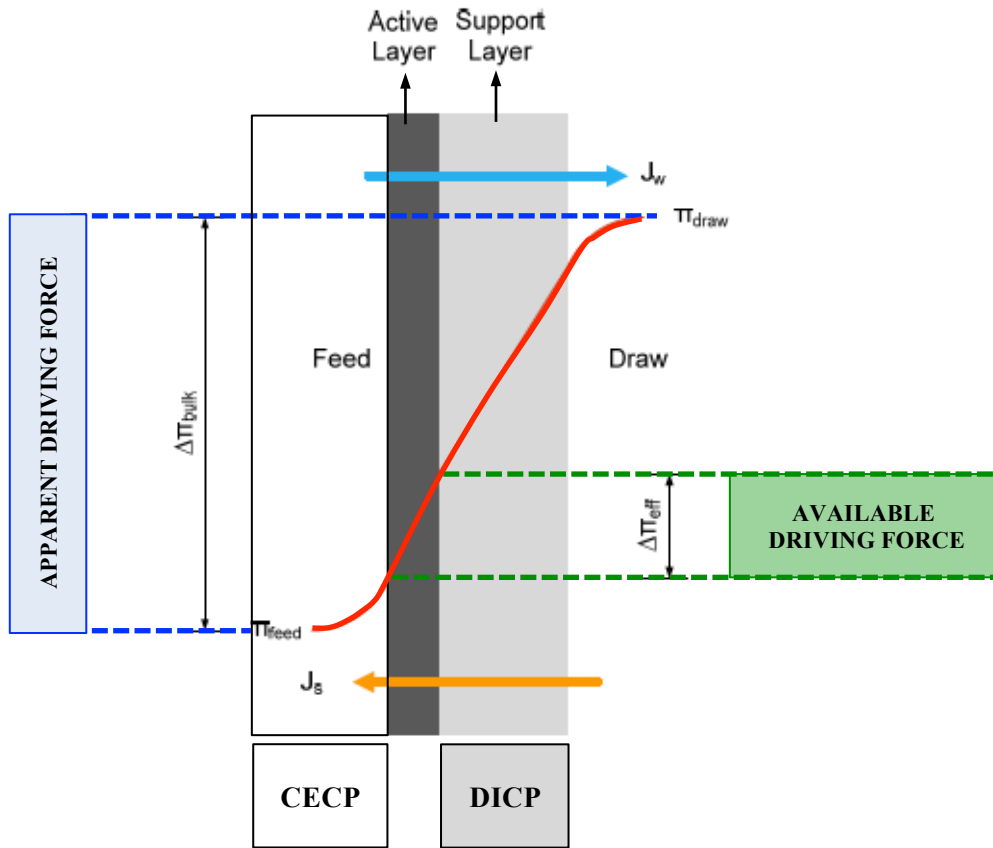


Figure 2.13: Schematic representation of concentration polarization in FO membranes.

The negative influence of dilutive internal concentration polarization on membrane performance has been evaluated using the solution-diffusion transport-theory [41]. The resulting water flux can be expressed by Equation 2.15:

$$J_w = \frac{1}{k} \ln \frac{A\pi_{\text{draw}} + B}{A\pi_{\text{feed}} + B + J_w} \quad (2.15)$$

Where A and B are respectively the water and solute permeability constant, π_{draw} is the osmotic pressure of the draw solution, π_{feed} is the osmotic pressure of the feed solution. K is the solute diffusion resistance within the support layer, which represents the diffusivity of the solute through the support layer of the membrane, and can be calculated as expressed in Equation 2.16 [4]:

$$K = \frac{t\tau}{\varepsilon D_s} = \frac{S}{D_s} \quad (2.16)$$

Where t, τ and ε are respectively membrane thickness, tortuosity and porosity whereas D_s is the solute diffusion coefficient. The ratio (τ/ε) is generally expressed by S, the membrane structural parameter. It is an intrinsic parameter that influences directly the water flux magnitude.

However, McCutcheon and Elimelech [42] have introduced a more complex model that takes into account both ECP and ICP in FO process. According to their theory, ECP and ICP affect the water flux at the same time and consequently the water flux (J_w) expression can be rewritten as follows:

$$J_w = A[\pi_{\text{draw}} \exp(-J_w k) - \pi_{\text{feed}} \exp(J_w/k)] \quad (2.17)$$

FO membranes have to be designed in order to minimize both ICP and ECP. This is the reason why thin film composite membranes seem to be the best solution to achieve high values of permeability and rejection.

2.3.6 Development of FO membranes

The first studies on FO were carried out by using reverse osmosis membranes. McCutcheon and Elimelech investigated TFC-RO membranes stating that these membranes exhibited high salt rejection but also low fluxes due to intense ICP [5-6]. These sub-optimal performances arise from the structure of the membrane. The typical TFC-RO membranes consist of an aromatic polyamide active layer fabricated over a substrate generally made of hydrophobic polysulfone (PSU) reinforced by a non-woven fabric (Figure 2.14).

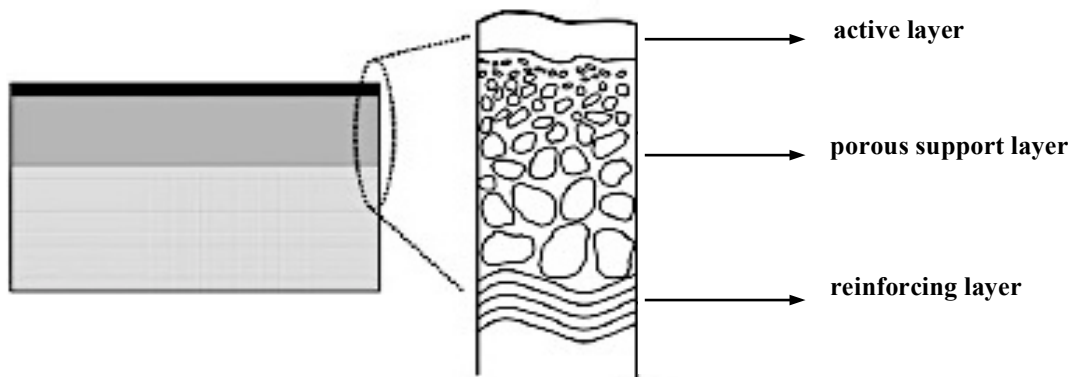


Figure 2.14: Schematic illustration of typical thin film composite membranes for RO [1].

The hydrophobic nature of this support layer, along with its thickness and high tortuosity, negatively affects the permeation efficiency of forward osmosis and increases the internal concentration polarization (ICP), thus reducing water flux [43-44]. Furthermore, RO composite membranes show high structural parameter (S) as well as high thickness in order to maintain their integrity under high-pressure conditions. These factors have a negative effect on FO performance because they increase ICP [45].

The realization of the first specific membranes for forward osmosis dates back to the early 2000s [5]. Cellulosic membranes were the first membranes developed specifically for FO applications. These membranes were widely used for FO not only because of their mechanical strength and resistance to oxidation and chlorine environments, but mostly for their high hydrophilicity, which improves water fluxes and reduces fouling propensity [1]. They are made of cellulose acetate and fabricated using the conventional phase inversion process followed by heat annealing. Hydration Technology Inc. (HTI) produced asymmetric cellulose triacetate membrane (CTA), which are currently available on the market and used for a broad

range of applications. Nevertheless, they are affected by several issues, such as low salt rejection, degradation by microorganism and limited pH working range [8]. Other companies, such as Oasys (Boston) started to commercialize FO membranes but in limited quantities. However, despite all the advantages respect to the traditional TFC-RO membranes mentioned above, cellulose acetate membranes are less resistant to hydrolysis.

In 2005, Chung et al. [46] developed a new FO membrane made of polybenzimidazole (PBI). This membrane seemed to be very promising because of the intrinsic properties of PBI, such as mechanical and chemical stability, but the salt rejection values were unsatisfactory. In order to improve the rejection, PBI membranes were modified by adding polyethersulfone (PES) and polyvinylpyrrolidone to the casting solution. The resulting membrane showed a thin selective layer supported by a porous structure leading to high FO performance.

Nowadays, the attention is focused on the realization of tailored composite membranes fabricated *via* phase inversion technique followed by interfacial polymerization. TFC-FO membranes are indeed the most promising candidates for FO processes because, unlike asymmetric membranes made of a singular polymer, the active and the support layers can be optimized independently by combining their specific properties [45].

The ideal TFC-FO membrane consists of an anisotropic structure including a highly selective active layer, which leads to high solute selectivity and low reverse solute diffusion and a hydrophilic and highly porous support layer in order to maximize water flux and minimize ICP. Furthermore, TFC-FO membranes must be thermally, mechanically, and chemically stable, as well as resistant to oxidation. These membranes have a similar structure to that of TFC-RO and a similar fabrication procedure. The greatest differences are the hydrophilicity and the morphology of the support layer that are crucial for regulating ICP in FO.

Therefore, TFC-FO membrane should present a porous support layer with finger-like pores (Figure 2.15). This morphology, characterized by straight vertical pores with low tortuosity parameter, seemed to be fundamental for optimizing FO performances because the finger-like structure lead to lower ICP. Accordingly, the modification of both properties and structure of the support layer, such as increasing the hydrophilicity, tailoring the porous morphology and decreasing the thickness, were considered a valid approach to improve FO efficiency. A more hydrophilic and thin substrate leads to higher water flux and lower ICP [43]. This is the reason why TFC-FO membranes are characterized by a thinner and more hydrophilic substrate layer than the traditional thin film composite membranes used for reverse osmosis.

Nowadays, the typical TFC-FO membrane consists of an ultrathin PA active layer fabricated with interfacial polymerization on top of a polysulfone or polyethersulfone modified support layer. The support layer is fabricated *via* phase separation technique; usually non-solvent induced phase separation; whereas the highly selective PA layer is typically realized via interfacial polymerization of *m*-phenyldiamine (MPD) and trimesoyl chloride (TMC).

As mentioned above, polysulfones, despite their excellent chemical, thermal and mechanical stability, are hydrophobic. However, this material can be modified for FO by both increasing the hydrophilicity and optimizing the porous structure of PSU-based substrate [8-43]. The introduction of a porous structure with a reduced structural parameter and low tortuosity is indeed a potential route to reduce ICP and to enhance water flux [5].

As far as hydrophilicity is concerned, several chemical modifications of the polysulfone have been investigated. Namely, sulfonation, carboxylation, and addition of NPs to the polymeric PSU-backbone [47]. Therefore, several hydrophilic polymers were tested as potential materials for the fabrication of modified supports, such as sulfonated copolymers based on polyethersulfone, sulfonated poly(ether ketone), and poly-dopamine (PDA) or PVA.

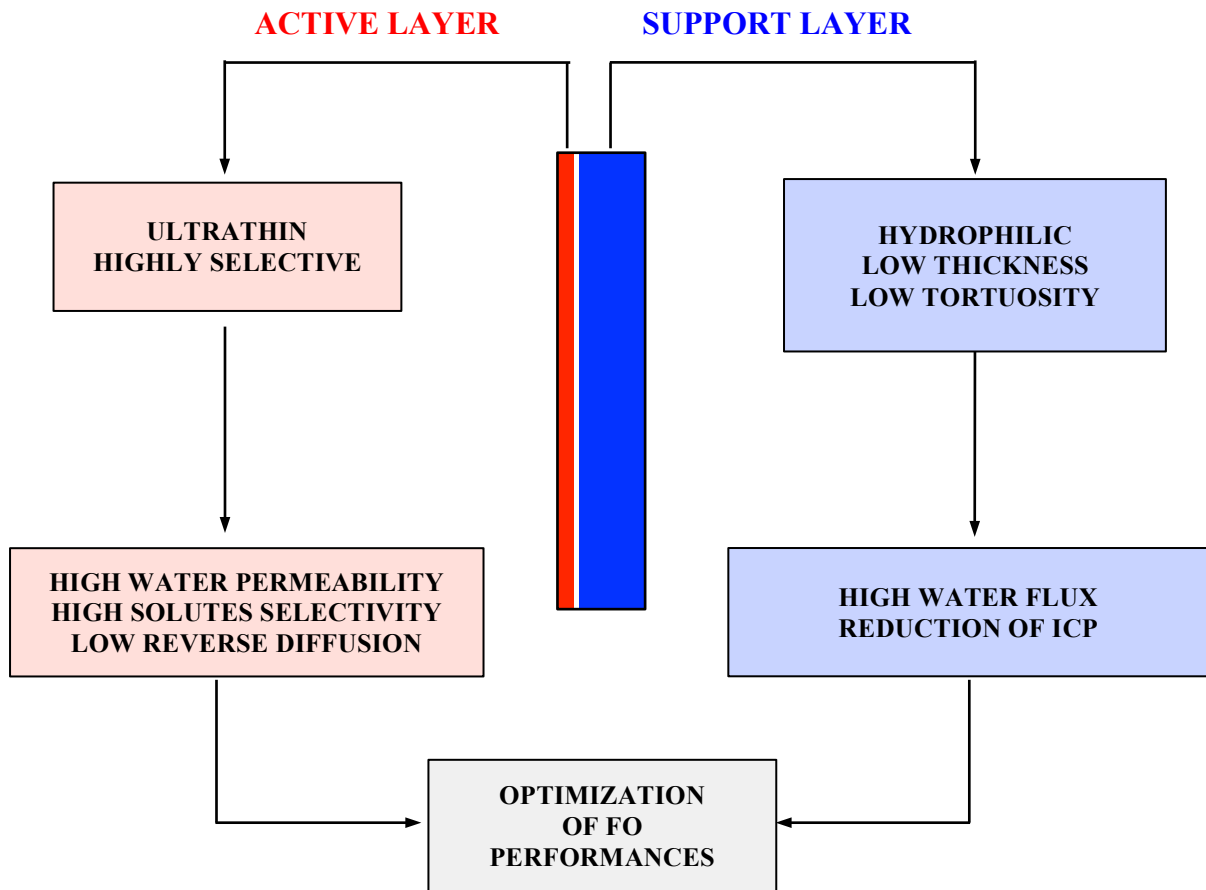


Figure 2.15: The ideal structure of a TFC-FO membrane.

The sulfonation of polysulfones appeared to be the most promising method to increase the hydrophilicity of the substrates because PSU can be easily functionalized by a variety of sulfonating agents via an electrophilic substitution reaction. Despite all of the advantages related to the increased hydrophilicity, hydrophilic polymers also have the following disadvantages [44]: 1) they are prone to swelling, which can decrease the mechanical strength of the membrane; 2) IP can occur not only on the support top surface but also into its pores. Accordingly, a good compromise has to be found.

Wang et al. [43] reported the introduction of sulfonated polymers into the membrane matrix to increase its hydrophilicity and highlighted the importance of the physicochemical properties of the support layer on the resultant FO performances. They fabricated TFC-FO membranes with a porous support layer made by blending PES and sulfonated PSU to enhance both the wettability and the long-term stability. Finger-like pores characterize these support layers.

Widjojo's group [8] fabricated TFC-FO membranes with a support layer containing 50% of a sulfonated polyphenylsulfone (SPPSU). These membranes show a porous substrate that enhances water flux, while their increased hydrophilicity improves the wettability and also reduces internal concentration polarization.

Sahebi et al. [44] realized TFC-FO membranes *via* phase inversion followed by IP, using as casting solution a blend of polyethersulfone and sulfonated polyethersulfone. They observed the behaviour change of the support with the increase of the sulfonated polymer degree. They concluded that higher hydrophilicity can be achieved by increasing the sulfonation degree.

They also reported that higher degree of sulfonation leads to a greater substrate porosity and to a lower structural parameter. Overall, the sulfonation route improves FO performances due to both the morphological variation of the support layer, and the enhancement of wettability.

Also Ren et al. [45] proposed sulfonated polysulfone blended with PSU as support layer materials for TFC-FO membranes. They noticed that by increasing the sulfonation degree of SPSU, the morphology of the support layer changed from a sponge-like to a finger-like porous structure, thus improving FO efficiency. Furthermore, these sulfonated layers have lower contact angle if compared to pure PSU layers, and consequently they mitigate ICP.

2.3.7 Fabrication of TFC-FO membranes

As mentioned in the previous section, TFC membranes are typically produced by a two-step procedure. The support layer is generally fabricated *via* non-solvent induced phase separation (NIPS), whereas the active layer is synthesized through interfacial polymerization (IP) [1-10-11].

Non-solvent induced phase separation technique was developed in the years 1958 to 1960 by Loeb-Sourirajan for the realization of the first anisotropic membranes. It consists of the precipitation of a concentrated casting solution by immersion in a non-solvent (typically water) bath. The immersion in the coagulation bath causes the precipitation of the polymer solution into two phases, a solid polymer-rich phase generating the membrane matrix and a liquid polymer-poor phase, which leads to the formation of the interconnected porous structure [1]. The resulting anisotropic structure is due to the fact that the top surface of the casting solution precipitates first leading to the formation of a finely microporous layer. This top layer slows the exchange phenomena between solvent and non-solvent, so the bottom layer precipitates more slowly generating a more porous structure. NIPS process is schematically illustrated in Figure 2.16.

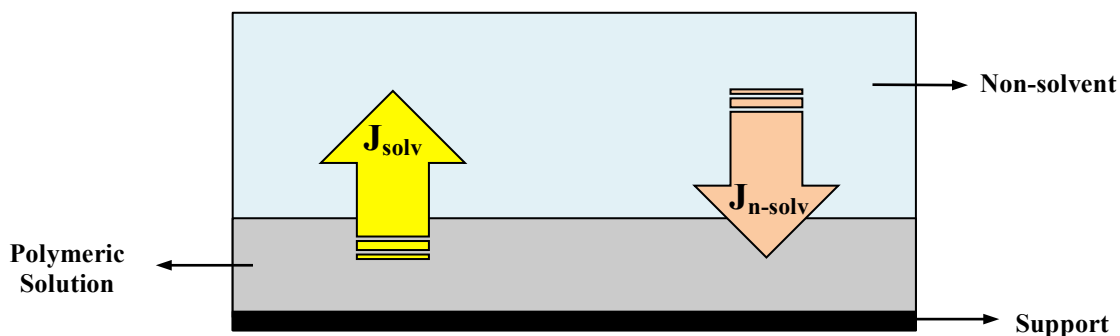


Figure 2.16: Principles of non-solvent induced phase separation (NIPS) process.

The solvent and the non-solvent exchange by diffusion mechanism at the interface between the casting solution and the non-solvent: the solvent migrates towards the coagulation bath with a flux J_{solv} while the non-solvents diffuses reversely with a flux J_{n-solv} , leading to the formation of the membrane [10-14].

Overall, the anisotropic membrane structure depends on six factors [10-11-14]: 1) polymer nature and behaviour; 2) composition of the casting solution; 3) composition of the coagulation bath; 4) exposure time; 5) humidity and 6) temperature. Generally, thermoplastic and amorphous polymers with high molecular weight (such as PSU) are considered the ideal

polymers for the fabrication of membranes. Aprotic solvents, such as N-methyl-pyrrolydone (NMP), are typically the most used solvent for the preparation of the casting solution because they dissolve a broad range of polymer and lead to a very porous and anisotropic membrane structure [11].

Furthermore, both kinetics, in terms of exchange rate and phase separation velocity, and thermodynamic stability influence the morphology of the resulting membrane [11]. As far as the thermodynamics is concerned, the stability of the three-component system can be described with a ternary diagram as the one shown in Figure 2.17

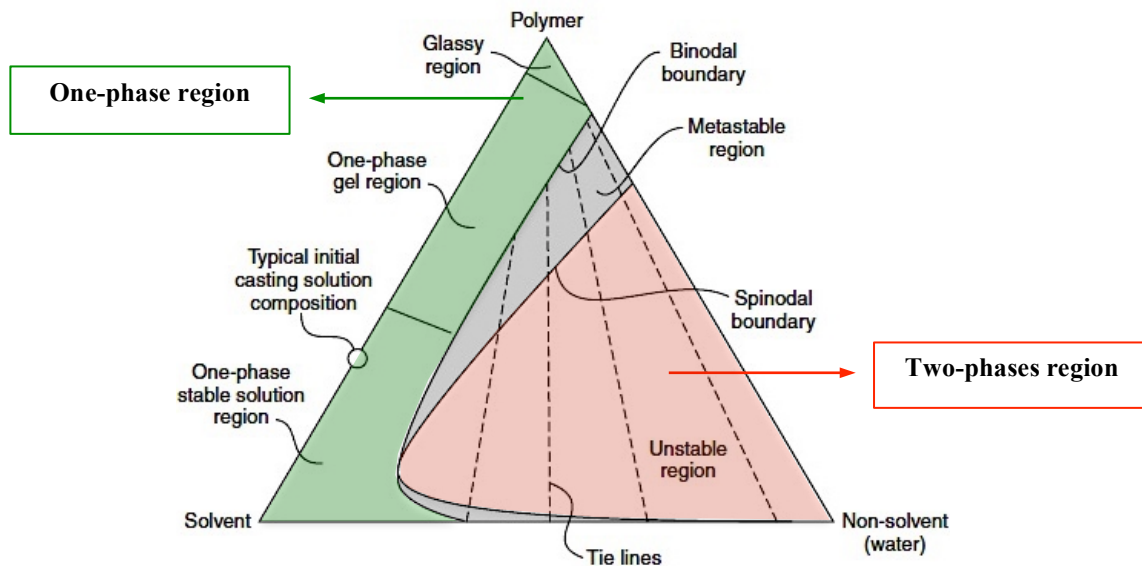


Figure 2.17: Three-component phase diagram used to explain phase separation processes.

The corners of the triangle represent the pure components, respectively the polymer, the solvent and the non-solvent (water). The diagram can be divided into three regions: a one-phase region that represents the complete miscible area, a metastable region whose extension decreases with the decrease in the molecular weight of the polymer and a two-phases region where the phase separation occurs, leading to the formation of a solid polymer-rich phase and a liquid polymer-poor phase. The one-phase region can be subdivided further into liquid, gel and glassy region depending on the polymer concentration in the casting solution. The casting solutions are typically prepared in the low-concentration liquid region (<25 wt%), whereas the transition liquid-gel and gel-glassy are generally placed respectively at a polymer concentration of 30-40 and 90 wt% [11].

The phase separation can be seen as a series of steps (Figure 2.18). Firstly, the casting solution is immersed in the coagulation bath and the exchange by diffusion mechanism starts: the solvent leaves the solution whereas water follows the reverse path. Then the polymer solution crosses the binodal boundary and enters into a metastable region where no separation occurs till the polymer nucleates. This step in the metastable region is influenced not only by the molecular weight of the polymer as mentioned above, but also by the viscosity of the solution that can postpone the precipitation. Finally, the phase separation occurs when the polymer solution crosses the spinodal boundary generating a solid and liquid phases with compositions linked by tie lines [11-14-15].

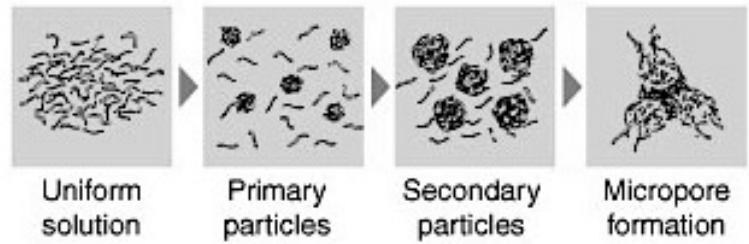


Figure 2.18: Steps of polymer precipitation.

Strathmann et al. [16] described the phase separation process as a line through the ternary diagram (Figure 2.19).

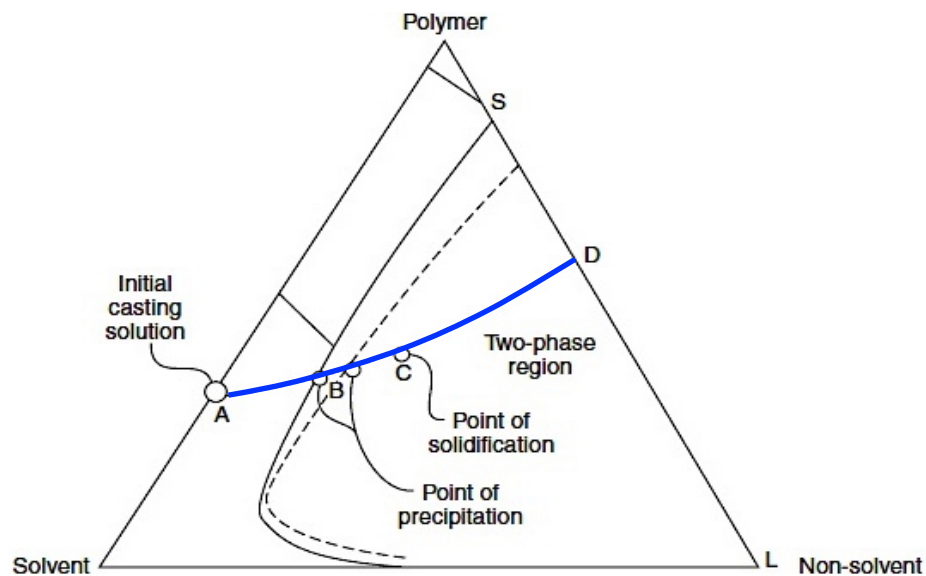


Figure 2.19: Schematic representation of phase separation as a line through the three-component phase diagram.

The initial casting solution composition is represented by point A. When the solution is immersed in water, the exchange mechanism starts and the system composition moves along the line AD reaching point B, which represents the concentration at which the polymer precipitation starts. As can be seen in the figure, the real position of the point B depends on the extension of the metastable region. As the process goes on, the viscosity increases and the polymer reaches its point of solidification (C). The process ends in point D, which represents the final membrane composition.

Turning now to the realization of the TFC active layer, the fabrication is realized *via* interfacial polymerization (IP). This process was first introduced by Emerson and Morgan in 1955 and then developed by Cadotte for the realization of TFC-RO membranes. The great advantage of this technique is the possibility of optimizing independently the properties of the skin layer and microporous substrate.

The process is based on the Schotten-Bauman polyamidation reaction. It consists in a step growth polymerization carried out at the liquid-liquid interface between two immiscible

solutions, a diamine and an organic chloride solutions [49]. The amine group reacts with the acyl chloride leading to the polymerization of the polyamide (Figure 2.20).

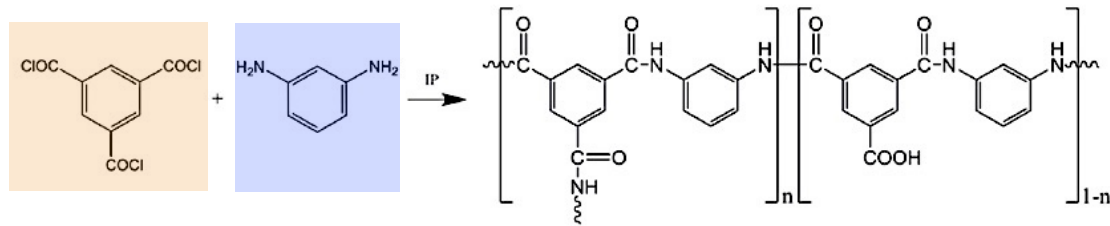


Figure 2.20: Interfacial polymerization between meta-phenylenediamine and trimesoyl chloride.

Therefore, the support layer is first soaked in an aqueous amine solution and then immersed into an acyl chloride solution. The interfacial polymerization reaction takes place at the interface between the two solutions, leading to the formation of an ultrathin polyamide layer. The TFC membrane thus formed is then subjected to curing through heat treatment (90-95 °C) to optimize the properties of PA layer by enhancing its adhesion to the substrate (Figure 2.21).

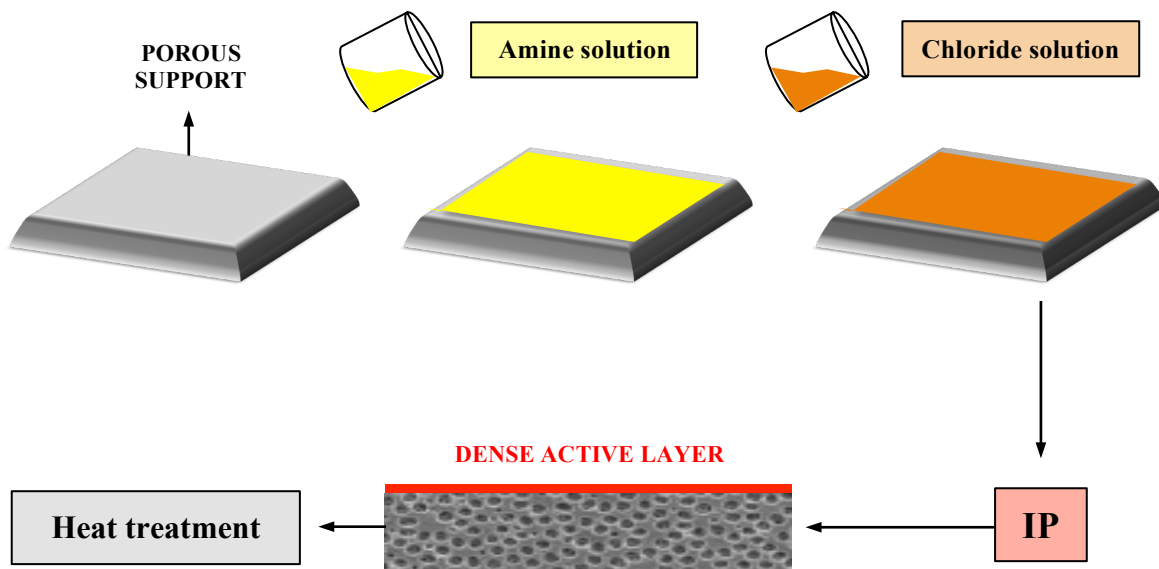


Figure 2.21: Schematic diagram of interfacial polymerization procedure.

2.3.8 Recent applications of forward osmosis

Due to its potential advantages, forward osmosis has been investigated for several industrial applications, namely: 1) wastewater reclamation [50]; 2) industrial wastewater treatments [4-5]; 3) desalination [4-5-17]; 4) fertigation, 5) brine concentration; 6) concentration of landfill leachate [51]; 7) liquid food processing [4]; 8) membrane bioreactor [4-5]; 9) drug delivery [5] and 10) medical product enrichment [5].

FO can be performed either in osmotic dilution mode as a stand-alone process or as a pre-treatment in hybrid systems [40] (Figure 2.22).

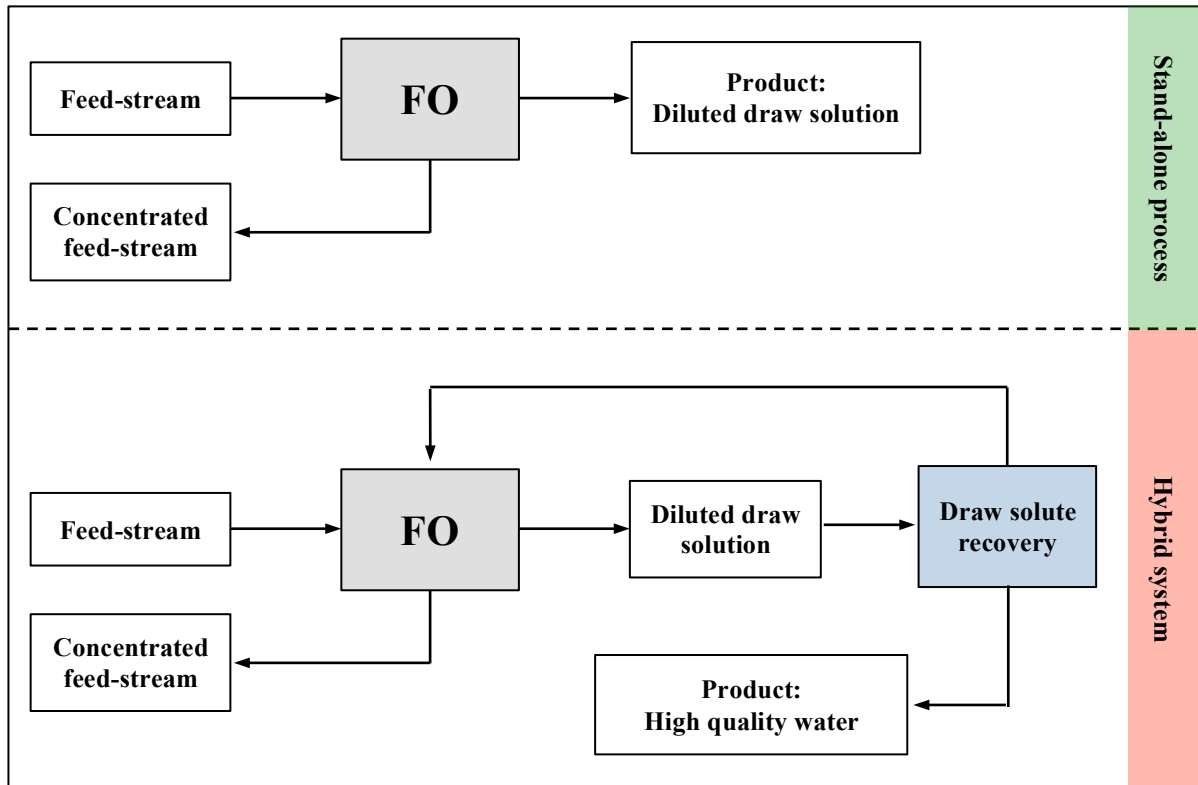


Figure 2.22: FO operation modes: osmotic dilution and pre-treatment modes.

In those applications where high quality products are not required, forward osmosis can be used in the osmotic-dilution mode as a stand-alone process, thus obtaining a dilute draw solution without any further reconcentration step. However, when high quality water is required, FO is used as a pre-treatment in a hybrid system [40].

In the latter case, FO is generally coupled with RO or distillation systems. Water first diffuses across the membrane and dilutes the draw solution due to FO pre-treatment. Then the draw solution is recovered for future FO reuses and high quality water is produced.

Among all the industrial applications, FO has been widely studied as a potential pre-treatment for sea-water desalination. McCutcheon et al. [27] described a hybrid desalination system using thermolytic draw solutes that can be easily recovered by heating. Khaydarov et al. [52] proposed a novel desalination hybrid system using solar power to recover the draw solution and produce high quality water. Other studies reported the possibility of using hybrid system FO-RO or FO-NF/UF. The great advantages of using FO as a pre-treatment include reduced fouling in the second step, lower energy input and no need of any chemical pre-treatment [5].

McCutcheon, Elimelech et al. [26] described a novel hybrid system for sea-water desalination, using an ammonia-carbon dioxide draw solution. First, seawater crosses the membrane diluting the ammonia-based draw solution. Then, the draw solution is recovered by column or membrane distillation processes.

However, despite all the potential advantages related to FO process, the lack of both high performance membranes and easily recoverable draw solution limits the industrialization of FO processes at a large scale.

2.4 Aim of the thesis and study objectives

The purpose of this thesis is the design of tailored membranes for forward osmosis applications.

According to previous studies reported in literature, thin-film composite (TFC) membranes seem to be the optimal choice because they can be custom-tailored. These membranes consist of an ultrathin selective polyamide layer on top of a porous support substrate that can be modified independently. The traditional substrate layers are fabricated from polysulfone. This polymer presents a high thermal and mechanical stability but is rather hydrophobic. Recent studies have shown that the increase in membrane hydrophilicity through the use of sulfonated polysulfone could improve the FO performance.

Therefore, the primary objectives of this work are to:

- prepare sulfonated polysulfones with different degrees of sulfonation
- fabricate sulfonated polysulfone (SPSU) membrane substrates
- prepare TFC membranes by synthesising a polyamide active layer onto the sulfonated substrates *via* interfacial polymerization
- evaluate membranes performance

3 Materials and methods

The experimental work is focused on the fabrication and characterization of thin-film composite membranes (TFC). These are made of three different layers as illustrated in Figure 3.1: an ultrathin, highly selective and nonporous superficial skin layer made of aromatic cross-linked polyamide (PA); a porous sulfonated-polysulfone (SPSU) middle layer formed on the top of a macroporous polyethylenetereftalate (PET) fabric providing the necessary mechanical strength to the membrane structure.



Figure 3.1: Schematic representation of a TFC membrane structure.

This chapter is first focused on synthesis of sulfonated polysulfone and its properties. Then, fabrication method of TFC membranes is described by dividing it into two consecutive steps: 1) fabrication of the support midlayer via UV-curing followed by non-solvent induced phase separation (NIPS) and 2) realization of the skin layer by interfacial polymerization.

In the second part of this section, different characterization techniques used to investigate the sulfonated polysulfone properties are discussed. These include thermogravimetric analysis (TGA), differential scanning calorimetry (DSC) and infrared spectroscopy (ATR-FTIR).

Membrane characterization is also illustrated in details. Namely, the different support SPSU layers have been investigated in terms of permeance and selectivity by using a lab-scale stirred dead-end system, whereas contact angle and cloud point measurements have been used to study their hydrophilicity. Then, the water permeance and the salt permeability constant of the TFC membranes were tested by using a FO lab-scale system.

3.1 Polysulfone (PSU) and sulfonated polysulfone (SPSU) properties

Polysulfone (PSU) belongs to a family of thermoplastics with high thermal stability, good mechanical properties, and excellent chemical resistance [53]. These properties, along with their commercial availability, make polysulfone one of the most widely used materials for membrane preparation. The chemical structure of polysulfone is illustrated in Figure 3.2.

PSU is typically used for the fabrication of asymmetric ultrafiltration membranes [54], and it is also widely used for the preparation of the support layer of TFC membranes for RO and

FO. Furthermore, unlike polyamide, polysulfone matrix is tolerant to aqueous chlorine over a broad range of pH values [55], making it suitable for the applications where the feed treatment or the membrane regeneration requires dissolved chlorine. Nowadays, various polysulfones are available on the market [56-57], having a slightly different structure and a molecular weight.

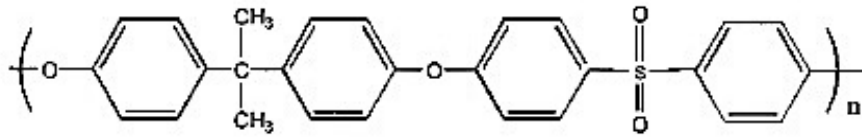


Figure 3.2 Chemical structure of PSU.

The Table 3.1 sums up the most important properties of this polymer.

Table 3.1: Key properties of polysulfone.

PSU
Amorphous structure with a glass transition of $\approx 185^{\circ}\text{C}$
Continuous Usage Temperature of $\approx 150^{\circ}\text{C}$
Heat Distortion Temperature of $\approx 175^{\circ}\text{C}$
Degradation temperature of 500°C
Excellent hydrolysis resistance
Broad chemical resistance
Limited weatherability and marginal UV resistance
High resistance to β , γ or X-rays and low microwave absorbance

However, polysulfone is also quite hydrophobic which results in low water flux through membrane pores. Therefore, the chemical structure of polysulfone has to be modified in order to improve its overall hydrophilicity and other properties. This can be achieved through addition of hydrophilic segments into the polysulfone backbone [58-59] or by introducing hydrophilic groups via photopolymerization or adsorption processes [60]. When the resulting polymer is used for membrane fabrication, its hydrophilic nature promotes wetting and mass transfer, resulting in higher water flux. Also, several studies [5-44-57] have reported a significant change in membrane morphology when modified polysulfone is employed.

As regards the addition of hydrophilic segments into the polymer backbone, one of the most widely used functional groups is represented by sulfonic acid ($-\text{SO}_3\text{H}$). The polysulfone can be easily functionalized by a variety of sulfonating agents via an electrophilic substitution reaction. The first sulfonation was reported in the patent literature by Quentin [61] who employed chlorosulfonic to introduce $-\text{SO}_3\text{H}$ groups along the commercially available polymer known as Udel® (Solvay Advanced Polymers). Although still in use [62-63], chlorosulfonic acid causes undesirable side reactions, such as chain scission, branching and/or cross-linking.

Several researchers utilized oleum (SO_3 dissolved in pure sulfuric acid) or sulfuric acid (98 wt. %), which could be used as both reactant and solvent [56-64-65]. When the latter is employed, polymer degradation equally occurs, making it difficult to control sulfonation

levels and to maintain good mechanical properties in the final product [66]. Others [67] have successfully employed mild sulfonation agents, such as trimethylsilyl chlorosulfonate, in order to minimize chain scissions. This method was therefore adopted in the present work. The chemical structure of sulfonated polysulfone is illustrated in Figure 3.3.

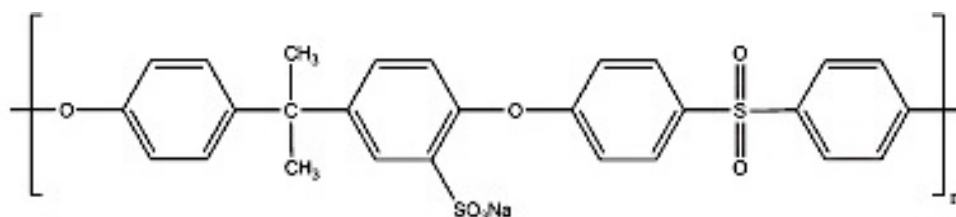


Figure 3.3: Chemical structure of sulfonated polysulfone.

3.2 Synthesis of SPSU

Synthesis of sulfonated polysulfone consists in the incorporation of sulfonate groups into the backbone of the polymer. The sulfonation procedure is illustrated in Figure 3.4.

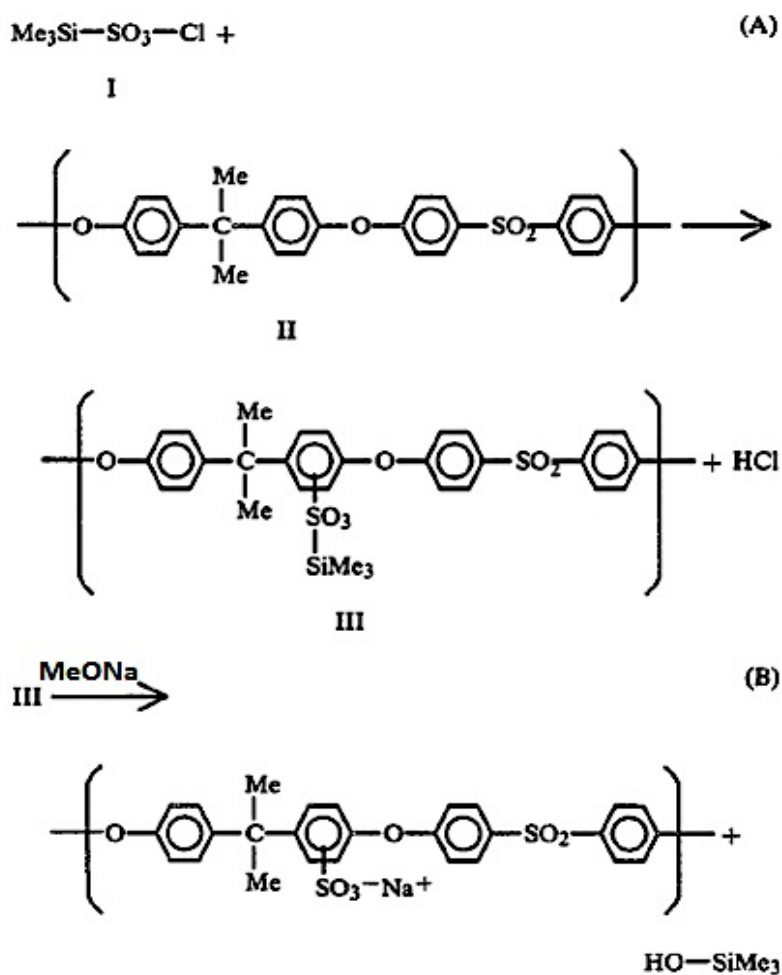


Figure 3.4: Schematic representation of the sulfonation procedure of a PSU unit using trimethylsilyl chlorosulfonate as sulfonating agent (Me indicates a methyl group).

As can be seen in the Figure 3.4, the first step of the reaction (A) consists in the electrophilic aromatic substitution of polysulfone (II) by means of trimethylsilyly chlorosulfonate (I). This leads to the formation of an intermediate (III), silyl sulfonate polysulfone, with concomitant release of a certain amount of HCl.

The intermediate is subsequently treated with sodium methoxide (MeONa), thus promoting basic hydrolysis of the silyl sulfonate bond and yielding the sulfonated polymer in salt form ($-\text{SO}_3^-\text{Na}^+$), more stable than the acid form (SO_3^-H^+) since it prevents any self-degradation due to the presence of sulfonic acid groups.

The polysulfone ($M_n \sim 22\,000$ g/mol) beads were first dissolved in dichloromethane (10% w/v) inside a three-neck round-bottom flask at room temperature as can be seen in Figure 3.5. The synthesis was performed under inert atmosphere as the presence of oxygen and water vapor can negatively interfere with the overall sulfonation process. The steady nitrogen flow was doubly useful since it removed HCl effluents formed during the substitution reaction. The necessary amount of trimethylsilyl chlorosulfonate was dissolved in 10-15 mL of dichloromethane and then added dropwise to the reaction mixture by means of a dropping funnel.

The reaction was left to proceed under continuous stirring for 24 hours. At this point, the cleavage of the silyl groups was obtained by adding a 15% w/w sodium methoxide/methanol solution to the reaction medium. The resin salt solution was then decanted into a nonsolvent bath of methanol (5:1 ratio by vol.), yielding a white precipitate isolated by filtration. The latter was washed several times with methanol and DI water and dried in an oven for 24 h at 105 °C.

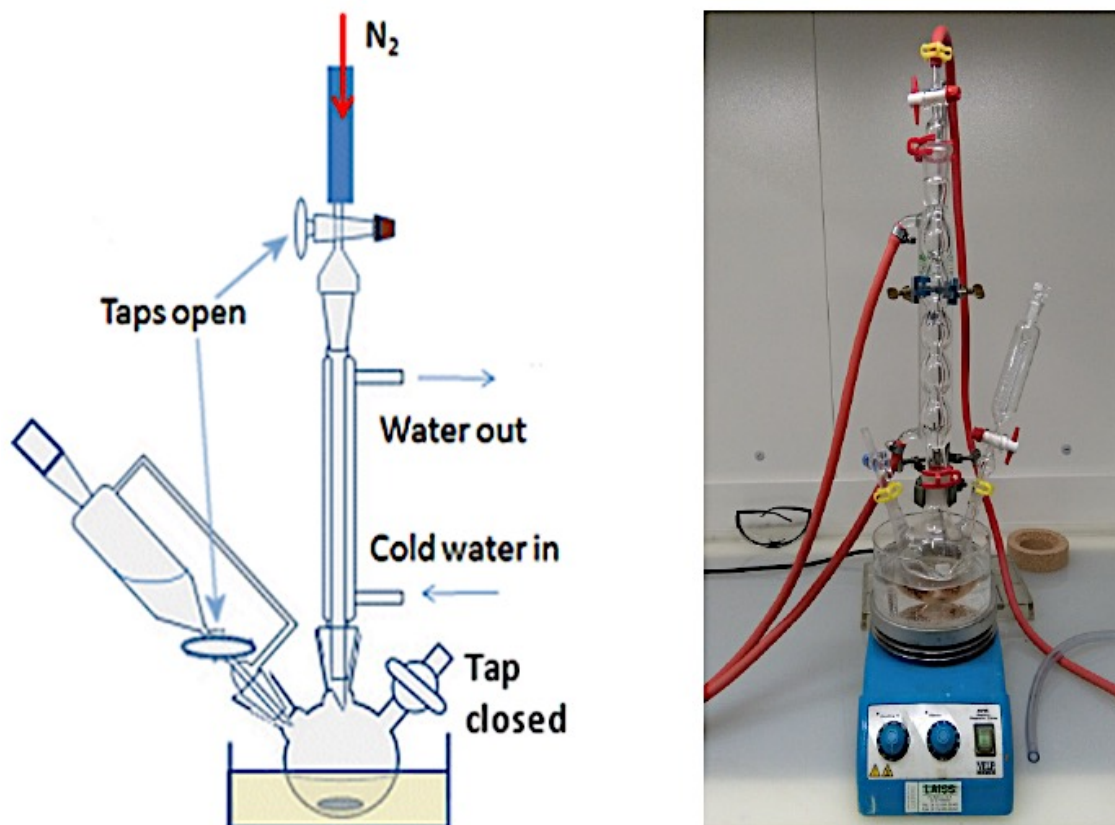


Figure 3.5: Synthesis set-up consisting of a three-neck round bottom flask equipped with mechanical stirrer, reflux condenser and nitrogen inlet.

The molar ratio of trimethylsilyl chlorosulfonate to polysulfone repeat unit has been specifically adjusted to achieve the desired degree of sulfonation, i.e the number of polymer repeat units which have been functionalized with a $\text{SO}_3^- \text{Na}^+$ group.

A number of differently functionalised polymers have been synthesised, by varying the molar ratio between trimethylsilyl chlorosulfonate (TMSCS) and polysulfone (PSU) repeat unit. Namely, the ratio of mole TMSCS/mole repeat unit has been set to 0.10, 0.25 and 0.50; the sample names have been assigned accordingly (Table 3.2, where SPSU stands for sulfonated polysulfone).

Table 3.2: List of the synthesized sulfonated polysulfone samples. The name has been assigned according to the theoretical degree of sulfonation.

Sample name	Mole TMSCS/mole repeat unit
SPSU_0.10	0.10
SPSU_0.25	0.25
SPSU_0.50	0.50

3.3 Fabrication of the SPSU-based membrane substrates

The first step of the fabrication of TFC membranes was the realization of the SPSU based asymmetric support layer on the top of the macroporous reinforcing mesh made of PET.

Asymmetric membranes are usually prepared via phase separation, typically NIPS [1-11-14-68]. In our case, a cross-linking step was added in order to improve the mechanical properties. In other words, the SPSU porous support layer was fabricated by a two-step method involving UV-curing followed by the traditional non-solvent induced phase separation [69-70]. The overall fabrication protocol can be divided into five main operations. Namely, 1) casting solution preparation, 2) casting plate preparation 3) casting solution deposition by means of a special casting blade, 4) irradiation of the as-cast polymeric film under a UV-curing flood lamp to achieve cross-linking and 5) immersion into DI water bath to induce the non-solvent induced phase separation. All these steps will be described in detail in the following sections. The schematic fabrication procedure is illustrated in Figure 3.6.

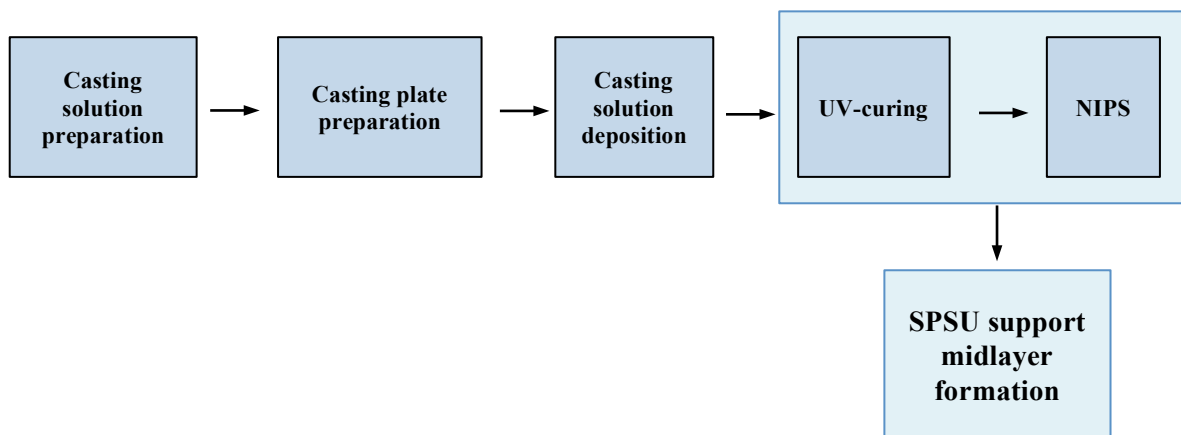


Figure 3.6: Complete fabrication protocol of the fabrication of the sulfonated support layer.

3.3.1 Casting solution preparation

Three types of sulfonated polysulfone with different degrees of sulfonation were used for the preparation of the support midlayers. For this purpose, 12% wt.% dope solutions of pure SPSU_0,10, of SPSU_0,25 blended with PSU in a 1:1 molar ratio and of SPSU_0,50/PSU 3:7 (in weight) were dissolved in N-methyl-2-pyrrolidone (NMP, anhydrous, 99.5%). The blended solutions were prepared in order to induce phase separation and prevent swelling of the sulfonated polymers [45].

The solutions were stirred continuously at room temperature for 6 hours to achieve the complete dissolution of the polymer and then left to stand in a desiccator overnight to allow the release of air bubbles. At this point, the solution was degassed in a vacuum-bell for 10 minutes using a vacuum pump MV20A (capacity 20 m³/h, final vacuum of 0.7 mbar).

In order to proceed with the UV-curing step, poly (ethylene glycol) diacrylate (PEGDA; M_n = 700 g/mol), acting as cross-linker) and the photoinitiator (phenylbis(2,4,6-trimethylbenzoyl)phosphine oxide) were added to the casting solution. The different formulations are summarized in the Table 3.3.

Table 3.3: Composition of the membrane support layers casting solutions.

Membranes	%wt	SPSU (%)	PSU (%)	PEGDA (%)	Photoinitiator (%)
SPSU_0,10	12	100	0	15	3
SPSU_0,25/PSU	12	50	50	10	3
SPSU_0,50/PSU	12	30	70	10	3

The percentage of PEGDA is referred to the total quantity of the casting solution (Equation 3.1), whereas the photoinitiator was always used at 3 wt.% and is referred to the quantity of the acrylic cross-linker:

$$\text{PEGDA}_{\text{wt}\%} = \frac{\text{PEGDA weight}}{\text{PEGDA weight} + \text{CASTING SOLUTION weight}} \times 100\% \quad (3.1)$$

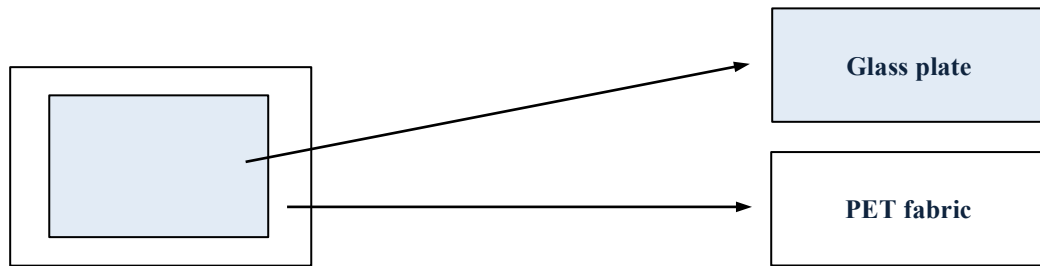
The cross-linker was added to the casting solution, which was stirred for 5 minutes. In a second step, the precise amount of photoinitiator was added to the solution that was stirred again for 5 min and then it was left to stand for another 5 min.

3.3.2 Casting plate preparation

The casting solution was cast on a PET macroporous fabric fixed on top of a glass plate by means of the water-resistant Fisherbrand[®] adhesive tape, allowing the PET fabric to remain in contact with the glass plate during the phase inversion process. This polyester mesh was employed as a reinforced fabric for the SPSU-based substrate, which exhibits poor mechanical strength if used alone. This is most likely due to water absorption by sulfonated groups resulting in polymer swelling and thus decreasing the resistance of the substrate layer [47-72].

The attachment of PET fabric on the glass plate was obtained as follows:

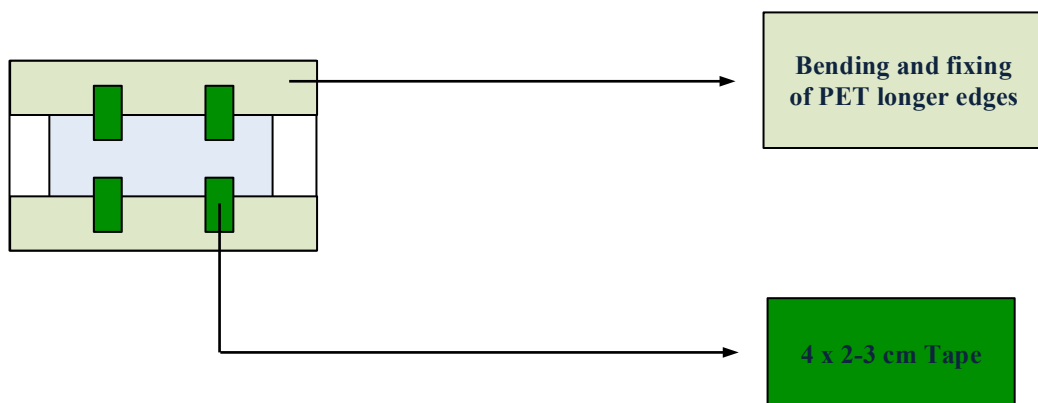
1. The PET fabric was cut out with slightly higher size with respect to that of the glass plate.



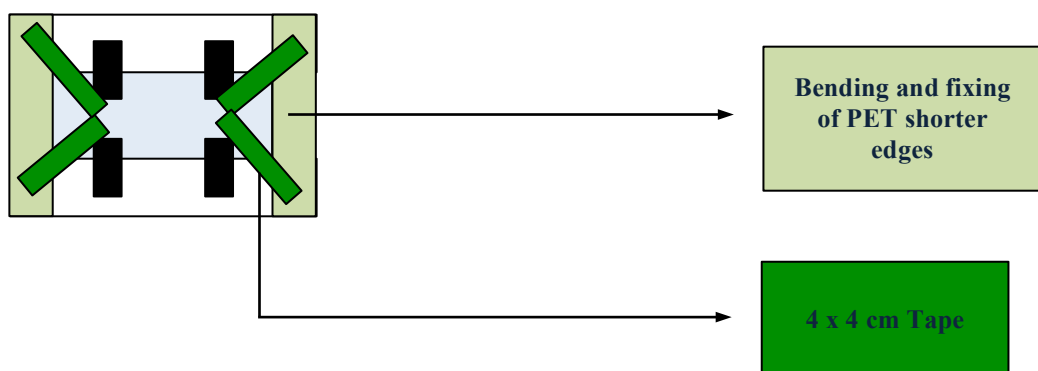
2. The adhesive tape was cut in several stripes as described below:

- 6 x 2-3 cm
- 4 x 4 cm
- 2 x 10 cm

3. The longer edges of the PET fabric were bended and fixed to of the glass plate with 4 x 2-3 cm stripes of the tape trying to avoid the formation of wrinkles and creases of PET.



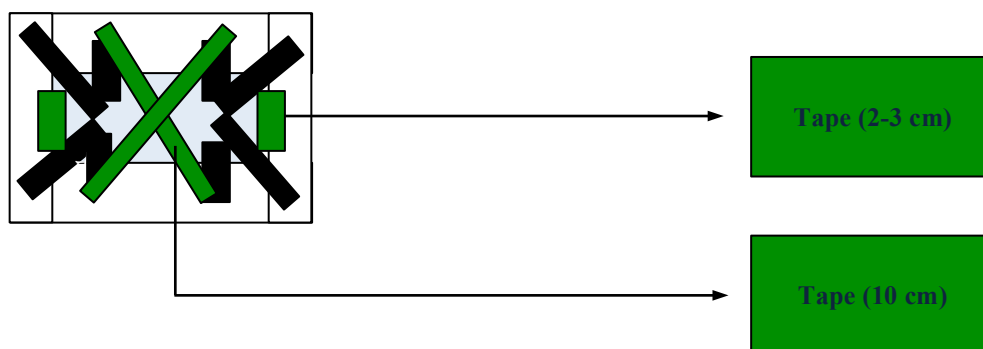
4. The shorter edges of the PET fabrics were bended and fixed to the backside of the glass plate with 4 x 4 cm tape stripes positioned diagonally. This step is more critical than the previous because the formation of creases at the corners is more frequent.



5. PET fabric was fixed to the back side of the glass plate with four more tape stripes:

- 2 x 2-3 cm stripes were positioned between the previous diagonal stripes that fixed the shorter edges

- 2 x 10 cm stripes forming an X as illustrated in the scheme below



6. The casting plate thus formed (Figure 3.7) was checked for the presence of creases and folds. The corner areas are more prone to the defect formation, which could lead to tape detachment during phase inversion (Chapter 3.3.5).

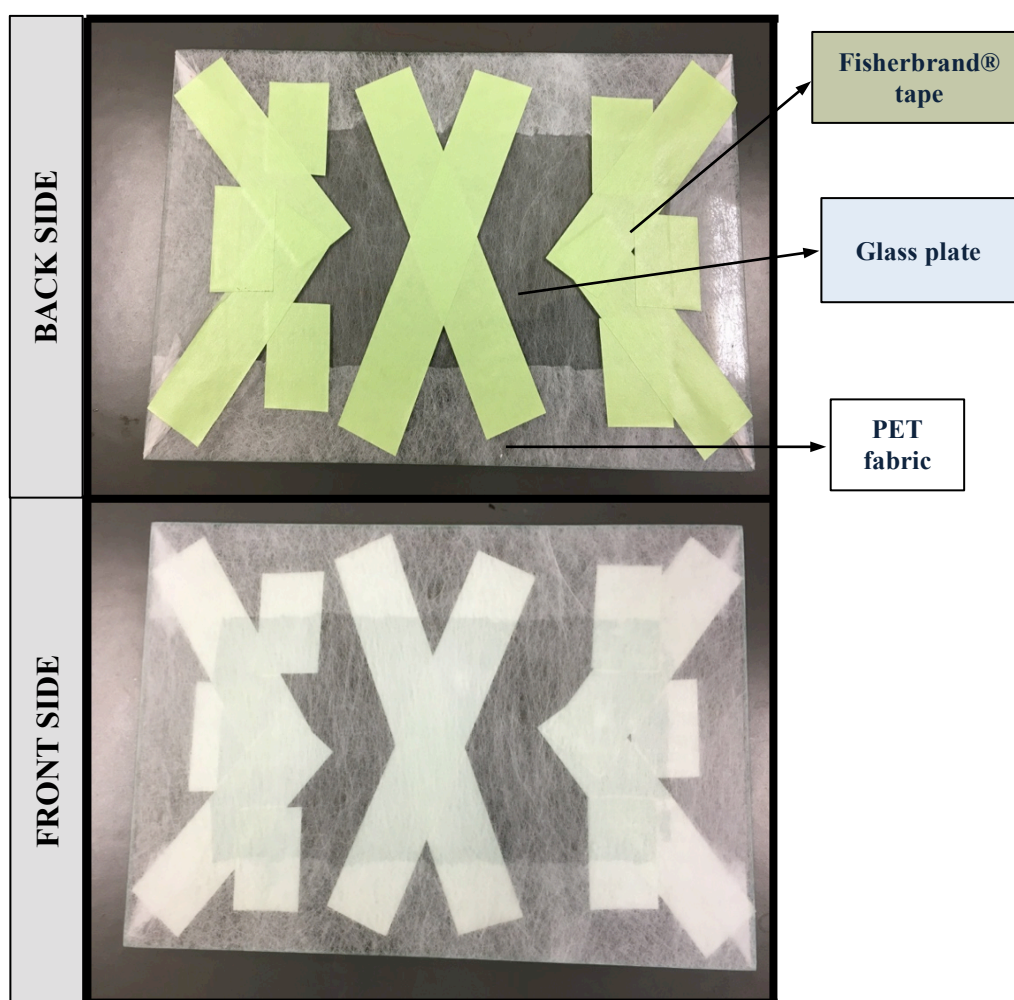


Figure 3.7: Casting support consisting of a glass plate covered by a PET fabric fixed onto its surface by means of a water-resistant adhesive tape.

3.3.3 Casting solution deposition

Once the casting plates were ready, it was possible to proceed with polymer solution deposition. For this purpose, the PET fabric was uniformly wetted by dropwise deposition of NMP. The polymer solution was then poured onto a small area of the top region of the plate and cast using a Gardco Microm II [11] hand-held film casting knife (Figure 3.8).

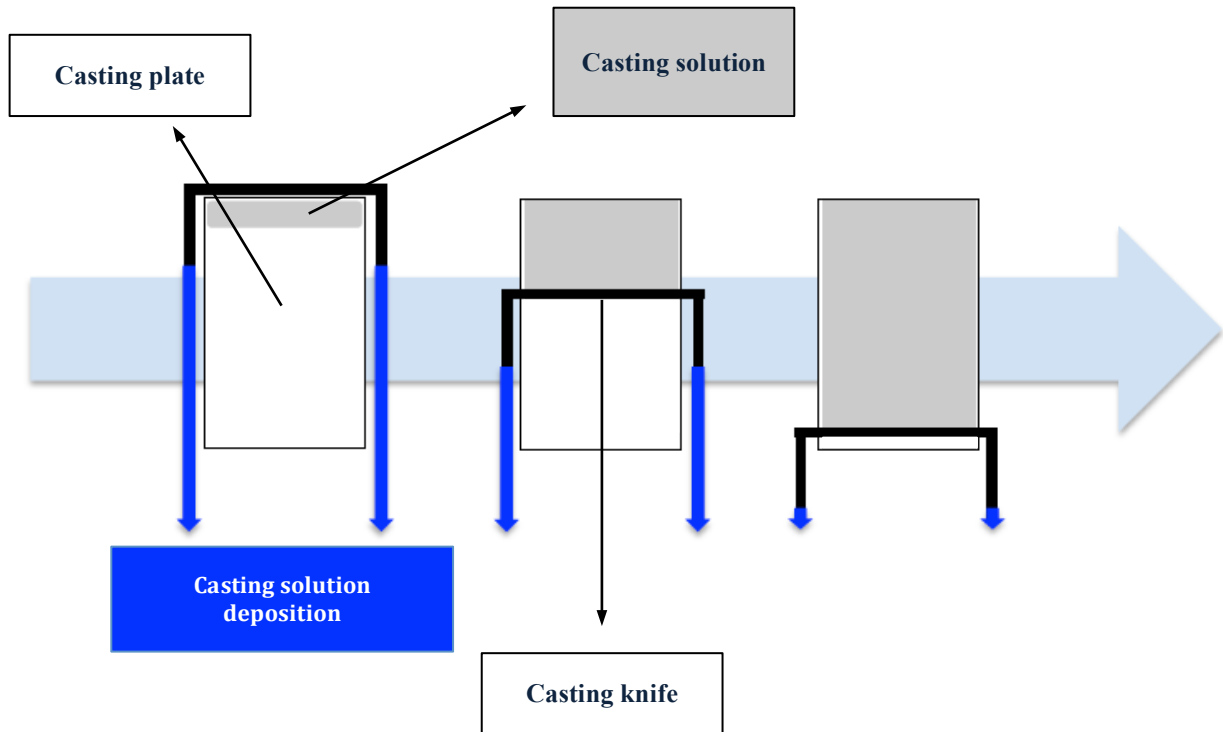


Figure 3.8: Schematic representation of the casting solution deposition by means of a hand-held film casting knife.

Gardco Microm II film casting knife, Figure 3.9, consists of a steel blade, two micrometers connected to the blade and an anodized frame with two end plates used by the operator to perform the deposition process. The micrometers are in contact with the upper edge of the blade, allowing it to be manually adjusted in order to set the gap between the blade and the casting plate, thus obtaining the membrane nominal thickness requested.



Figure 3.9: Gardco Microm II film casting knife.

Following this procedure, membrane films of SPSU_0.10, SPSU_0.25/PSU 50:50 and SPSU_0.50/PSU 30:70 were cast with a 150 μm nominal thickness.

3.3.4 UV - curing

As mentioned in chapter 3.3, a cross-linking step is required in order to improve the mechanical resistance of the SPSU membranes [47-73-74]. For this purpose, a difunctional acrylate (poly (ethylene glycol) diacrylate, PEGDA) and an acyl phosphine-type photoinitiator (phenylbis(2,4,6-trimethylbenzoyl)phosphine oxide) were added to the polymer dope prior to casting. Under UV-irradiation, phenylbis(2,4,6-trimethylbenzoyl)phosphine oxide photogenerates a radical initiator, setting off the chain-grow polymerization on the methacrylic double bond of PEGDA which leads to the formation of a cross-linked network (Figure 3.10) which entraps the sulfonated polysulfone.

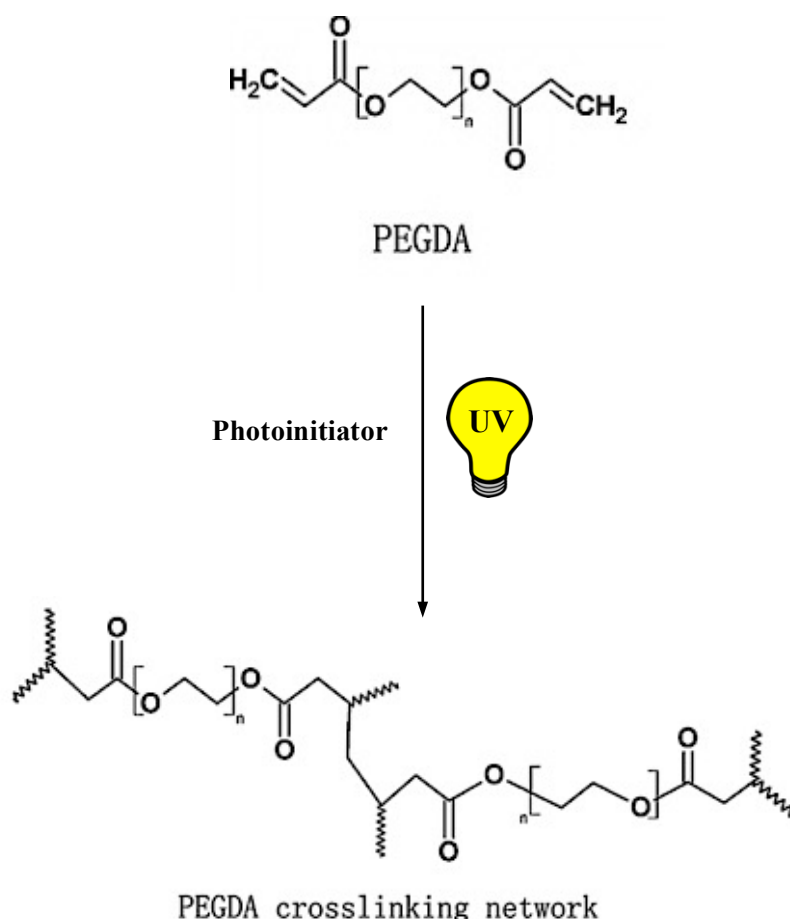


Figure 3.10: Formation of PEGDA cross-linked network.

Therefore, the SPSU porous support layers are produced by a two-steps method involving UV-curing and non-solvent induced phase separation (NIPS). Previous studies [73-74] have reported considerations about the influence on the performance of membranes based on polysulfones subjected to a two-step fabrication protocol including UV-curing and NIPS. They performed the curing step after the phase separation.

However, experimental evidences from more recent investigations [69-70] have shown the advantages of performing the photo-crosslinking step before the phase inversion in the coagulation bath: membranes were more stable and have a more uniform pores distribution. Accordingly, it was decided to follow this protocol (Figure 3.11).

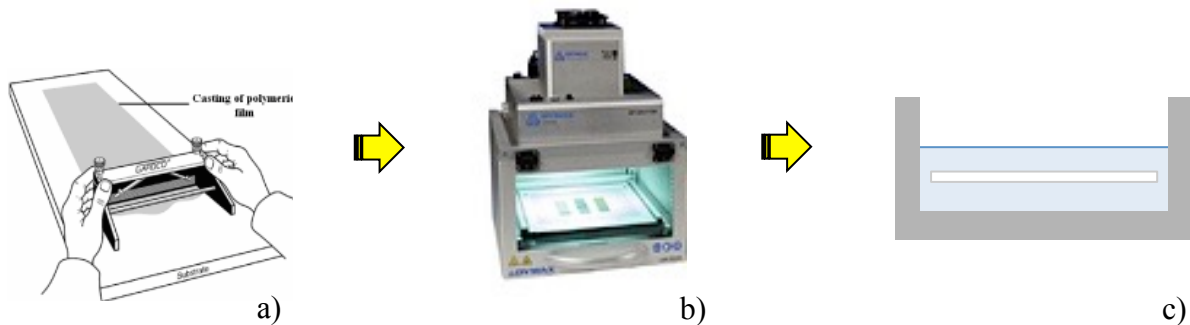


Figure 3.11: Representation of the experimental protocol selected for the realization of the support layer. After the deposition of the casting solution (a), the polymer is subjected to a photo-curing process (b) followed by NIPS (c).

Experimentally, cross-linking was achieved by irradiating the as-cast polymer films for 1 min under a Dymax ECE 5000-UV lamp, whose radiation peak is in the specific UVA-light range 320-390 nm, which is compatible with the absorption range of bis(2,4,6-trimethylbenzoyl)phenylphosphineoxide (350-450 nm).

The energy dose given for the curing process is fixed to 10.5 J/cm^2 . In order to guarantee the repeatability of the curing procedure, this value is periodically checked by means of the ACCU-CALTM 150 radiometer.

3.3.5 NIPS

According to the established fabrication protocol, the non-solvent induced phase separation was performed after UV-curing [70].

In the NIPS process [11-14] the freshly cast polymer film is quickly immersed into a coagulation bath containing a non-solvent (typically water), where an exchange of solvent and non-solvent takes place: the solvent moves from the solution to the coagulation bath, whereas the non-solvent moves towards the polymer solution leading to the formation of the porous membrane (Chapter 2.3.7).

Experimentally, once the UV-curing is over, the casting plate is immediately immersed into deionized (DI) water coagulation bath for 10 min at room temperature. Then the plate is moved into a second DI water bath and left there for 24 h to complete the phase-inversion process. It is possible to visually follow the phase separation by noting a colour shift of the casting solution film from transparent to white.

The experimental set-up is illustrated schematically in Figure 3.12.

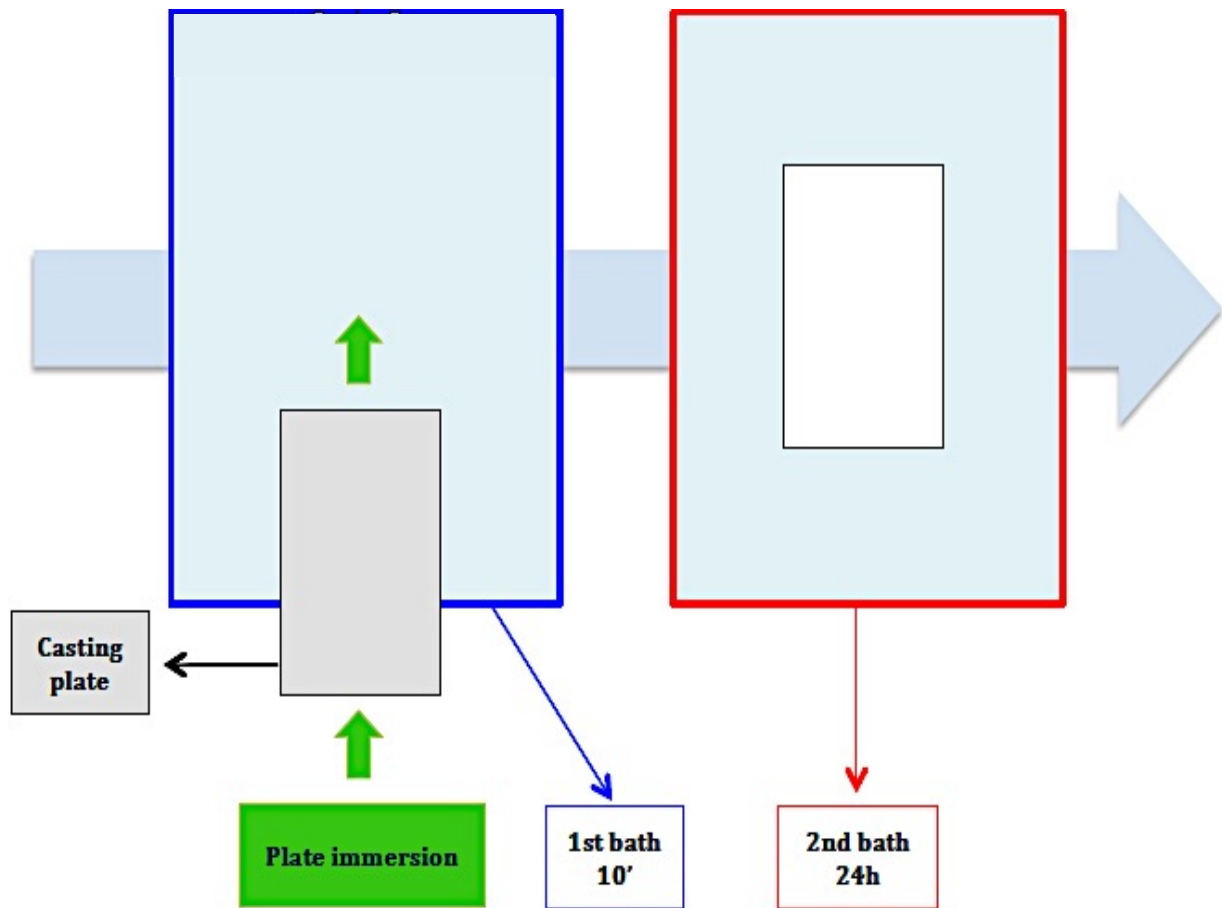


Figure 3.12: Laboratory-scale NIPS set-up.

Figure 3.13 illustrates a DI water coagulation bath containing membranes just immersed to complete the phase-inversion process.



Figure 3.13: Membranes immersed in the coagulation bath.

Twenty-four hours later, the casting plates were removed from the coagulation bath, cut along the corners (Figure 3.14) and stored in DI water until further use.

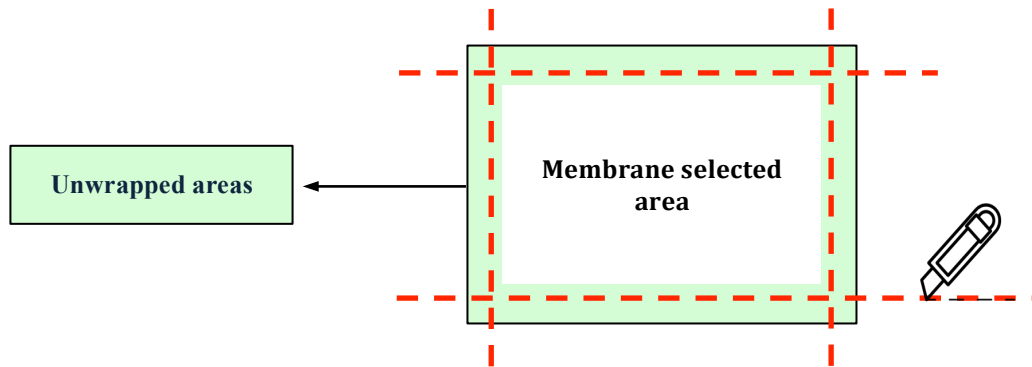


Figure 3.14: Removal of the corner areas of the membrane.

3.4 Polyamide active layer formation *via* interfacial polymerization

The final step in the fabrication of TFC membranes (Figure 3.15) consists in the synthesis of the active polyamide (PA) layer on substrate surface via *in-situ* interfacial polymerization (IP) [11-75-76].

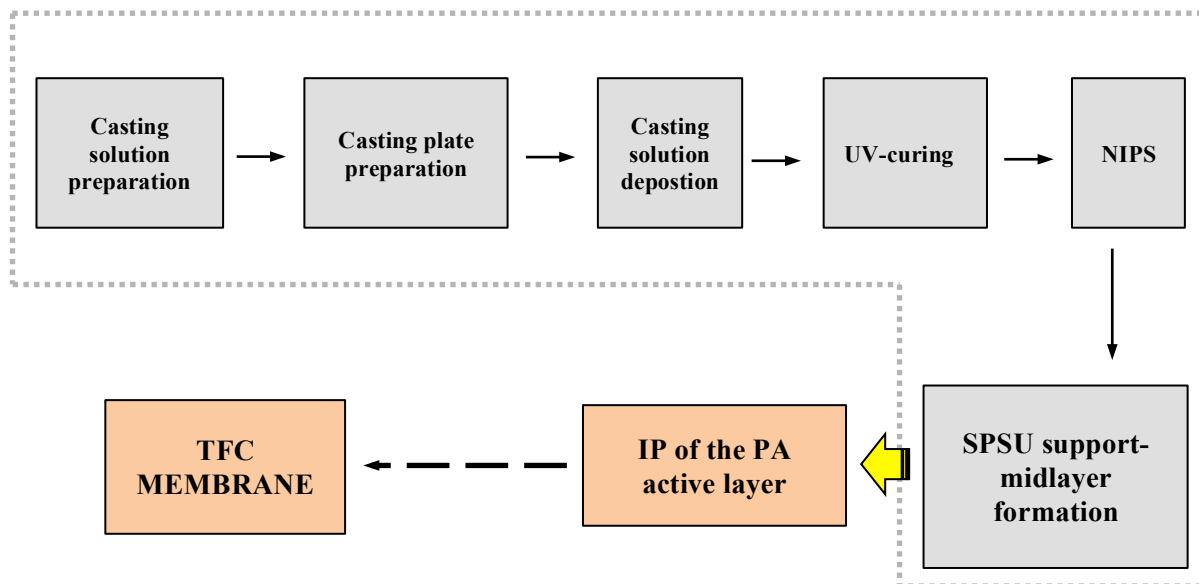


Figure 3.15: Schematic illustration of the complete fabrication process of TFC membranes including the final IP step.

Interfacial Polymerization, introduced by John Cadotte at FilmTec in 1981 and then developed at North Starch Research [77-78], consists of a multi-steps process aimed to the fabrication of an ultrathin and cross-linked PA layer characterized by high selectivity (Chapter 2.3.8). According to the traditional IP procedure, a polyamine solution is prepared and cast onto a microporous support layer that is generally an ultrafiltration membrane made

of polysulfone. Afterwards, the polymer support coated by the amine solution is immersed in an acyl solution where the amine and the acyl chloride react at the interface generating the cross-linked amide layer (Figure 3.16). The layer thus formed is very dense and selective [11].

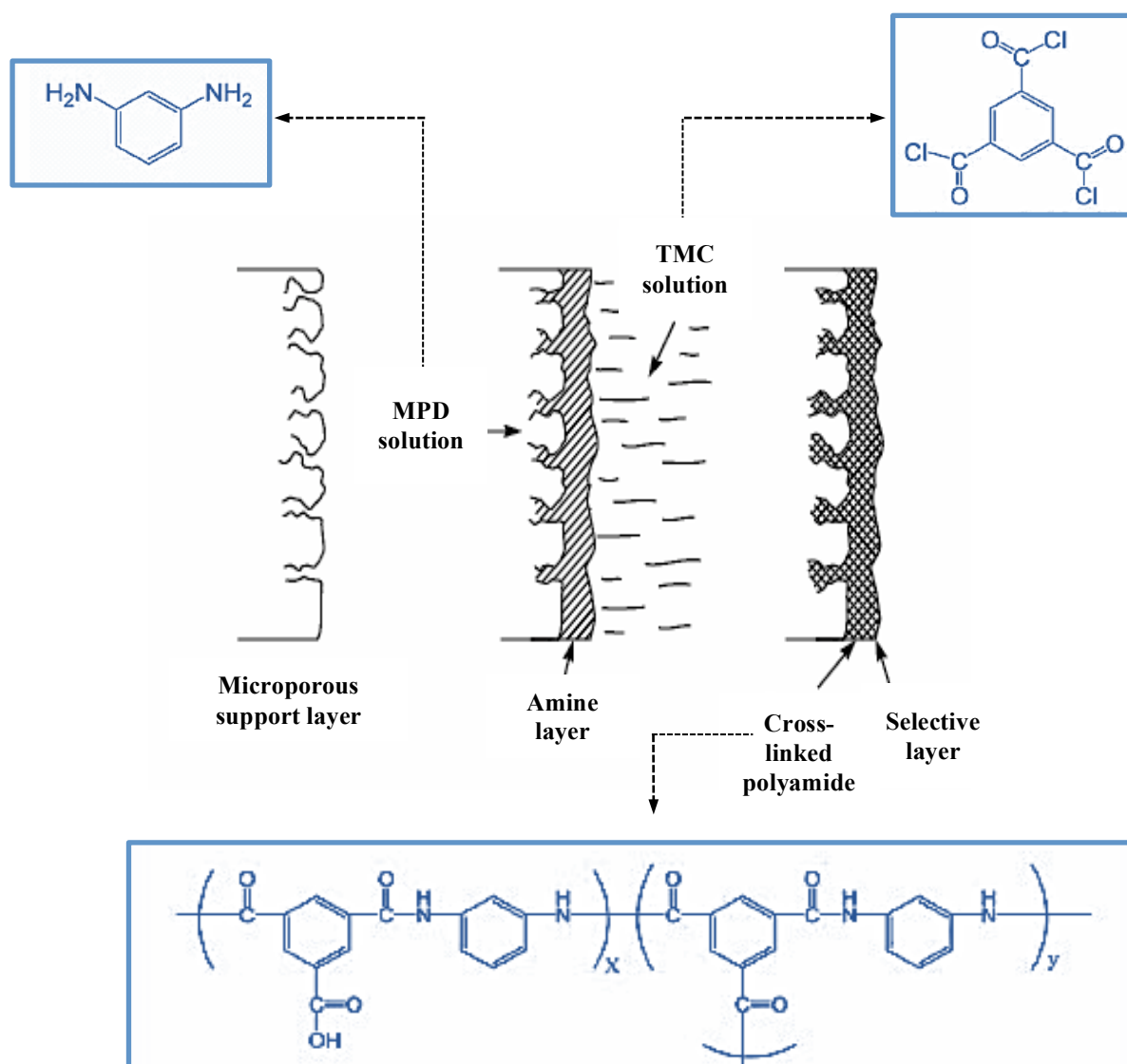


Figure 3.16: Schematic representation of the IP process. The microporous support layer is first immersed into MPD solution and then into a TMC solution to form cross-linked polyamide layer at the interface between the two components.

The experimental protocol used for the fabrication of the polyamide layer consists of two steps: the preparation of the different solution followed by the fabrication of the amide active layer onto the sulfonated substrates.

The polyfunctional amine solution was prepared by dissolving the *m*-phenylenediamine (MPD) in deionized (DI) water with a concentration of 3.4 wt.%. The solution was stirred to complete the dissolution. The polyfunctional acyl solution was prepared by dissolving the benzenetricarbonyl trichloride (TMC) in hydrocarbon solvent through stirring, taking care to avoid the evaporation of the solvent. The concentration of benzenetricarbonyl trichloride in the solution must be the 0.15% in weight.

The sodium hypochlorite bleach-solution (NaOCl) was prepared by adding 13 drops to 500ml of DI water, whereas, sodium metabisulfite solution was dissolved in DI water with a concentration of 1g/l.

The complete fabrication protocol of the PA layer is schematically illustrated in Figure 3.17.

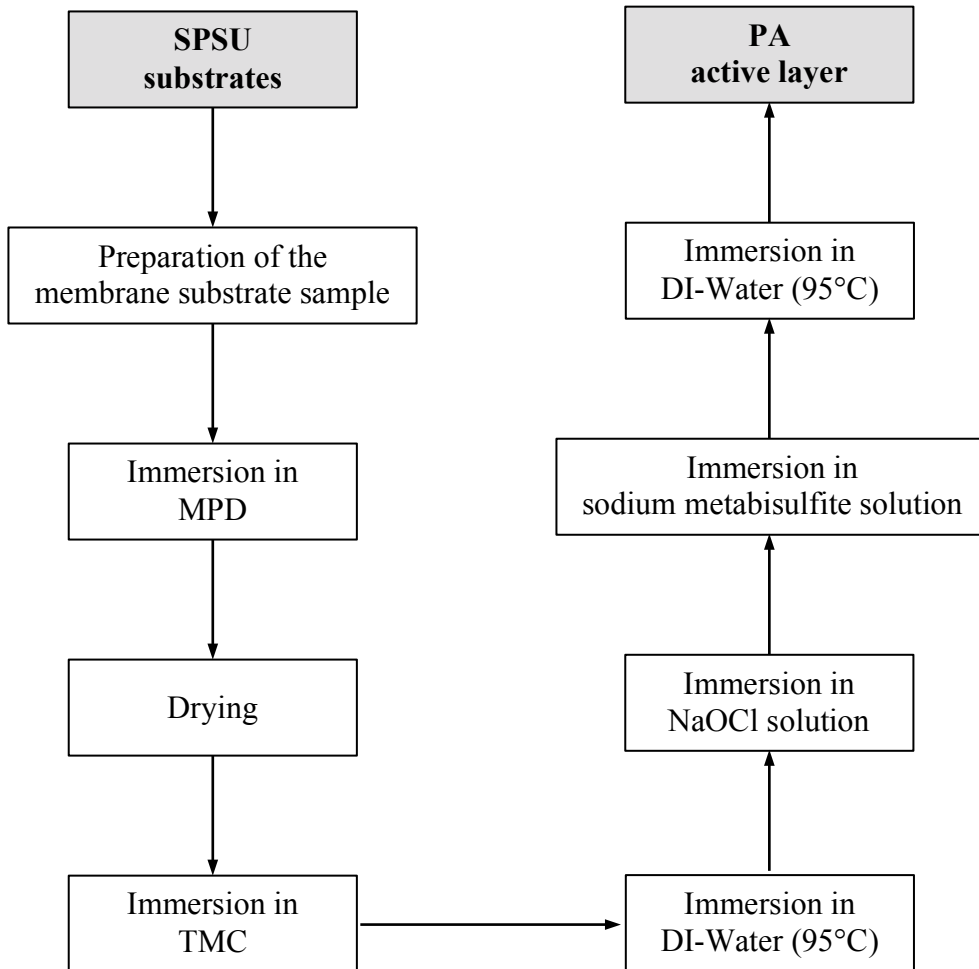


Figure 3.17: Schematic representation of the interfacial polymerization fabrication process.

First, a membrane sample of the support layer with dimensions close to 10x13 cm is cut and attached to the toughened glass (11x14 cm) with 4 stripes of Fisherbrand[®] adhesive tape (2x16cm; 2x19cm) keeping the active layer on top.

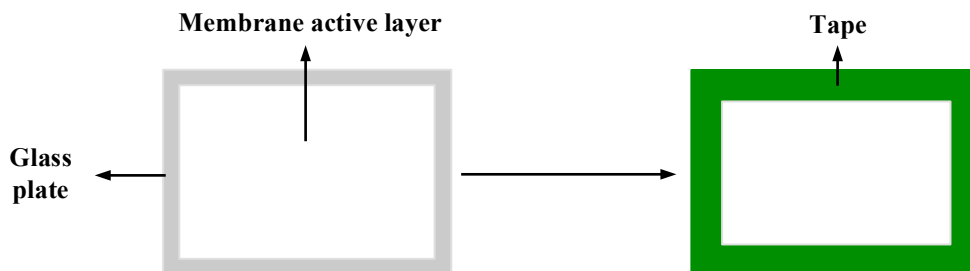


Figure 3.18: Preparation to the membrane sample to be subjected to IP.

The glass with the membrane sample is laid down for 2 minutes in a sloping bath containing the MPD solution. The glass is positioned so that only the active layer of the plate comes in contact with the amine solution (Figure 3.19).

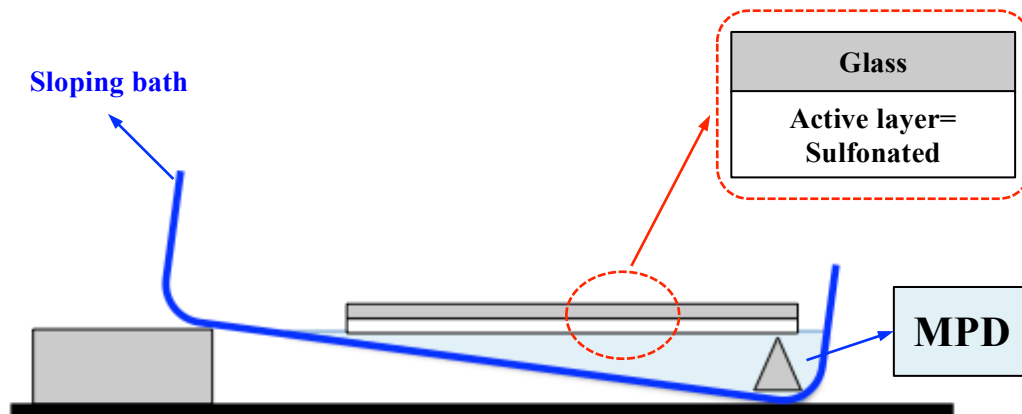


Figure 3.19: Immersion of the glass covered by the membrane sample into a sloping bath containing the polyamine solution.

After removing the plate from the MPD bath, the membrane is dried from the MPD solution in excess with an air gun. Next, the membrane sample is immersed for 1 minute in a bath filled up with the TMC solution. During this step the generation of the polyamide active layer occurs.

Then, the plate is kept outside the TMC solution for 2 minute and subsequently immersed in hot DI water (95 °C) for 2 minutes. The composite membrane thus formed, is removed from the DI-water bath and cut-away from the glass.

Next, the membrane is rinsed for 2 minutes in the NaOCl aqueous solution and then soaked in the sodium metabisulfite for 30 seconds. Membranes are subsequently dunked again in hot DI water (95 °C) for 2 minutes for a final wet curing step. Finally the membranes were washed thoroughly with DI-water before storage in DI-water at 4 °C.

This protocol was followed for the fabrication of TFC membranes starting from all of the support membranes investigated.

3.5 Characterization of sulfonated polymers

The different sulfonated polymers synthesised by varying the molar ratio between trimethylsilyly chlorosulfonate (TMSCS) and polysulfone (PSU) repeat unit were characterized using the following analytical techniques:

- 1 Differential Scanning Calorimetry (DSC)
- 2 Thermogravimetric Analysis (TGA)
- 3 Attenuated total reflection Fourier transform infrared (ATR-FTIR) spectroscopy

3.5.1 Differential scanning calorimetry (DSC)

Differential scanning calorimetry is a thermoanalytical technique used to investigate the response of polymers to heating.

The analysis is carried out in a measurement chamber in which two different crucibles made of alumina or platinum are positioned on top of heaters controlled by a computer.

The first crucible contains the sample (S) whereas the second is empty and is used as a reference (R). A specific software controls the temperature in the chamber and regulates the heating rate. When the sample undergoes a physical transformation, such as phase transitions, it will require more or less heat than the reference to maintain both at the same temperature [79].

This difference in the heat flux versus temperature is recorded and plotted. In the thermogram thus obtained the temperature is given on x-axis whereas the difference in the heat flow is taken on y-axis. Regarding the heat-flow, there is a convention according to which exothermic reaction are characterized by positive peaks.

The following Figure 3.20 shows the working principle of the DSC described above.

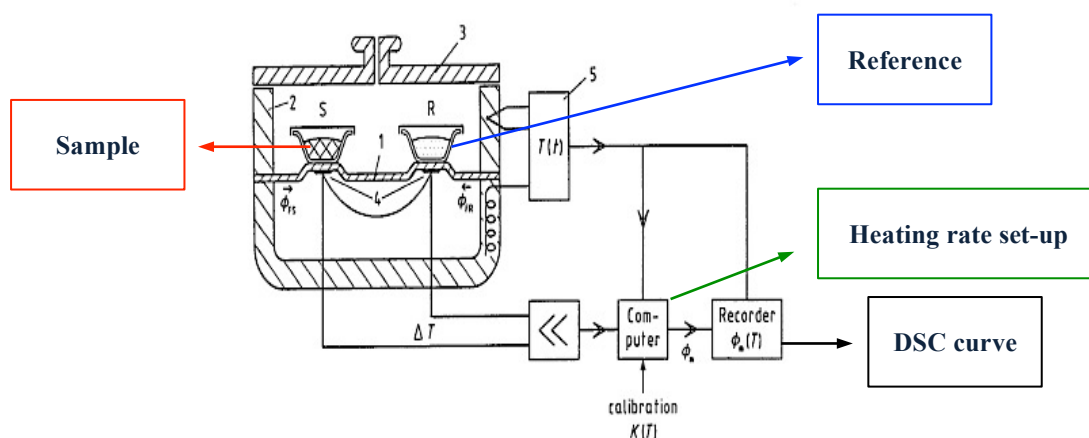


Figure 3.20: Schematic illustration of a Differential Scanning Calorimeter.

This technique gives information about heat capacity, glass transition, crystallization temperature and crystalline percentage, phase transition, thermal stability and melting temperature [79-80].

In this work, DSC was used to study the variation in the glass transition temperature (T_g) of the following sulfonated polysulfones: SPSU_0.10, SPSU_0.25 and SPSU_0.50. The results were compared to that of PSU. The analysis was carried out in the heat-flux configuration, using a Mettler Toledo DSC1 calorimeter.

The experiments were performed at a heating rate of 10 °C/min up to 280 °C under 50 ml/min N_2 atmosphere, using Al-40 μ l crucibles. The recorded data were evaluated using STARe software.

3.5.2 Thermogravimetric analysis (TGA)

TGA is a thermogravimetric analysis in which changes in physical and chemical properties of materials are measured as a function of increasing temperature (constant heating rate), or as a function of time (constant temperature or constant mass loss) [81].

This technique studies materials mass change caused by different thermal events, such as oxidation, reduction, degradation and decomposition, allowing to evaluate the thermal stability of a specific material subjected to a specific heating rate under a controlled atmosphere.

The analysis is carried out in a measurement chamber (Figure 3.21) where a sample inserted into a thermo-resistant crucible is positioned on an electronic micro-thermobalance. The temperature inside the chamber is controlled by thermocouples.

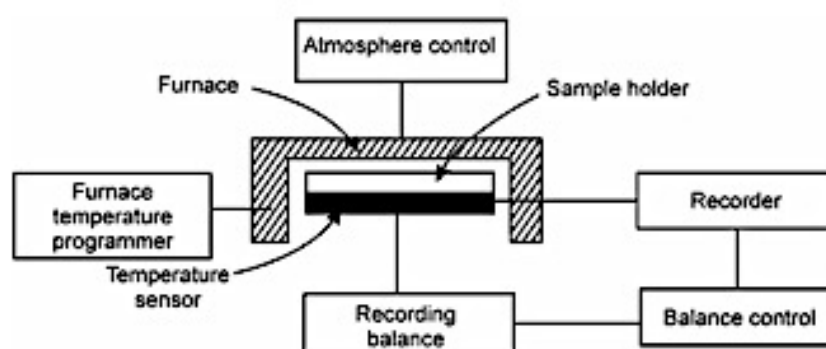


Figure 3.21: Working principle of a TGA analyzer.

The crucible can be made of alumina, quartz, platinum, graphite, glass or stainless steel and should resist to temperatures that are at least 100 K greater than the temperature reached in the experiment. Crucibles differ also in terms of geometry and the choice is closely related to the typology of the sample [81-82].

This balance is able to evaluate with extreme precision the weight loss of the sample during the heating rate and is connected to a software that records the weight variations and extrapolates a graph. The experimental results are presented as *thermogram* plotting the mass change versus temperature [81].

In the present work, the thermogravimetric analysis was used to investigate the thermal behaviour of sulfonated polymers (SPSU_0.10, SPSU_0.25 and SPSU_0.50) as compared to that of pristine polysulfone (PSU), with a particular focus on the trend of the weight loss relative to the degradation range of sulfonate groups (270-400 °C).

The tests were performed on a TGA/SDTA851^o analyzer used in dynamic mode.

The sample (10-12 mg) was placed in an alumina crucible and then positioned on the micro-thermobalance. The experiment was run up to 650 °C under 60 ml/min nitrogen flux using a three-step heating rate: 1) an isotherm at 40 °C for 10 min, 2) 40-140 °C at a heating rate of 20 °C/min and 3) 140-650 °C at a heating rate of 10 °C/min. A blank curve was always recorded with the same heating rate before analyzing the sample and then automatically subtracted to the sample curve. The recorded data were evaluated using STARe software.

3.5.3 Attenuated total reflection Fourier transform infrared (ATR-FTIR) spectroscopy

The Fourier Transformation IR Spectroscopy is a well-established spectroscopic technique used to characterize, identify, and quantify substances [83].

The Attenuated Total Reflectance Fourier Transformation IR Spectroscopy (ATR-FTIR) simplifies the analysis because it allows the sample to be examined without any additional preparation required for the traditional FTIR.

The working principle of this technique is schematically illustrated in Figure 3.22.

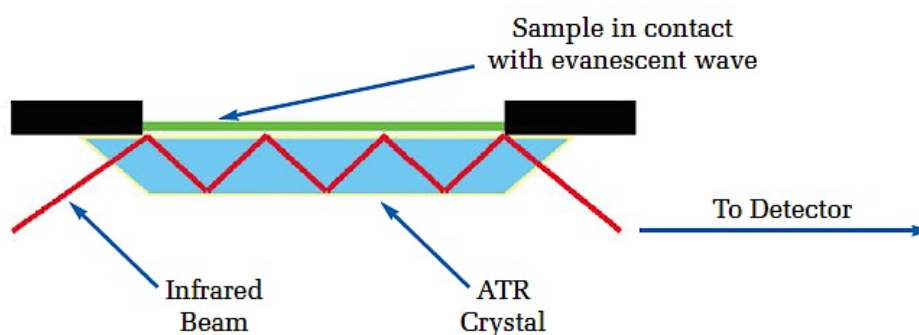


Figure 3.22: Schematic representation of an ATR system.

An IR-beam is first sent with a specific angle onto the surface of a dense crystal (generally a diamond) characterized by high refractive index. Then an evanescent wave generated by the internal reflectance is directed towards the backside of the sample. It penetrates beyond the sample surface for 0.5-5 μm , therefore the sample must be in close contact with the crystal. This wave interacts with the sample and gets attenuated in those IR regions where the sample absorbs energy. These absorption regions are closely related to the chemical structure of a specific substance and can be considered a fingerprint of each functional group of the chemical species [84].

This technique was used after the sulfonation reaction in order to confirm the introduction of sodium sulfonate groups into the polymer backbone.

ATR-FTIR spectra of SPSU_0.10, SPSU_0.25 and SPSU_0.50 were recorded in transmission mode using a Nicolet iS50 FT-IR Spectrometer equipped with ATR diamond crystal accessory (Thermo Scientific, Madison, WI) in the range of 4000-650 cm^{-1} (16 scans with 4 cm^{-1} resolution). A background was recorded before each measurement. The recorded spectra were evaluated using OMNIC software and compared to that of pristine PSU.

3.6 Characterization of the membrane substrates

The sulfonated polysulfone membrane substrates obtained *via* UV-curing+NIPS procedure were characterized in terms of their physicochemical properties. Namely, static contact angle analysis was employed to investigate substrate wettability, whereas turbidity measurements were used to determine the cloud points of the synthesised polymers prior to substrate casting.

Substrate performance was then evaluated in terms of pure water permeance and selectivity, using a stirred-dead end filtration cell and a UV-Spectrophotometer.

3.6.1 Static contact angle measurements

Static contact angle measurements were employed to investigate the wettability of the pristine polysulfone and that of the sulfonated polysulfones. The wettability is an important property in membrane design since, all other parameters being equal, a more hydrophilic membrane would have a higher water flux.

According to the theory by Thomas Young [92], the surface wettability of a material is related to the contact angle of a liquid droplet on the solid surface as expressed in the Equation 3.2:

$$\gamma_{lv}\cos\theta_Y = \gamma_{sv} - \gamma_{sl} \quad (3.2)$$

where γ_{lv} , γ_{sv} and γ_{sl} are respectively the liquid-vapour, solid-vapour and solid-liquid interfacial or surface tension and θ_Y is the contact angle. Small contact angles ($<90^\circ$) mean that the surface is easily wettable and is commonly called *hydrophilic*. On the other hand, when contact angle is higher than 90° , the surface is considered *hydrophobic* or not wettable. [93].

The surface properties of the pristine PSU and that of the SPSU_0.10, SPSU_0.25/PSU 50:50 and SPSU_0.50/PSU 30:70 mixtures was investigated using the Kruss DSA100 drop shape analyzer (DSA) in the sessile drop standard configuration. DSA [62-63] is an imaging method used for the determination of the contact angle, which measures the shadow image of a sessile drop dripped onto the sample surface. First, a drop of a specific volume (μl) is dripped onto the surface of a solid thin film to be tested. Then, once the drop comes in contact with the film, it's lightened and a grey-scale image is captured and elaborated by the drop shape analyzer (Figure 3.22).

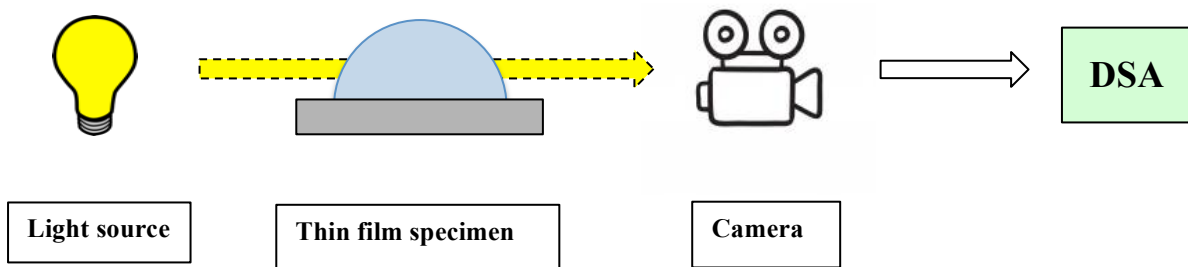


Figure 3.23: Schematic diagram of DSA working principle.

DSA software recognises the drop outline while the operator has to fix the baseline (contact line between the liquid drop and the solid surface). It is possible to select among four different geometrical methods (circle, conic section, polynomial and Young-Laplace method) in order to fit the drop shape and calculate the contact angle (θ) that is the angle measured between the fitted shape line and the detected baseline (Figure 3.24).

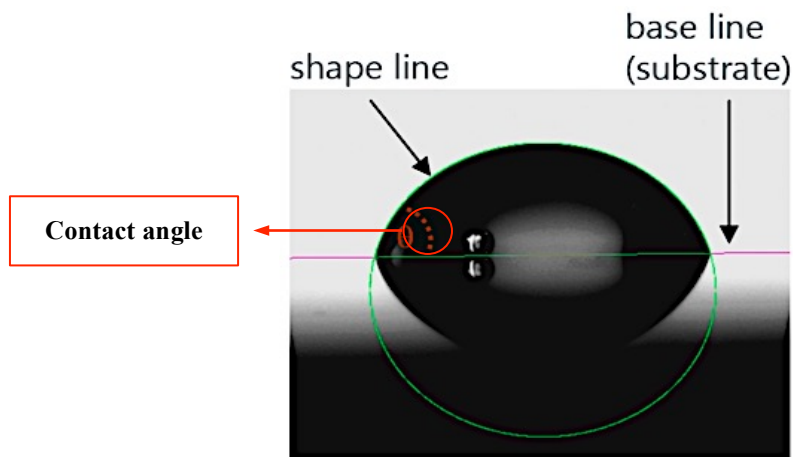


Figure 3.24: Contact angle determination.

The contact angle measurements were conducted not on the membrane themselves, but on the corresponding thin films so as to avoid experimental errors due to the membrane porosity. For this purpose, 12 wt.% PSU, SPSU_0.10, SPSU_0.25/PSU 50:50 and SPSU_0.50/PSU 30:70 solutions in NMP were prepared. Thin films were cast by dropwise deposition of polymer solution on a glass microscope slide. The samples were then placed into a laboratory oven in order to induce solvent evaporation (3 h at 105 °C). Subsequently, the thin films were carefully lifted from the glass slides and immediately used for the analysis. A 10 μ l DI-water droplet has been chosen and the measurements were conducted at room temperature.

Contact angle were measured using Advance Drop Shaper software and the final value was taken as an average of six measurements for each sample taken at random locations in order to minimize the experimental error [45] (Figure 3.25).

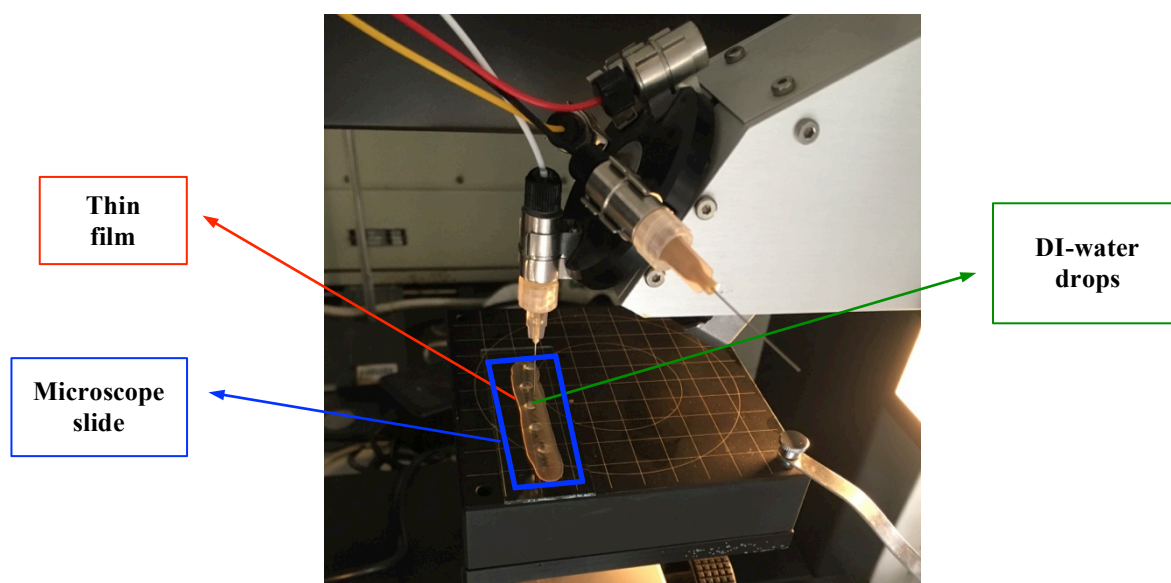


Figure 3.25: Experimental set-up of the contact angle drop shape analysis. The final value of contact angle is taken as an average of six DSA measurements.

3.6.2 Cloud Point measurements

Cloud point measurements were used to better understand the phase separation properties of the membrane forming systems (polymer, solvent and non-solvent).

The thermodynamics of a three-components system is conventionally described by a ternary diagram (Figure 3.26). One important feature of this plot is the so-called *cloud point* representing the transition from the one-phase stable solution region (on the left) to a thermodynamically unstable region where phase separation occurs.

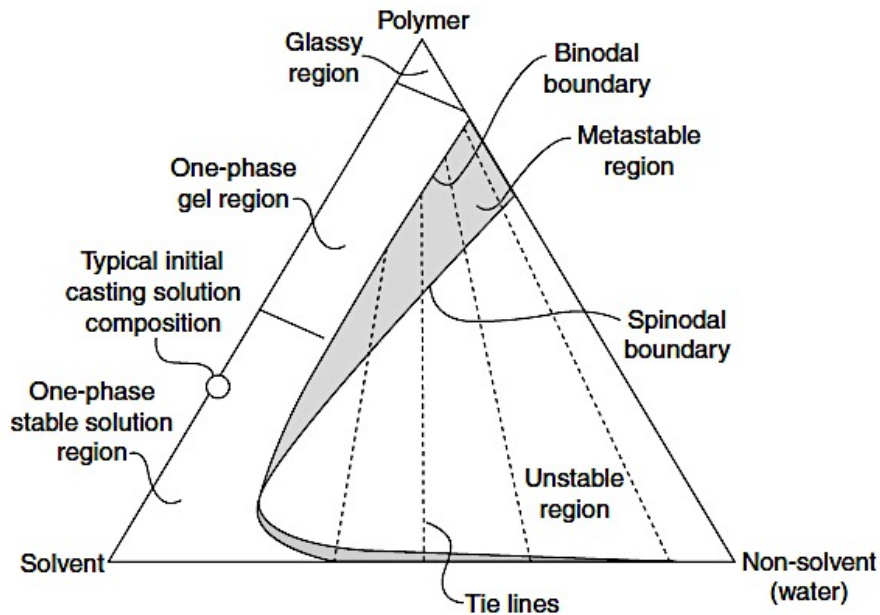


Figure 3.26: Phase diagram of a three components system (Polymer/Solvent/Non-solvent).

The cloud point value is unique for any specific three-component system. Therefore, it is important to investigate the influence of the sulfonation on the thermodynamic equilibrium between solvent, non-solvent and polymer (pristine PSU vs. sulfonated polysulfone).

Cloud point values for a given concentration of the polymer were determined by titration [87-88]. According to this method, different volumes of non-solvent/solvent were added to solutions with various polymer contents while continuously stirring [45]. The addition continued until turbidity occurred [57]. The composition of the solution on the onset of turbidity represents the transition concentration between the one-phase and the two-phase regions of the phase-diagram, i.e. the system's cloud point [90].

In other words, the cloud point measurements were performed to determine the amount of the non-solvent needed to induce the phase separation by NIPS process with PSU or SPSU based solutions [60].

Experimentally, NMP solutions with 15-20-25 wt% PSU contents were prepared and poured into 100 ml glass bottles. Then a NMP/water mixture (4:1 in weight) was added drop by drop by means of a syringe while continuously stirring the solution until the turbidity could be visually detected [89] (Figure 3.27).

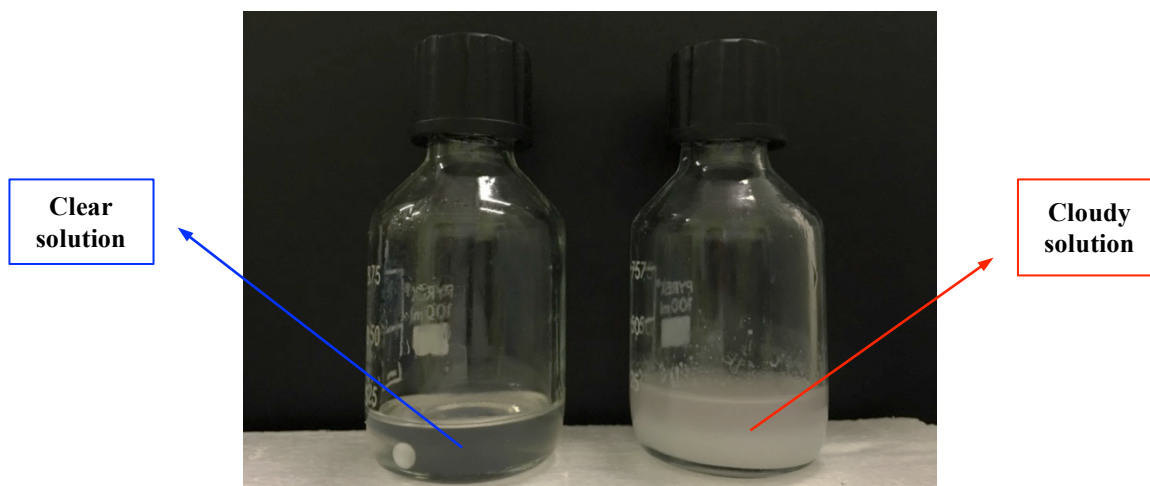


Figure 3.27: Turbidity occurrence during a cloud point measurement as compared to the clear starting solution (on the left).

The first part of the experiment was conducted at room temperature (25 °C). However, once the turbidity has been detected, the mixtures were heated up to 70 °C for 15 minutes and left to cool down to room temperature under constant stirring. If the turbidity persisted, the cloud point has been reached; otherwise, another small amount of NMP/water mixture would be added and the procedure repeated as before [57]. This step is important because there is a possibility that phase separation occurs only locally, meaning that the real cloud point has not yet been reached [57].

Finally, mass balance was used to determine the weight of each of the components in the system. The cloud points of SPSU_0.10 and that of the two mixtures (SPSU_0.25/PSU 50:50 and SPSU_0.50/PSU 50:50) were determined following the same protocol.

The experimental set-up of the process described above, is illustrated in Figure 3.28.

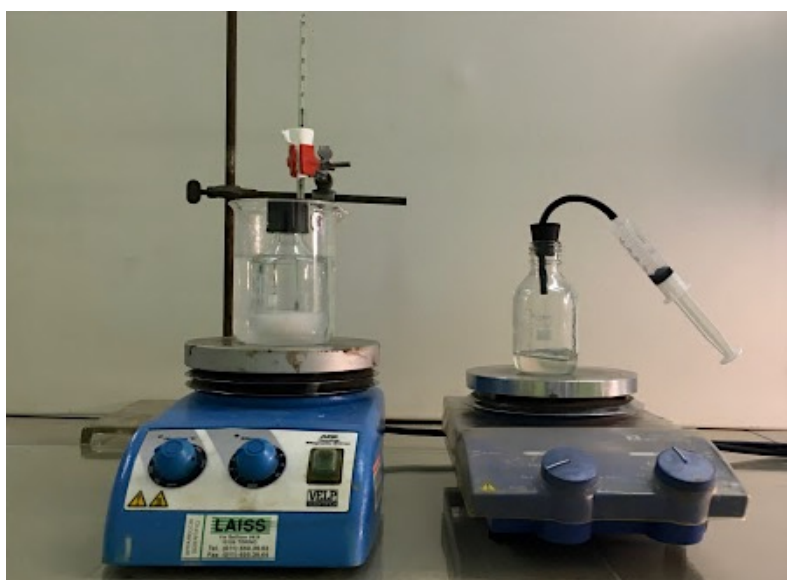


Figure 3.28: Experimental set-up of the Cloud point measures.

3.6.3 Mass transport tests

Mass transport tests were used to determine the pure water permeance and the selectivity of the membrane substrates.

The pure water permeance (A) is one of the most important parameters in membrane characterization. It represents the volume of water that passes through a membrane per unit time, per unit area and per unit of transmembrane pressure ($L\ m^{-2}\ h^{-1}\ bar^{-1}$). In other words, this parameter indicates the flux obtained with pure water per unit of transmembrane pressure and represents an easy and straightforward way to evaluate initial performance of a membrane.

The pure water permeance is defined by the following equation [63-97]:

$$A = \frac{V}{S \cdot \Delta t \cdot \Delta P} \quad (3.3)$$

where A is the pure water permeance ($LMHbar^{-1}$), V is the collected volume of the permeate, ΔP is the transmembrane pressure, S is the membrane effective surface area and Δt is the time of the test.

The experiments were performed using a lab-scale dead-end ultrafiltration system [63-94-95] (Figure 3.29), with the feed flow perpendicular to the membrane.

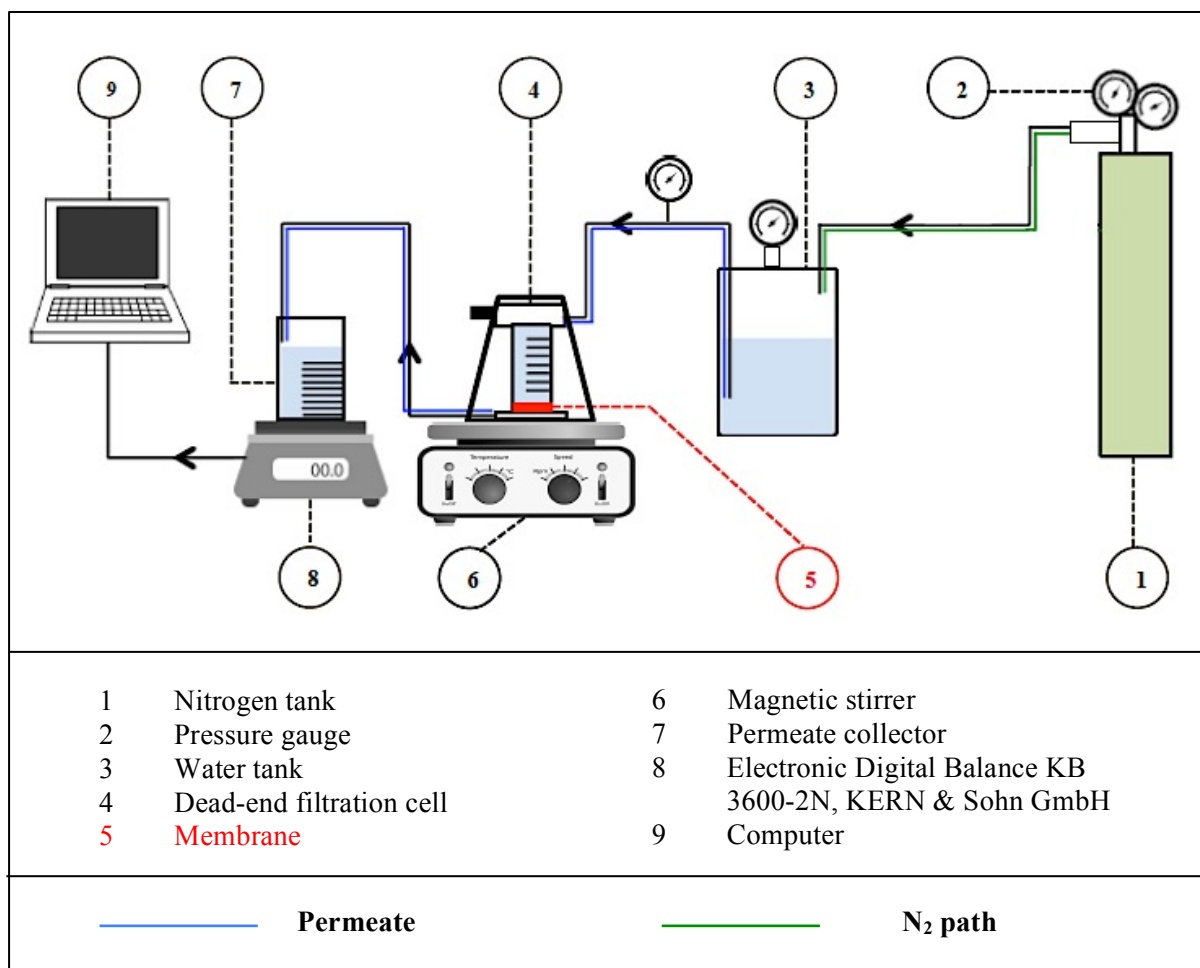


Figure 3.29: Schematic diagram of the lab-scale dead-end ultrafiltration system used for the evaluation of the support layer permeance.

The ultrafiltration cell (10 mL, Amicon 8010, Millipore Co.) was linked to both a nitrogen tank, acting as a compressor, and to a DI-water reservoir (Figure 3.29). The permeate mass is measured over time with a laboratory scale connected to computer.

First, a circular membrane sample (25 mm in diameter and effective area of 4.1 cm²) is washed with ultrapure water and then inserted into the holder of the Amicon cell [96], with the active side facing upwards. Then an O-ring is placed on top of the membrane and the cell is assembled as illustrated in Figure 3.30.

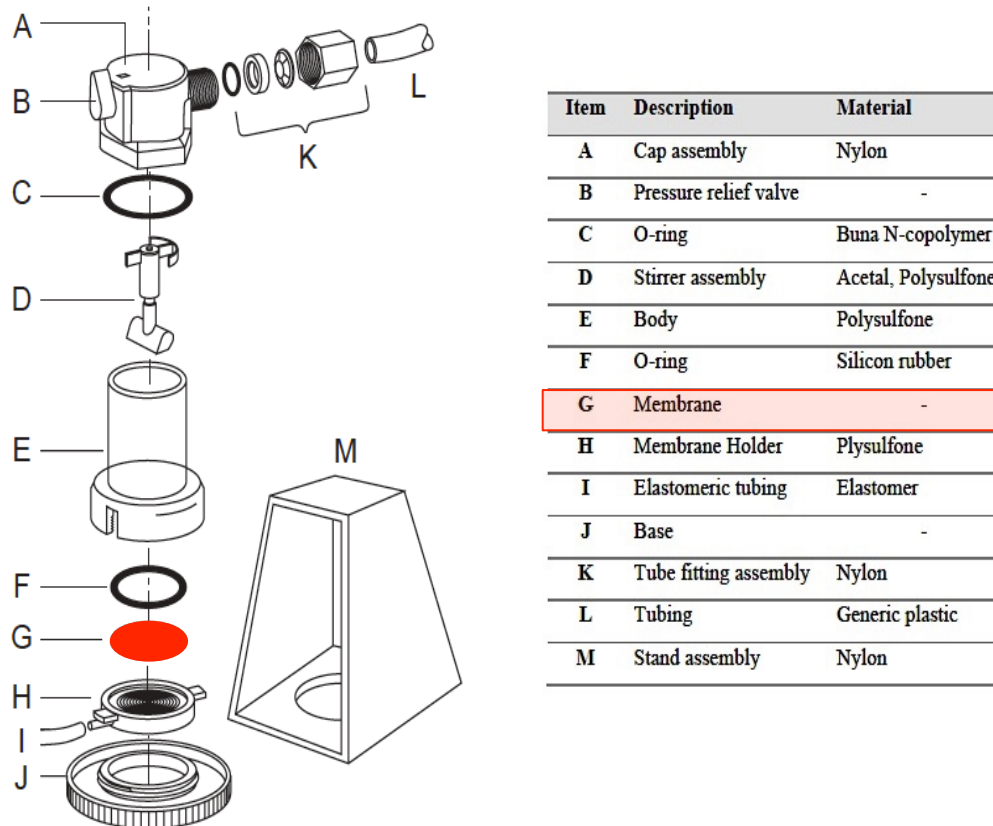


Figure 3.30: Expanded view of the Amicon Cell 8010 produced by Millipore Corporation.

At this point, the N₂ tank is opened and the cell is pressurized until a pressure of 12 psi has been reached. This pressure is kept constant for 10 minutes in order to compact the membrane; then it is reduced to 10 psi to perform the test.

During the test, the nitrogen flux forces the DI water contained in a 10 L vessel into the cell. Once the latter is filled up, the DI water starts to permeate the membrane. The permeate is collected into a beaker placed on an electronic balance that measures the mass variation every minute. The balance is connected to a computer equipped with Winwedge Software that evaluates the recorded data.

The measurements of the pure water permeance were conducted on the following sulfonated polysulfone membrane supports: SPSU_0.10, SPSU_0.25/PSU 50:50 and SPSU_0.50/PSU 30:70. The test was repeated three times for each batch of membranes and the values were averaged.

Coming to the selectivity of membrane substrates, the average pore size was indirectly evaluated through rejection tests followed by spectroscopic analysis.

Rejection (or retention) represents the quantity of the solute held back by the membrane and can be expressed by the Equation 3.4:

$$R(\%) = \left(1 - \frac{C_p}{C_f}\right) \times 100\% \quad (3.4)$$

where C_p is the solute concentration of the permeate, whereas C_f is the solute concentration in the feed solution.

The filtration experiment was performed with a lab-scale stirred dead-end ultrafiltration cell (Amicon 8010, Millipore Co.), using LUDOX® HS-40 colloidal silica 50 wt.% suspension in H₂O. These colloidal particles have an average hydrodynamic diameter of 32 nm.

The experimental set-up is very similar to the one used for the permeability test, except for the 10 L water tank, which is not necessary in this case (Figure 3.31).

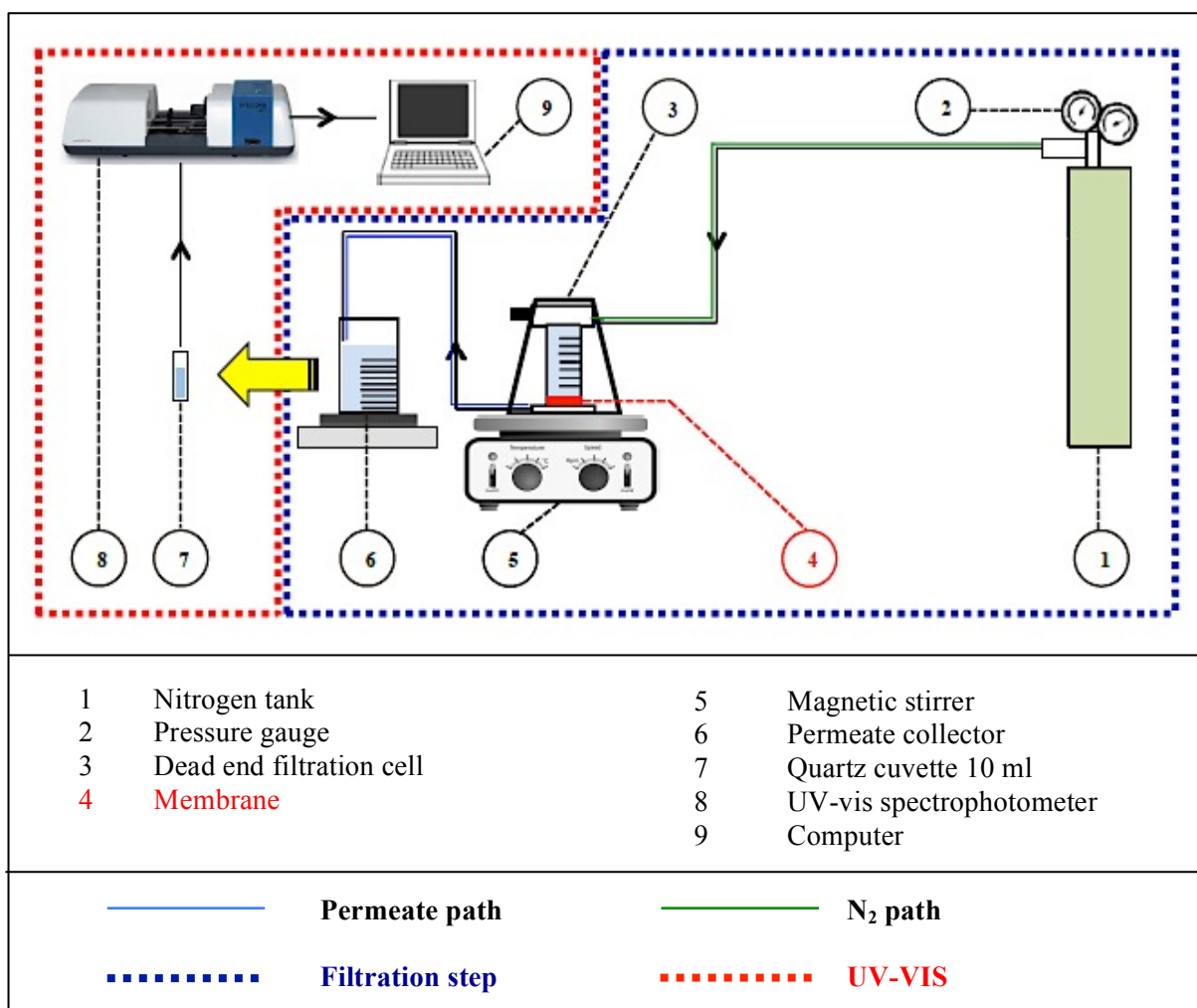


Figure 3.31: Schematic diagram of the experimental set-up used for the determination of membrane support selectivity.

The membrane sample (25 mm in diameter and effective area of 4.1 cm²) is placed in the Amicon cell as described in chapter 3.6.3, and filled with a 7 g/L LUDOX® HS-40 solution. The cell is pressurized for 10 min at 12 psi to compact the membrane within the holder. The pressure is then reduced to 10 psi and 6 mL of permeate are collected into a vial. The solution

in the cell was continuously stirred throughout the test to prevent gel formation on membrane surface.

The permeate was then transferred in a 10 mL quartz cell in order to perform the spectroscopic analysis. Hence the colloidal silica concentration in the permeate was determined *via* UV-Vis spectroscopy, thus obtaining the rejection value.

The following membrane substrates were examined: SPSU_0.10, SPSU_0.25/PSU 50:50 and SPSU_0.50/PSU 30:70. Each membrane type was tested three times and the final values were averaged.

3.6.3.1 UV-Vis spectroscopy

According to the working principles of this technique [98] (Figure 3.32), a beam of UV or visible light is filtered by a monochromator. The selected wavelength passes through a cell containing the sample and part of radiation is absorbed. The absorbance is expressed by the Equation 3.5:

$$A = \log_{10}(I_0/I) \quad (3.5)$$

where A is the absorbance, I_0 is the intensity of the incident light and I is the intensity of the light transmitted by the sample.

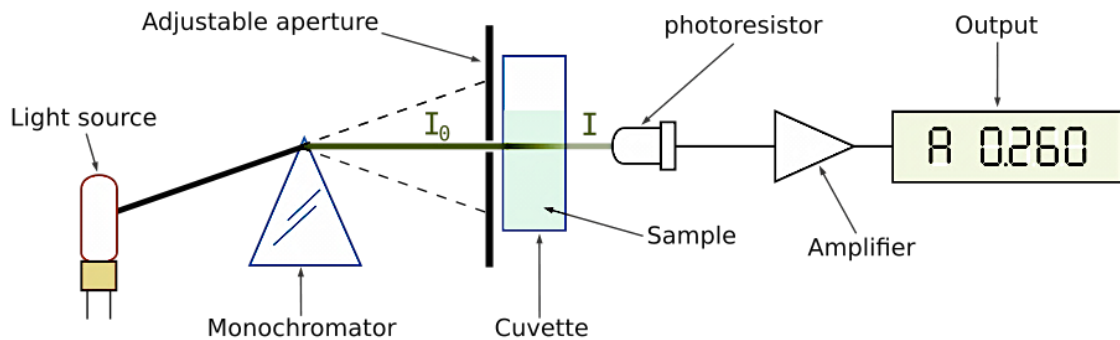


Figure 3.32: Schematic diagram of UV-visible Spectrometer working principle.

This analytical technique allows to determine the concentration of an absorbing species in solution, using the Beer-Lambert law (Equation 3.6) [98]:

$$A = \varepsilon \cdot b \cdot C \quad (3.6)$$

where A is the absorbance, ε [$\text{m}^{-1}\text{cm}^{-1}$] is the molar absorptivity, C [M] is the molar concentration of the absorbing specie whereas b [cm] is the optical path of the light through the sample.

The measurements were performed using a Specord S600 spectrophotometer equipped with a cell carousel. The absorbance was related to the concentration using a calibration curve.

The latter was obtained by measuring the absorbance of solutions with known concentrations of LUDOX® HS-40. The resulting curve is expressed by the following equation:

$$y = 0,3136 \cdot x \quad (3.9)$$

where y is the absorbance and x is the concentration [mg/ml]. This expression was used to calculate the concentration of the permeate, and therefore the rejection through Equation 3.4.

3.7 FO performances of TFC membranes

Typically, membrane performance in FO process is described in literature [7-9] in terms of water fluxes (J_w), reverse solute fluxes (J_s), and resistance to the diffusion of the solute across the support layer of the TFC membrane. Nevertheless, J_w and J_s are not intrinsic parameters of the membrane, because they are closely related to the specific hydrodynamic conditions and also to both the nature and the concentration of the draw solution that determines the osmotic gradient at the interface.

Therefore, the performances of the membranes were evaluated with an alternative approach [99] that focuses the attention on three intrinsic parameters: water permeance (A), salt permeability constant (B) and structural parameter (S). A and B describe the performances of the active layer, whereas S is related to the support layer. Those values can be calculated with an Excel-based algorithm starting from the governing equations of mass-transport across a FO membrane (Figure 3.33).

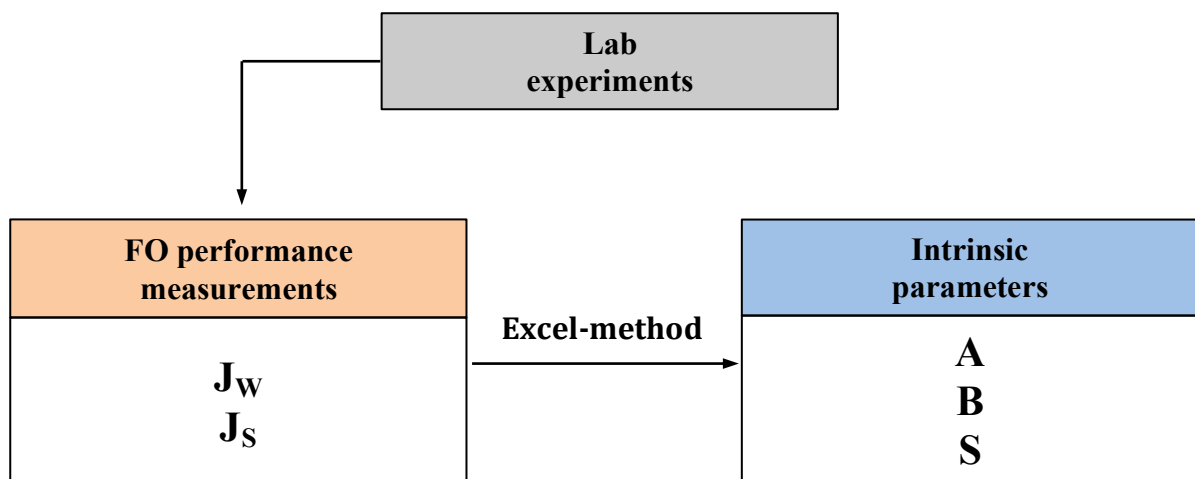


Figure 3.33: Protocol followed for the determination of the intrinsic parameters.

The experiments were performed with a lab-scale FO system (Figure 3.34 and 3.35) using DI-water as feed solution and concentrated NaCl solution as draw solution.

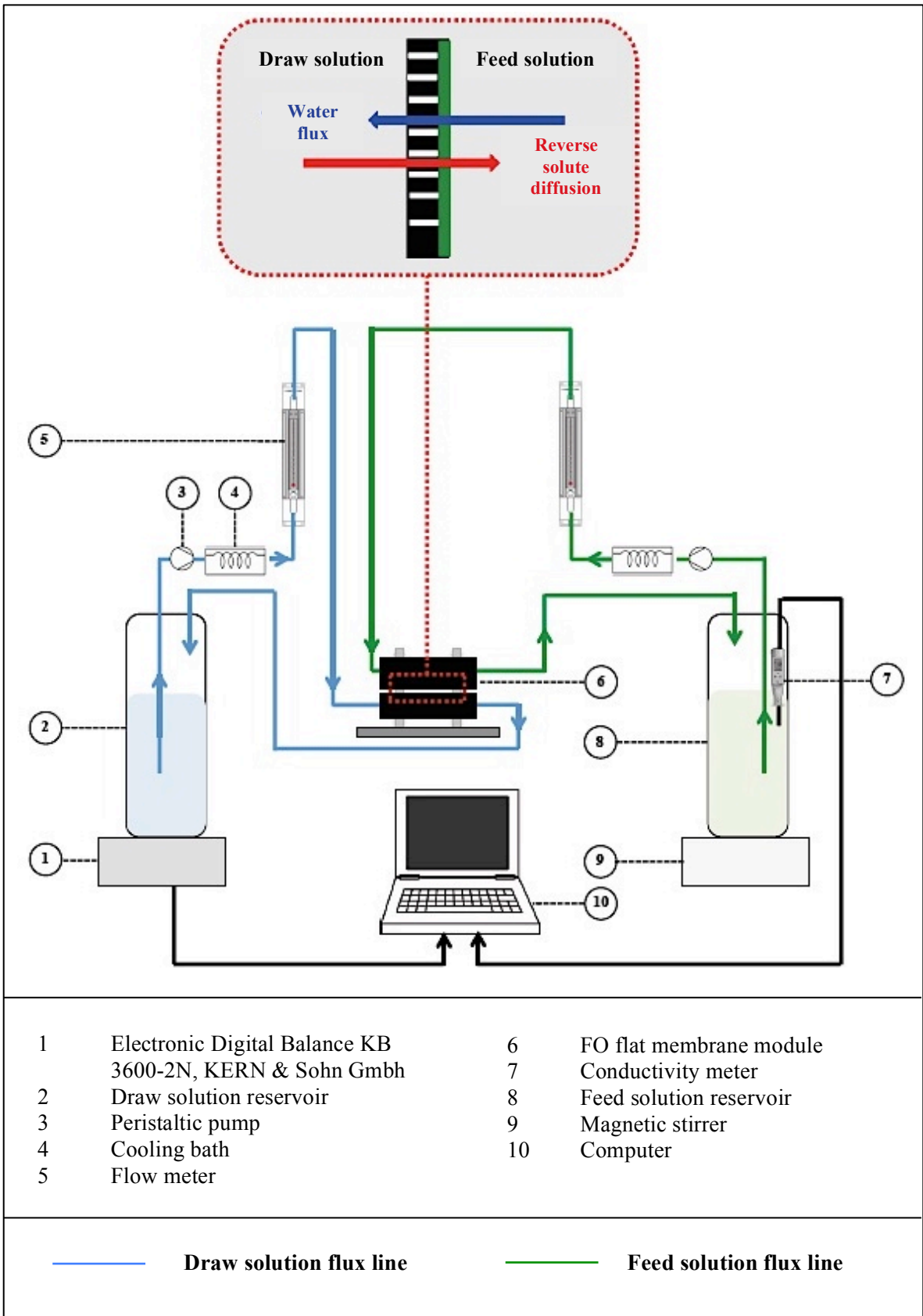


Figure 3.34: Schematic diagram of the lab-scale FO system used experimentally for the characterization of the composite membrane.

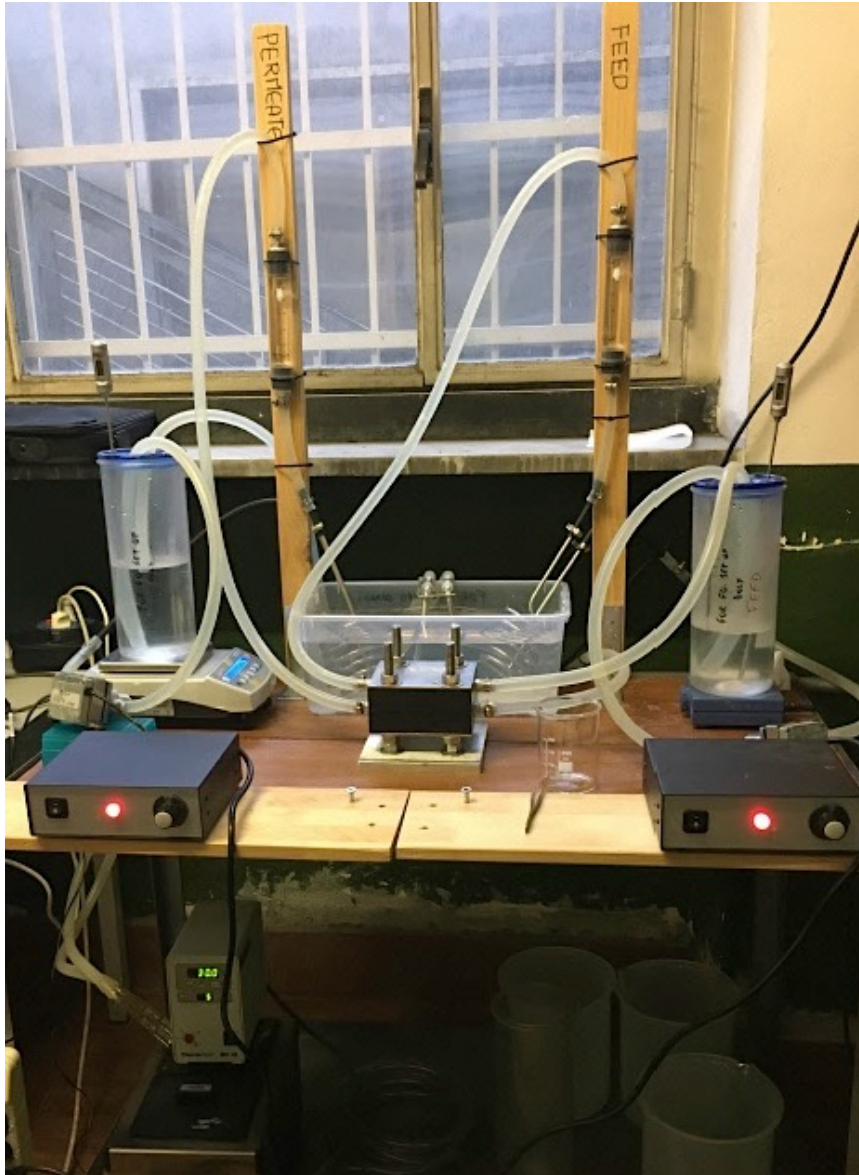


Figure 3.35: Lab-scale FO system.

The membrane sample with a nominal surface area of 19.8 cm^2 is placed in the cell-housing unit with the PA active layer facing the feed solution (Figure 3.36).



Figure 3.36: FO membrane cell.

The cell unit is connected to the draw solution (DS) and the feed solution (FS) reservoirs, which are positioned respectively onto an electronic balance and a magnetic stirrer. The solution co-current flow starts by switching on the two peristaltic pumps.

Both the draw and the feed solutions are thermostated at 25 ± 0.5 °C by means of a thermostatic bath regulated by a cooler. A thermometer constantly controls the temperature. This operation is fundamental because any variation can influence the diffusion properties of the solute. The filtration test starts when both the DS and FS reach the membrane-housing unit. According to forward osmosis working principle (Chapter 2.3), water diffuses across the membrane towards the draw solution side because of the osmotic pressure gradient between the FS and the DS. At the same time, the solute of the DS diffuses in the opposite direction, i.e., from the draw solution to the feed side. This reverse diffusion is detected by measuring the changes in the conductivity of the feed solution every minute. For this purpose a conductivity meter is placed in the FS reservoir.

The test was carried out with different DS concentrations, so that the experimental protocol was divided in five stages. At the end of each stage, a specific volume of the NaCl-DS was added to increase the concentration of the draw solution in the DS-reservoir, generating an increase in the osmotic pressure and thus also an increase in both J_w and J_s values. The following Table 3.4 sums up all of the DS concentration used for each of the five stages of the test.

Table 3.4: Concentration of the NaCl draw solution used for each of the five stages of the test. The second column of the table represents the volume (mL) of draw solution, which has to be added to the draw solution reservoir for each stage. Before starting with the first stage, the DS-reservoir was filled with 1 L of DI-water.

C_i [mM]; $i=[1-5]$	Volume of DS added to the DS-reservoir (mL)
50	25.64
200	85.47
350	101.01
500	121.21
650	148.15

Water and reverse solute fluxes were evaluated for each stage: the balance positioned underneath the DS-reservoir records the weight variation of the draw solution whereas the conductivity meter analyses the variation in the conductivity of the FS due to the reverse diffusion process. The recorded data are transferred to a computer, where Winwedge Software extracts J_w from the weight values and J_s from the conductivity measurements. Finally, water permeance (A), salt permeability constant (B), and structural parameter (S) were calculated simultaneously with the Excel-based algorithm of Tiraferri et al. [99].

The test was repeated three times for each batch of membranes and the final values were averaged.

4 Results and discussion

In this section, the results from the experimental analysis described in Chapter 3 will be presented and discussed in order to evaluate the potential use of sulfonated polysulfone membranes for forward osmosis applications. This chapter is divided into three parts:

- Characterization of sulfonated polysulfones
- Characteristics and performances of membrane substrates
- Preliminary studies on TFC membranes

In the first section, results from thermal and spectroscopic characterizations are presented. The results are also discussed by focusing on the influence of the sulfonation degree on polysulfone thermal behaviour.

In the following section, characteristics and performance of membrane substrates are evaluated. First, the compositions of the casting dopes selected for the fabrication of the sulfonated support *via* UV+NIPS are justified. Then, results from contact angles measurements are evaluated and compared. Also, the interaction between the solvent and the sulfonated polysulfones is investigated in order to evaluate the phase separation behaviour of the different casting solutions.

The last part of the chapter is focused on membrane performance. The permeance and selectivity of the membrane substrates are evaluated and compared. Finally, preliminary results on FO performance of the membrane are discussed evaluating concerns encountered and future challenges.

4.1 Characterization of sulfonated polymers

In this section, results from differential scanning calorimetry, thermogravimetical analysis and ATR-FTIR spectroscopy performed on the samples listed in Table 4.1 will be discussed to assess the effectiveness of sulfonation of the synthesized polysulfones. The results will be evaluated by making a comparison with the traditional behaviour of PSU and focusing on the influence of the sulfonation degree.

Table 4.1: Sulfonated polysulfone samples characterized through DSC, TGA and ATR-FTIR.

Sample name	Theoretical sulfonation degree
PSU	0
SPSU_0.10	0.10
SPSU_0.25	0.25
SPSU_0.50	0.50

4.1.1 Effect of sulfonation on glass transition temperature

Differential Scanning Calorimetry was used to investigate the glass transition temperature (T_g) of the sulfonated polymers and its dependence on the sulfonation degree.

DSC curves of each sample are presented in Figure 4.1.

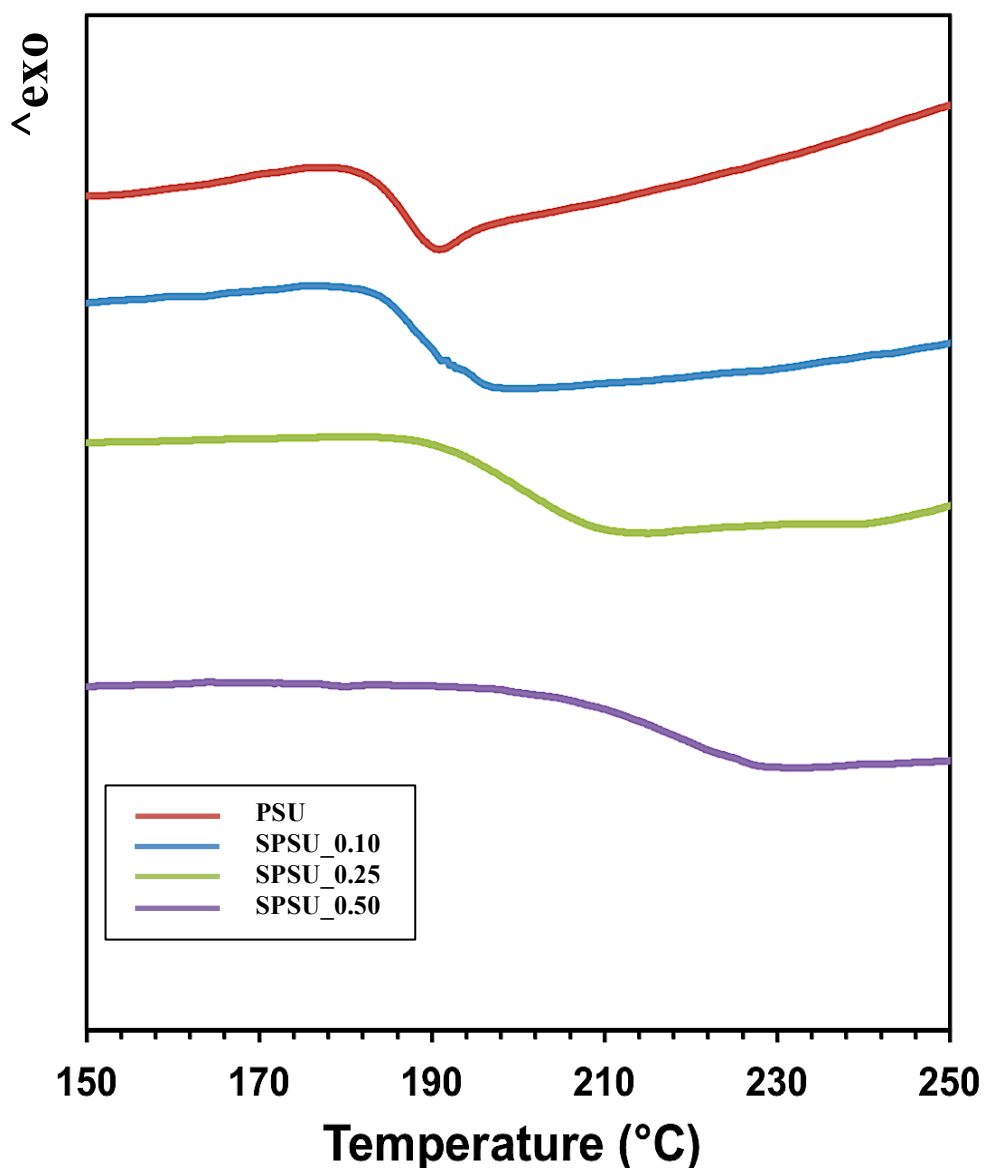


Figure 4.1: Comparative DSC curves of polysulfone and sulfonated polysulfone samples, reported in the range of 150-250 °C.

The results reported in Table 4.2 reveal a higher T_g for the sulfonated samples as compared to the pristine polysulfone. The transition temperatures of SPSU samples were detected in the range 190-220 °C, whereas the T_g of polysulfone (185 °C) is in good agreement with values reported in the literature (185-190 °C) [56].

Table 4.2: Glass transition temperature of PSU and SPSU samples.

Sample name	T _g [°C]
PSU	185
SPSU_0.10	190
SPSU_0.25	200
SPSU_0.50	220

The increase in the glass transition temperature is due to the substitution of hydrogen atoms of the aromatic rings by sodium sulfonate groups. The introduction of -SO₃Na groups along the polysulfone backbone has two effects [100]: 1) higher molecular bulkiness and 2) greater intermolecular interaction by sulfonated pendent ions (ionomer effect). The introduction of bulky groups generates steric hindrance, which limits the intersegmental motion reducing both the flexibility and the mobility of ether groups. Moreover, electrostatic interactions between ion clusters can increase the immobilization effect on polysulfone main chain [100-101-102]. Overall, both these effects contribute to the glass transition temperature increase. In other words, more energy is required for the chains to move and allow the polymer to reach the rubbery state.

4.1.2 Effect of sulfonation on thermal stability

The thermal stability of sulfonated polysulfones was investigated by TGA analysis. The tests were performed on polysulfones with different degrees of sulfonation in order to examine the effect of sulfonation on the thermal behaviour of the polymers. TGA thermograms of each sample are illustrated in Figure 4.3.

Polysulfone behaviour is in close agreement with the results reported in the literature [90]. As illustrated in Figure 4.2, PSU shows only one weight loss at 500 °C, which is assigned to the thermal decomposition of the polymeric backbone. Different observations can be made for the sulfonated samples. In all the cases, TGA curves show a similar multiple-step weight loss. The first weight loss between 270 and 400 °C is ascribed to thermal desulfonation [90-100], which involves the formation of SO and SO₂ gases. The second step above 450 °C is due to the degradation of the polymeric backbone. Furthermore, SPSU samples show lower degradation temperature than PSU. The degradation onset of the polymer backbone slightly decreases as the sulfonation degree increases (Table 4.3). This behaviour can be ascribed to the presence of sulfonate groups that reduce the symmetry of the macromolecule, thus leading to a lower thermal stability of the polymer backbone.

Table 4.3: Onset of degradation of PSU and SPSU samples.

Sample name	T onset-degradation [°C]
PSU	500
SPSU_0.10	480
SPSU_0.25	450
SPSU_0.50	430

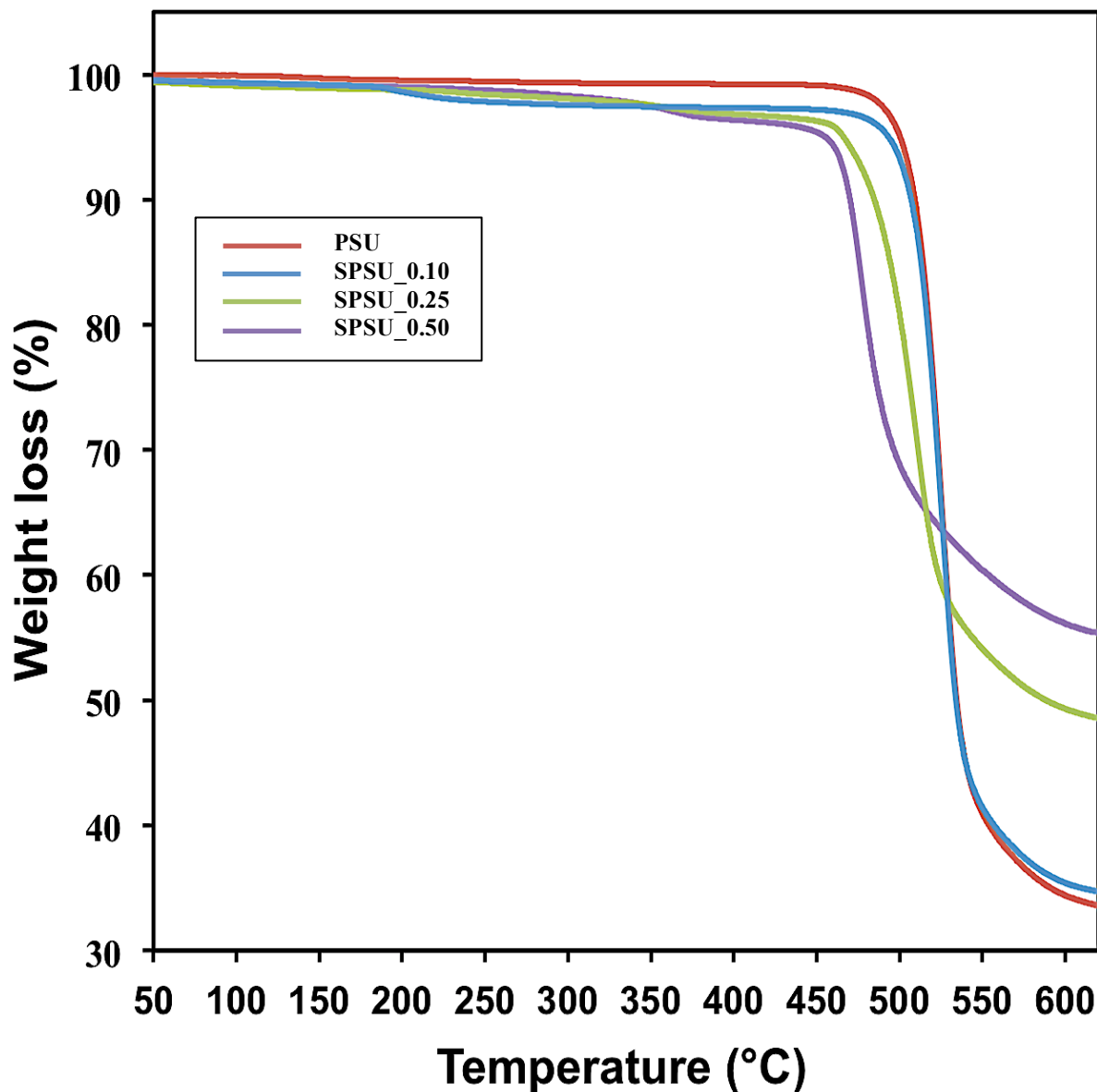


Figure 4.2: Comparative TGA thermograms of polysulfone and sulfonated-polysulfone samples, reported from 50 to 620 °C.

4.1.3 Confirmation of sulfonation by ATR-FTIR spectroscopy

The effectiveness of the sulfonation reaction was also confirmed by FTIR analysis.

The spectra presented in Figure 4.3 show the characteristic peak of sulfonate symmetric stretching in aromatic polymers at 1040 cm^{-1} , thus confirming the presence of sulfonate groups in the polymer backbone [56-57-90]. The sulfonation is usually also detected by the characteristic asymmetric stretching vibration at $1150\text{-}1170\text{ cm}^{-1}$. However, this band is not clearly visible on the recorded spectra because of overlapping with other bands. It also can be observed that the intensity of the peak at 1040 cm^{-1} increases as the sulfonation degree is increased. The other typical IR bands of polysulfones and sulfonated derivatives are reported in Table 4.4 [106].

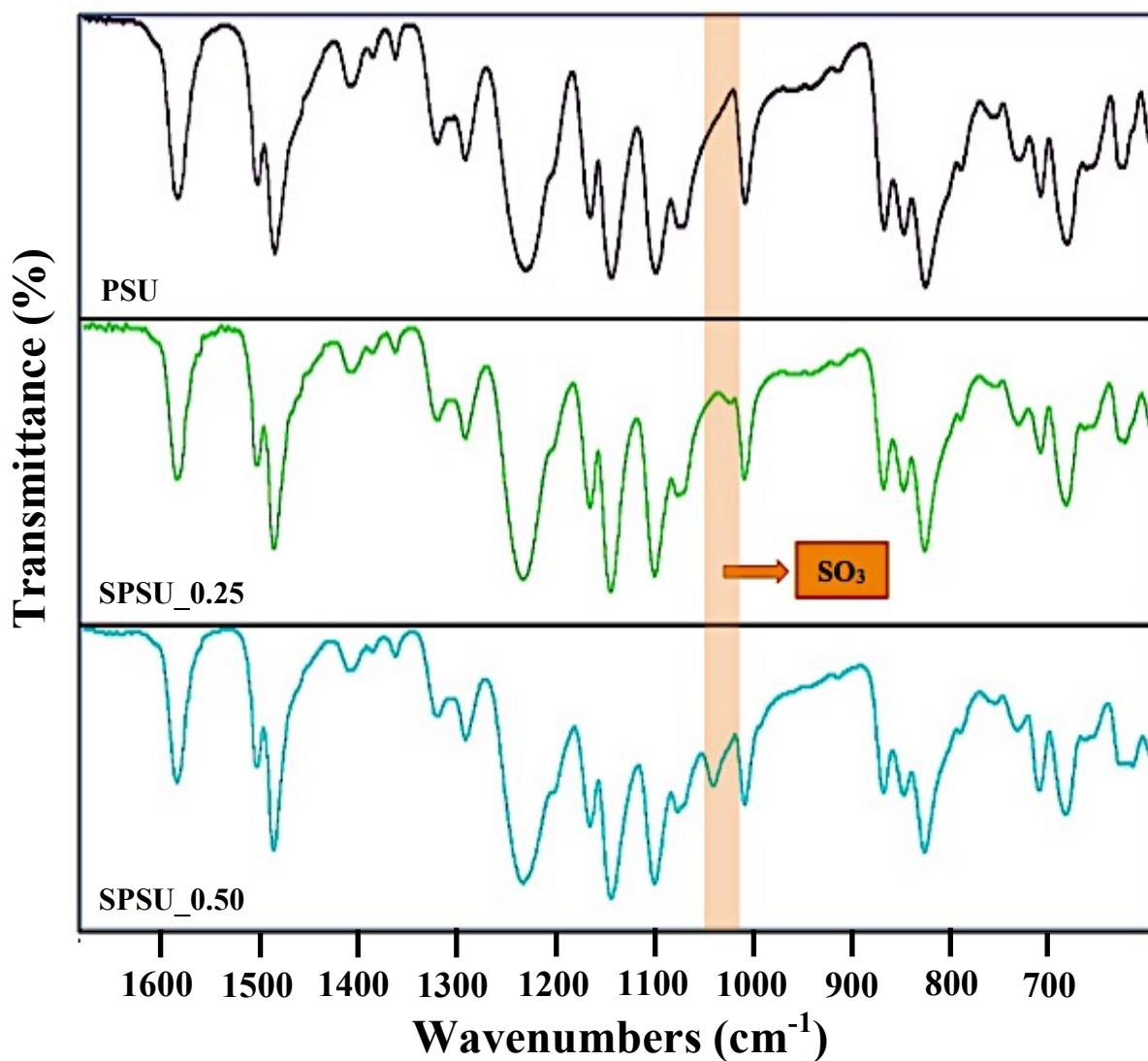


Figure 4.3: Transmittance spectra of pristine PSU and sulfonated-polysulfone samples (SPSU_0.25 and SPSU_0.50) reported from 650 to 1650 cm^{-1} .

Table 4.4: IR bands of polysulfones and sulfonated derivatives [106].

Wavenumber (cm^{-1})	Bands
3600-3200	O-H stretching vibrations
2980-2880	Asymmetric and symmetric C-H stretching vibrations of methyl group
1590-1485	Aromatic C=C stretching
1412	Asymmetric C-H bending of methyl group
1365	Symmetric C-H bending of methyl group
1244	Asymmetric C-O-C stretching of ether group
1170	Asymmetric stretching of sulfonate group
1107-1092	Aromatic ring vibrations
1040	Symmetric stretching of sulfonate group

4.2 Characterization of the membrane substrates

The following sections will be focused on membrane substrates.

First, the choice of the casting solutions will be justified considering the influence of the sulfonation degree on membranes fabrication and mechanical stability. Then, substrates wettability will be discussed evaluating the results from contact angle measurements. Further, cloud points results will be presented and compared.

Finally, the results of permeability and selectivity tests will be presented comparing performances of the different substrates.

4.2.1 Casting solution composition

The final casting solution compositions for the fabrication of the support layer are a result of preliminary studies carried out using polysulfones with various degrees of sulfonation.

Several dope compositions have been tested, varying not only the sulfonation degree, but also the polymer concentration in the casting solution. However, the main problem was related to the sulfonation degree of sulfonated polysulfone. Namely, membranes fabricated using highly sulfonated casting solutions faced three main concerns:

1. Low stability and low adhesion to the support could be visually observed during phase separation (Figure 4.4A): the polymer precipitates detaching from the support
2. No phase separation occurs when the sulfonation degree is too high. The polymer solution generates a dense gel phase once immersed in the coagulation bath (Figure 4.4B).
3. Slow precipitation rates due to the hydrophilic nature of SPSU

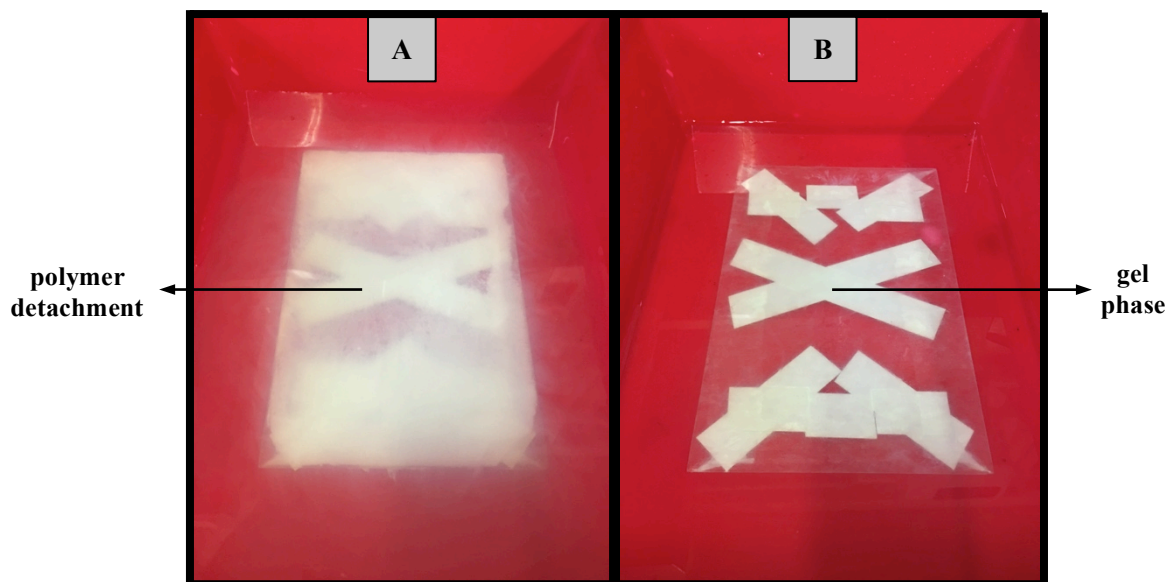


Figure 4.4: Influence of sulfonation degree on phase separation process: a) polymer detachment during phase inversion; b) formation of a gel phase.

Therefore, according to these observations, the theoretical sulfonation degrees of polysulfones were fixed to 0.10, 0.25 and 0.50. However, also SPSU_0.25 and SPSU_0.50 face low stability due to their high hydrophilicity.

This is the reason why polymer blends consisting of PSU and SPSU_0.25 or SPSU_0.50 at different concentrations were used for the preparation of the casting dopes. Contrary, SPSU_0.10 did not present these issues during phase separation. In this case, blending was not necessary.

Nevertheless, membranes prepared from polysulfone/sulfonated polysulfone blends still showed low mechanical stability due to high water swelling. This problem was overcome by adding a crosslinking step, using poly (ethylene glycol) diacrylate (PEGDA) as cross-linking agent (Chapter 3.3.4). The UV-induced cross-linking leads to the formation of a tight network of PEGDA that entraps sulfonated polysulfones. This procedure allows to prepare membranes with improved mechanical resistance.

Therefore, the final fabrication protocol was tailored according to the sulfonation degree of the polymer (Figure 4.5).

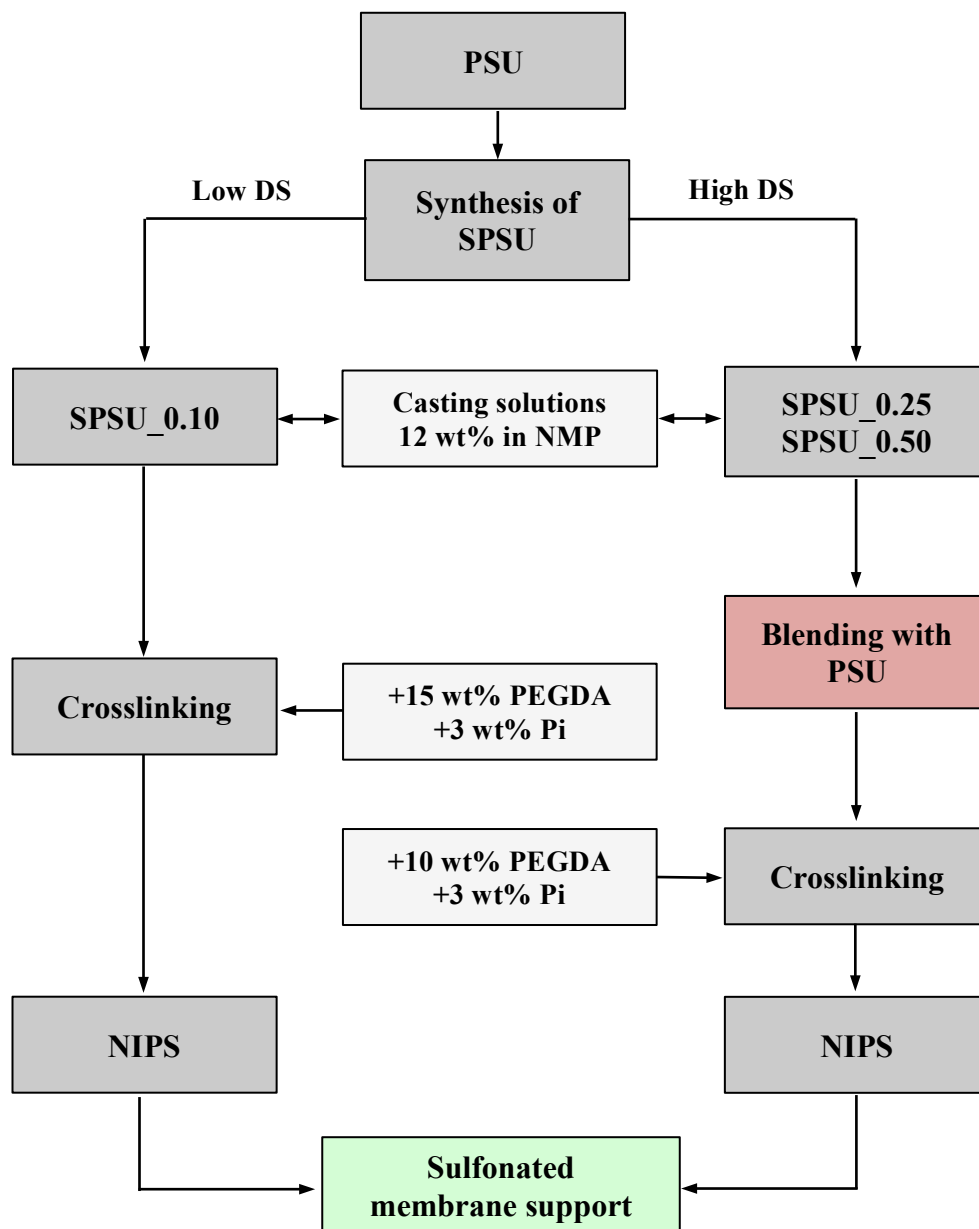


Figure 4.5: Schematic representation of the fabrication protocol used for membrane substrates preparation.

4.2.2 Substrates wettability

Water contact angle measurements were used to investigate the wettability of the sulfonated polysulfone thin films. As mentioned in Chapter 3.6.1, the measurements were carried out using dense thin films, since the surface porosity of the support layer could affect the test due to the penetration of water droplets.

Theoretically, the presence of sulfonated functional groups in the polysulfone backbone should increase the hydrophilicity of the polymer, thus enhancing the wettability of membrane support. These groups compete with water in both hydrogen bonds and weak Van der Waals interactions, leading to lower contact angles and higher wettability [63].

Results from water contact angle measurements (Figures 4.6 and 4.7) have confirmed this hypothesis.

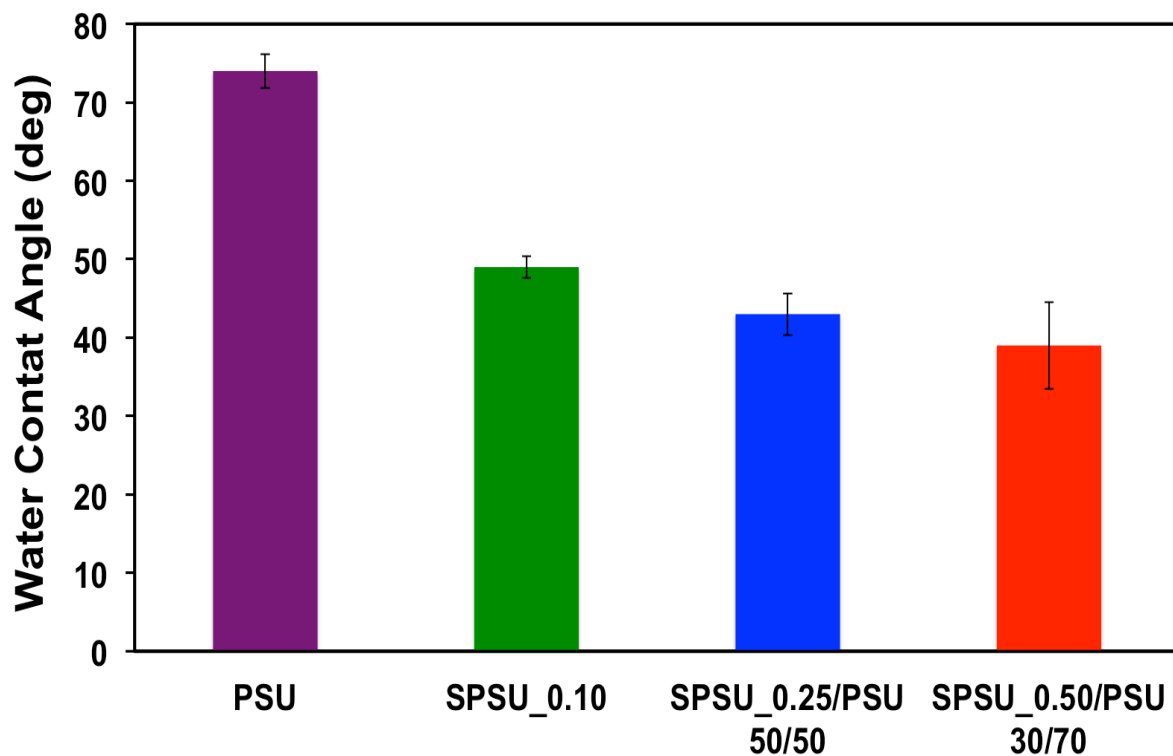


Figure 4.6: Contact angles of PSU, SPSU_0.10, SPSU_0.25/PSU 50:50 and SPSU_0.50/PSU 30:70. The error bars represent the standard deviations of each measurement from the average value.

The graph reported in Figure 4.6 shows that the contact angle of PSU is higher than that of sulfonated membranes. The value obtained from polysulfone is 74.5° , whereas, as expected, contact angle decreases as the degree of sulfonation increases [104]: SPSU_0.10 shows an average value of 49° , while the two blend systems present an even lower contact angle ($39-43^\circ$). These last two have a very similar contact angle, in spite of the significant difference in the sulfonation degree. This behaviour can be ascribed to the different contents of SPSU and pristine PSU in the two blend systems.

The standard deviations are in the acceptable range. The slight variations of the results can be due to experimental errors and to the heterogeneity of the samples.

Looking at the behaviour of the sulfonated samples, the observable variability can be ascribed to the presence of more hydrophilic regions, as a result of an uneven sulfonation.

Images of droplets deposited on top of the different thin films are shown in Figure 4.7. The morphology of the droplets suggests a higher wettability of sulfonated sample. This finding is consistent with the results discussed above.

Overall, we can conclude that sulfonated polysulfones are more hydrophilic than pristine polysulfone, making membrane substrates more wettable.

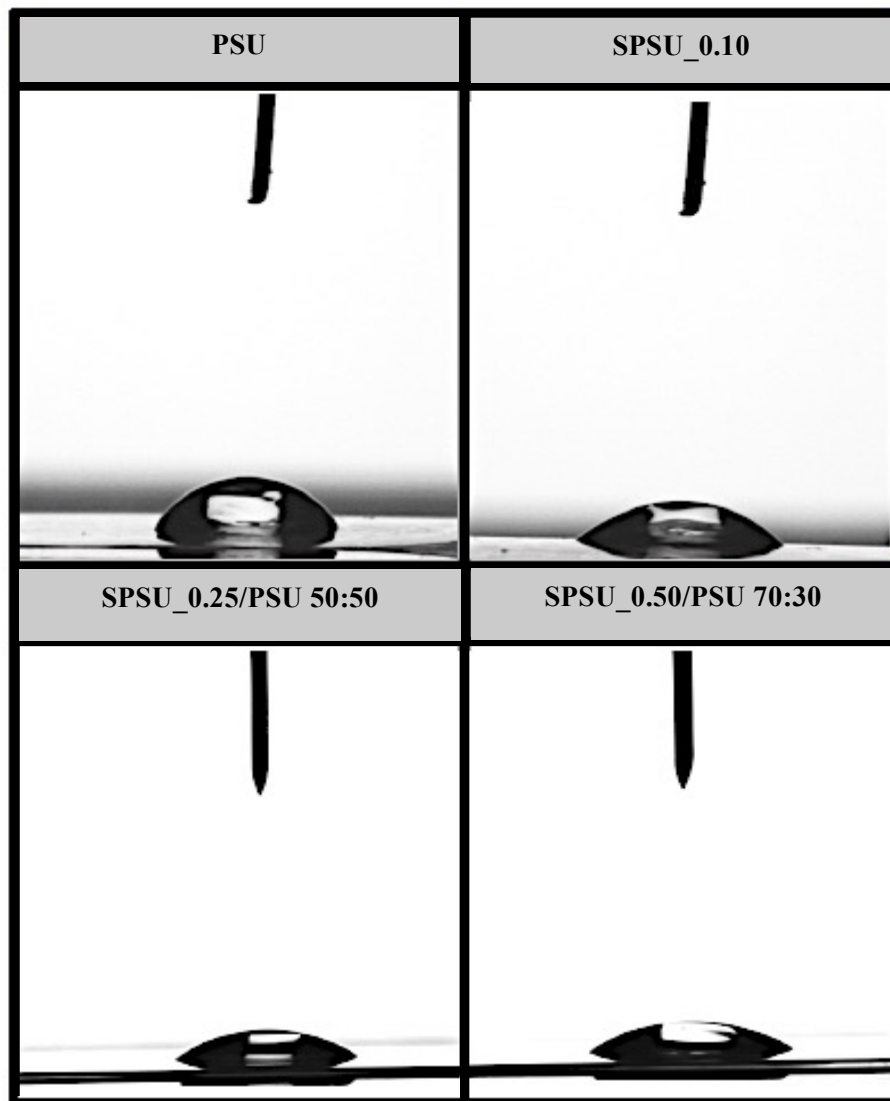


Figure 4.7: Images of droplets deposited onto PSU, SPSU_0.10 and blended thin films (SPSU_0.25/PSU 50:50 and SPSU_0.50/PSU 30:70).

4.2.3 Interaction between polymer, solvent and non-solvent

Cloud point measurements were used to investigate the phase separation properties [86].

Cloud point data and binodal curves of PSU, SPSU 0.10, SPSU_0.25/PSU 50:50 and SPSU_0.50/PSU 50:50 are shown on the ternary diagram illustrated in Figure 4.8. The term “polymer” is generic and refers to the polymeric content of each casting solution (PSU, SPSU 0.10, SPSU_0.25/PSU 50:50 or SPSU_0.50/PSU 50:50).

It can be observed that, in the sulfonated polysulfones, the area of the one-phase region bordered by the binodal curve increases with respect to that of pristine polysulfone. In other words, it means that the path taken from the sulfonated solution to reach the two-phases borderline will be longer [45]. It can be concluded that sulfonated dopes require high water content to induce phase separation, even if the amount to be added is relatively small.

This is a common trend for sulfonated polymers: they tend to delay the demixing process if compared to the non-sulfonated polymers [9]. This phenomenon can be ascribed to the greater water-affinity of sulfonated polysulfones, as observed by contact angles measurements. The presence of sulfonate groups, capable of forming hydrogen bonds with water, leads to slower precipitation rates during phase inversion. This enhanced affinity to water translates into longer exchange phenomena between the polymer solution and the water bath before phase separation [57].

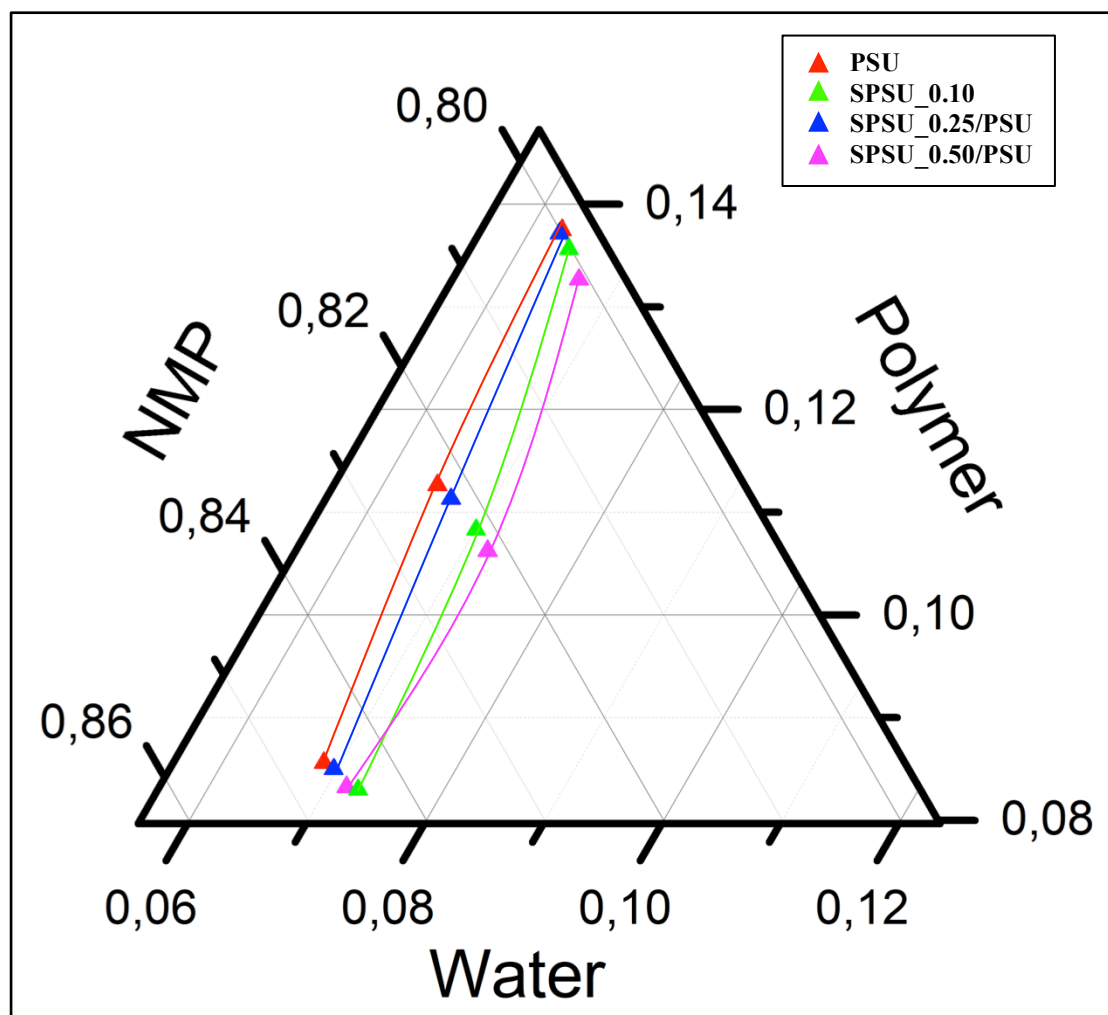


Figure 4.8: Ternary phase diagram for PSU, SPSU_0.10, SPSU_0.25/PSU 50:50 and SPSU_0.50/PSU 50:50.

4.2.4 Pure water permeance of sulfonated substrates

Substrates permeance was investigated in order to confirm their potential use as support layers for thin film composite membranes in forward osmosis applications.

As discussed in Chapter 3.6.3, the experiments were performed with DI-water using a lab-scale dead-end ultrafiltration cell (Amicon 8010, Millipore Corporation).

Results are the average of three measurements for each membrane. Pure water permeance values for SPSU 0.10, SPSU_0.25/PSU 50:50 and SPSU_0.50/PSU 30:70 membrane substrates are shown in Figure 4.9.

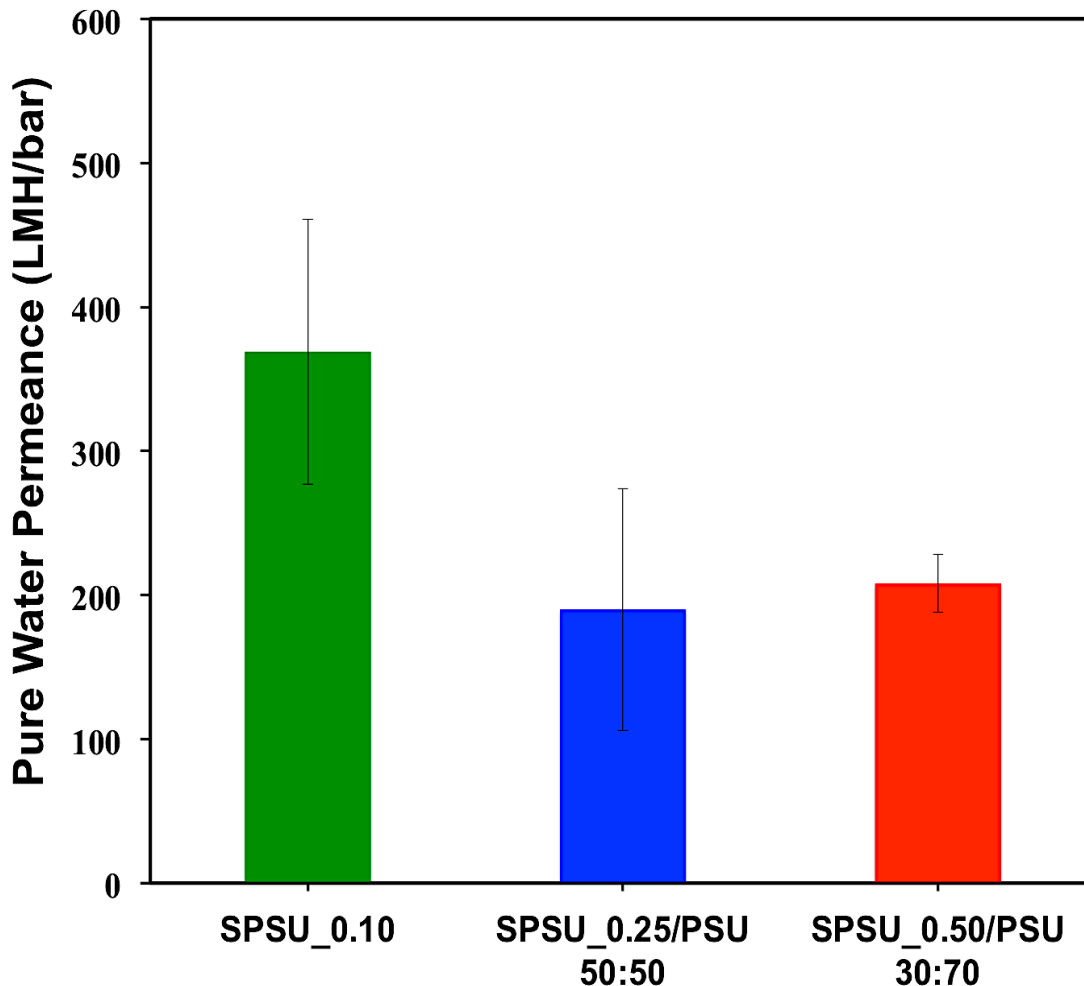


Figure 4.9: Pure water permeance of SPSU 0.10, SPSU_0.25/PSU 50:50 and SPSU_0.50/PSU 30:70 membrane substrates. Results are taken as the average of three tests for each membrane sample. The error bars represent the standard deviations of each measurement from the average value.

As can be seen from the graph reported in Figure 4.9, the pure water permeance of SPSU_0.10 membrane was found to be 369 LMH/bar, whereas the blended membranes SPSU_0.25/PSU 50:50 and SPSU_0.50/PSU 30:70 showed very similar permeance values, respectively 190 and 209 LMH/bar. Based on these results, there is no evidence of a growth trend in pure water permeance due to the increase of sulfonation degree of polysulfones, actually the highest value is that of SPSU_0.10. It should however be noted that a growth trend is not necessarily expected because water flux is almost totally influenced by pores distribution and not only by wettability increase.

As concerns the standard deviation, we can conclude that they are in the acceptable range in view of the fact that these membranes were labmade. Hence, there are several factors that can affect the fabrication step, thus leading to a variation in membrane permeance.

First, although the same fabrication protocol was followed, membranes show regions characterized by the presence of macrovoids. It has been assumed that their formation was caused by the presence of bubbles in the casting solution. As mentioned in Chapter 3.3.1, the photoinitiator was added to the casting dope that was subsequently stirred for 5 min and then left to stand for another 5 min. Nevertheless, it is plausible that some air bubbles remained entrapped in the solution leading to the generation of these bigger pores

Also, as it has already been pointed out, the blade is manually adjusted to set the gap from the casting plate. This means that the membrane nominal thickness can differ from the required value of 150 μm . It is clear how difficult it is to monitor all these factors that inevitably affect the results.

Overall, the permeance of all the membrane samples lies within the typical ultrafiltration range (100-1000 LMH/bar), which was our target. These permeability values have confirmed the potential use of sulfonated polysulfones membranes as support layer for TFC membranes in FO applications.

4.2.5 Selectivity of sulfonated substrates

The selectivity of sulfonated substrates was evaluated in order to investigate average membrane surface pore size.

The measurements were carried out on the same samples used for the pure water permeance measurements. As described in Chapter 3.6.4, the average pores size was indirectly evaluated through rejection tests followed by spectroscopic analysis. The rejection test was performed with a lab-scale dead-end ultrafiltration cell (Amicon 8010, Millipore Corporation), using LUDOX[®] HS-40 colloidal silica having an average diameter of 32 nm. The rejection value was then obtained by evaluating the concentration LUDOX[®] HS-40 in the permeate by an UV- Spectrophotometer.

The results illustrated in Figure 4.10 are the average of three tests for each sample. The rejection of SPSU_0.10 membrane was found to be 68%, whereas membranes SPSU_0.25/PSU 50:50 and SPSU_0.50/PSU 30:70 membranes exhibit a rejection of 72% and 66% respectively. Since the average hydrodynamic diameter of the silica particles is 32 nm, the over 66% rejection means that the membrane pore size can be placed in the 30-40 nm range. This was our target value: bigger pores would lead to uneven deposition of polyamide layer, leaving “gaps” on the membrane surface. These pore dimensions lies within the ultrafiltration range; therefore these results correlate well with the permeance values discussed above.

As stated for permeance results, we can conclude that the standard deviations reported in Figure 4.10 are in the acceptable range.

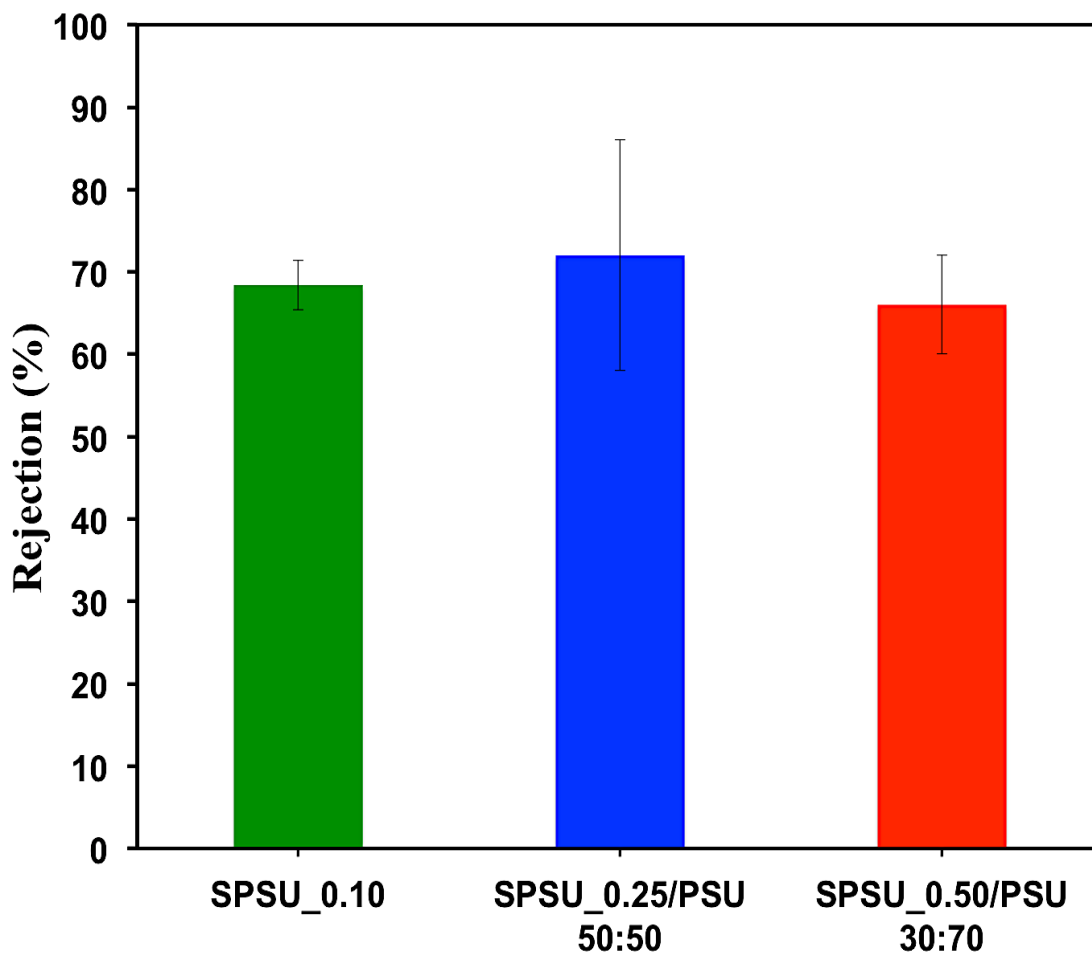


Figure 4.10: Rejection percentage of SPSU 0.10, SPSU_0.25/PSU 50:50 and SPSU_0.50/PSU 30:70 membrane substrates. Results are taken as the average of three measurements for each membrane sample. The error bars represent the standard deviations of each measurement from the average value.

The following Table 4.5 summarises the results obtained from the characterization tests performed on all of the membrane substrates investigated in this study.

Table 4.5: Properties of SPSU membrane substrates.

Membrane ID	Permeability [LMH/bar]	Rejection [%]
SPSU_0.10	369 ± 112	68 ± 3
SPSU_0.25/PSU 50:50	190 ± 104	72 ± 14
SPSU_0.50/PSU 30:70	209 ± 20	66 ± 6

4.3 TFC membranes

Since the defined targets for substrates performances have been achieved, all of the membranes investigated (both SPSU_0.10 and blended membranes SPSU_0.25/PSU 50:50 and SPSU_0.50/PSU 30:70) were subjected to interfacial polymerization in order to create

thin-film composite membranes. The polyamide active layer was realized onto the different substrates following the fabrication protocol defined in Chapter 3.4.

4.3.1 FO performances

FO performances were tested with the aim of calculating the intrinsic membrane parameters, namely: 1) water permeance, 2) salt permeability constant and 3) structural parameter. The measurements were performed with a lab-scale FO system using DI water as feed solution and NaCl as draw solution (Chapter 3.7).

Preliminary results were overall not satisfactory. These findings seem to be consistent with the enhanced hydrophilicity of the substrate layer, which poses several disadvantages. Namely, the rough membrane surface and the potential presence of macrovoids can cause the uneven distribution of the polyamide layer. In addition, interfacial polymerization within the pores instead of just at the top might lead to lower permeance [107]. We have also encountered some practical issues during the interfacial polymerization procedure, such as poor adhesion of the adhesive tape to the surface of the membrane substrate.

However, studies are still in progress to optimize the fabrication protocol of the polyamide layer. Further investigations on the interaction between the active layer and the sulfonated support are required.

5 Concluding remarks

In this thesis work, the potential application of sulfonated polysulfone for the fabrication of TFC membranes for FO was examined.

First, a series of sulfonated polysulfones with different degree of sulfonation (SPSU_0.10, SPSU_0.25 and SPSU_0.50) have been prepared by introducing hydrophilic sodium sulfonate groups *via* an electrophilic substitution reaction. The level of sulfonation was adjusted by varying the molar ratio between polysulfone and the sulfonating agent (trimethylsilyl chlorosulfonate).

DSC, TGA, ATR-FTIR results have confirmed the effectiveness of sulfonation, thus validating the synthesis protocol. Sulfonated polymers have shown higher glass transition temperatures (from 190 °C to 220 °C) than polysulfone; thermal degradation between 270 °C and 400 °C, ascribable to the desulfonation process, and IR transmittance band at 1040 cm⁻¹, which is the typical peak of sulfonate symmetric stretching in aromatic polymers. These findings are in good agreement with previous studies on sulfonated polysulfones reported in the literature.

Then, sulfonated polysulfone membrane substrates were fabricated *via* phase inversion procedure. It was necessary, however, to blend sulfonated polysulfone with the pristine polysulfone to achieve phase separation. An embedded polyethylene terephthalate fabric was employed in order to improve the mechanical and chemical properties of the support layer. UV-curing was used to induce cross-linking and further enhance the mechanical resistance of the membrane substrates.

The contact angle measurements showed a significant increase in hydrophilicity in the polysulfone/sulfonated polysulfone blend systems. These results suggest that the overall membrane hydrophilicity can be tuned by changing the polymer ratio in the polysulfone/sulfonated polysulfone blend. Cloud point measurements were used to build a ternary phase diagram for the membrane forming systems. The data indicate that the much higher affinity of the hydrophilic sulfonated polymer to water (a non-solvent) results in a delayed demixing as compared to that of the non-sulfonated membranes.

The pure water permeance of the membrane substrates varies in the range of 200 – 400 L m⁻² h⁻¹ bar⁻¹ with the average pore size of around 30 – 40 nm. These results indicate that the membrane substrates are in the range of ultrafiltration, thus meeting the expectation for the realization of membrane substrates for FO.

In conclusion, we have successfully synthesized sulfonated polysulfone using a mild sulfonating agent in a one-step process. The sulfonated polymer was then employed to prepare membranes with a stable hydrophilic surface, which can be used as stand-alone membranes in ultrafiltration applications or as substrates for forward osmosis thin-film composites. As concerns with TFC membranes, studies are still in progress to better understand the interaction between the polyamide active layer and the sulfonated substrates.

References

- [1] G. M. Geise, H. S. Lee, D. J. Miller, B. D. Freeman, J. E. McGrath, D. R. Paul, Water Purification by Membranes: The Role of Polymer Science, *Journal of Polymer Science, Part. B: Polymer Physics*, vol. 48, 1685-1718, 2010
- [2] UNEP, *Vital Water Graphics: An Overview of the State of the World's Fresh and Marine Waters*, 2nd ed.; UNEP: Nairobi, Kenya, 2008
- [3] R. Valladares Linares, Z. Li, M. Elimelech, G. Amy, H. Vrouwenvelder, *Recent Development in Forward Osmosis Processes*, IWA Publishing, 2017
- [4] T. Y. Cath, A. E. Childress, M. Elimelech, Forward osmosis: Principles, applications, and recent developments, *Journal of Membrane Science* 281 (2006) 70–87
- [5] S. Zhao, L. Zou, C. Y. Tang, D. Mulcahy, Recent developments in forward osmosis: Opportunities and challenges, *Journal of Membrane Science* 396 (2012) 1– 21
- [6] D. Li, Y. Yan, H. Wang, Recent advances in polymer and polymer composite membranes for reverse and forward osmosis processes, *Progress in Polymer Science* 61 (2016) 104-155
- [7] J. Wei, C. Qiu, C. Y. Tang, R. Wang, A. G. Fane, Synthesis and characterization of flat-sheet thin film composite forward osmosis membranes, *Journal of Membrane Science* 372 (2011) 292–302
- [8] N. Widjojo, T. S. Chung, M. Weber, C. Maletzko, V. Warzelhan, A sulfonated polyphenylenesulfone (sPPSU) as the supporting substrate in thin film composite (TFC) membranes with enhanced performance for forward osmosis (FO), *Chemical Engineering Journal* 220 (2013) 15–23
- [9] N. Widjojo, T. S. Chung, M. Weber, C. Maletzko, V. Warzelhan, The role of sulphonated polymer and macrovoid-free structure in the support layer for thin-film composite (TFC) forward osmosis (FO) membranes, *Journal of Membrane Science* 383 (2011) 214– 223
- [10] Lyonnaise des eaux, *Water Treatment Membrane Processes*, McGraw-Hill, 1996
- [11] R. W. Baker, *Membrane technology and applications*, 2nd edn., Wiley, Chichester, 2004
- [12] An overview of Membrane Technology and Theory, <http://www.kochmembrane.com/PDFs/Application-Bulletins/KMS-Membrane Theory.aspx>, 18/11/2017
- [13] Ultrafiltration Technical manual, <http://www.aquamarinewater.co.za/ultrafiltration/pdf/UFTechManual.pdf>, 18/11/2017
- [14] F. Tasselli, E. Drioli, L. Giorno, Non-solvent Induced Phase Separation Process (NIPS) for membrane preparation, *Encyclopedia of Membranes*, DOI 10.10007/978-3-642-40872-4_1823-1,2014
- [15] M. Mulder, *Basic principles of membrane technology*, Kluwer, Dordrecht, 1996
- [16] H. Strathmann, P. Scheible and R.W. Baker, A Rationale for the Preparation of Loeb Sourirajan-type Cellulose Acetate Membranes, *J. Appl. Polym. Sci.* 15, 811, 1971

- [17] G. Han, S. S. Chan, and T. S. Chung, Forward Osmosis (FO) for Water Reclamation from Emulsified Oil/ Water Solutions: Effects of Membrane and Emulsion Characteristics, *ACS Sustainable Chem. Eng.* 2016, 4, 5021–5032
- [18] S. Zhao, L. Zou, C. Y. Tang, D. Mulcahy, Recent developments in forward osmosis: opportunities and challenges, *J. Membr. Sci.* 2012, 396, 1–21.
- [19] G. Han, S. Zhang, X. Li, N. Widjojo, T. S. Chung, Thin film composite forward osmosis membranes based on polydopamine modified polysulfone substrates with enhancements in both water flux and salt rejection, *Chem. Eng. Sci.* 2012, 80, 219–231.
- [20] K. L. Lee, R. W. Baker, H. K. Lonsdale, Membranes for power generation by pressure-retarded osmosis, *J. Membr. Sci.* 8 (1981) 141–171.
- [21] S. Loeb, L. Titelman, E. Korngold, J. Freiman, Effect of porous support fabric on osmosis through a Loeb-Sourirajan type asymmetric membrane, *J. Membr. Sci.* 129 (1997) 243-249
- [22] B. D. Coday, P. Xu, E. G. Beaudry, J. Herron, K. Lampi, N. T. Hancock, T. Y. Cath, The sweet spot of forward osmosis: Treatment of produced water, drilling wastewater, and other complex and difficult liquid streams, *Desalination* 333 (2014) 23–35
- [23] B. Mi, M. Elimelech, Gypsum scaling and cleaning in forward osmosis: measurements and mechanisms, *Environ. Sci. Technol.* 44 (2010) 2022–2028
- [24] S. Lee, C. Boo, M. Elimelech, S. Hong, Comparison of fouling behavior in forward osmosis (FO) and reverse osmosis (RO), *J. Membr. Sci.* 365 (2010) 34–39
- [25] N. Akther, A. Sodiq, A. Giwa, S. Daer, H.A. Arafat, S.W. Hasan, Recent advancements in forward osmosis desalination: A review, *Chemical Engineering Journal* 281 (2015) 502–522
- [26] J. R. McCutcheon, R. L. McGinnis, M. Elimelech, A novel ammonia–carbon dioxide forward (direct) osmosis desalination process, *Desalination* 174 (2005)1–11
- [27] J. R. McCutcheon, R. L. McGinnis, M. Elimelech, Desalination by ammonia–carbon dioxide forward osmosis: influence of draw and feed solution concentrations on process performance, *Journal of Membrane Science* 278 (2006) 114–123
- [28] M. M. Ling, T. S. Chung, Desalination process using super hydrophilic nanoparticles via forward osmosis integrated with ultrafiltration regeneration, *Desalination* 278 (2011) 194–202
- [29] S. Adham, J. Oppenheimer, L. Liu, M. Kumar, Dewatering Reverse Osmosis Concentrate from Water Reuse Applications using Forward Osmosis, *WateReuse Foundation Research Report*, 2007
- [30] D. Li, X. Zhang, J. Yao, G.P. Simon, H. Wang, Stimuli-responsive polymer hydrogels as a new class of draw agent for forward osmosis desalination, *Chemical Communications* 47 (2011) 1710–1712
- [31] Q. Ge, M. Ling, T. S. Chung, Draw solutions for forward osmosis processes: Developments, challenges and prospects for the future, *Journal of Membrane Science*, Volume 442, 1 September 2013, Pages 225-237
- [32] A. Achilli, T. Y. Cath, A. E. Childress, Selection of inorganic-based draw solutions for forward osmosis applications, *Journal of Membrane Science*, Volume 364, Issues 1–2, 15 November 2010, Pages 233-241
- [33] K. L. Hickenbottom, N. T. Hancock, N. R. Hutchings, E. W. Appleton, E. G. Beaudry,

- P. Xu, T. Y. Cath, Forward osmosis treatment of drilling mud and fracturing wastewater from oil and gas operations, *Desalination* 312 (2013) 60–66
- [34] N. T. Hancock, T. Y. Cath, Solute coupled diffusion in osmotically driven membrane processes, *Environmental Science & Technology* 43 (2009) 6769–6775
- [35] T.Y. Cath, D. Adams, A.E. Childress, Membrane contactor processes for wastewater reclamation in space: II. Combined direct osmosis, osmotic distillation, and membrane distillation for treatment of metabolic wastewater, *Journal of Membrane Science* 257 (2005) 111–119
- [36] D. L. Shaffer, J. R. Werber, H. Jaramillo, S. Lin, M. Elimelech, Forward osmosis: Where are we now?, *Desalination* 356 (2015) 271–284
- [37] S. Lee, C. Boo, M. Elimelech, S. Hong, Comparison of fouling behavior in forward osmosis (FO) and reverse osmosis (RO), *Journal of Membrane Science* 365 (2010) 34–39
- [38] Z. Y. Li, V. Yangali-Quintanilla, R. Valladares-Linares, Q. Li, T. Zhan, G. Amy, Flux patterns and membrane fouling propensity during desalination of seawater by forward osmosis, *Water Research* 46 (2012) 195–204
- [39] Y. Wang, F. Wicaksana, C.Y. Tang, A.G. Fane, Direct microscopic observation of forward osmosis membrane fouling, *Environmental Science & Technology* 44 (2010) 7102–7109
- [40] D. Roy, M. Rahni, P. Pierre, V. Yargeau, Forward osmosis for the concentration and reuse of process saline wastewater, *Chemical Engineering Journal* 287 (2016) 277–284
- [41] S. Loeb, L. Titelman, E. Korngold, J. Freiman, Effect of porous support fabric on osmosis through a Loeb–Sourirajan type asymmetric membrane, *Journal of Membrane Science* 129 (1997) 243–249
- [42] J. R. McCutcheon, M. Elimelech, Influence of concentrative and dilutive internal concentration polarization on flux behavior in forward osmosis, *Journal of Membrane Science* 284 (2006) 237–247
- [43] K. Y. Wang, T. S. Chung, G. Amy, Developing Thin-Film-Composite Forward Osmosis Membranes on the PES/SPSf Substrate Through Interfacial Polymerization, *March 2012 Vol. 58, No. 3, AIChE Journal*
- [44] S. Sahebi, S. Phuntsho, Y. C. Woo, M. J. Park, L. D. Tijing, S. Hong, H. K. Shon, Effect of sulphonated polyethersulfone substrate for thin film composite forward osmosis membrane, *Desalination* 389 (2016) 129–136
- [45] J. Ren, B. O'Grady, G. deJesus, J. R. McCutcheon, Sulfonated polysulfone supported high performance thin film composite membranes for forward osmosis, *Polymer* 103 (2016) 486–497
- [46] K. Y. Wang, T. S. Chung, J. J. Qin, Polybenzimidazole (PBI) nanofiltration hollow fiber membranes applied in forward osmosis process, *Journal of Membrane Science* 300 (2007) 6–12
- [47] X. Ding, Z. Liu, M. Hua, T. Kang, X. Li, Y. Zhang, Poly(ethylene glycol) crosslinked sulfonated polysulfone composite membranes for forward osmosis, *J. Appl. Polym. Sci.* 2016
- [48] P. Zhong, X. Fu, T. S. Chung, M. Weber, C. Maletzko, Development of Thin-Film Composite forward Osmosis Hollow Fiber Membranes Using Direct Sulfonated Polyphenylenesulfone (sPPSU) as Membrane Substrates, *Environ. Sci. Technol.* 2013, 47, 7430–7436

- [49] G. Odian, Principles of Polymerization, Wiley Interscience, 4th edn., 2004
- [50] J. L. Cartinella, T. Y. Cath, M. T. Flynn, G. C. Miller, K. W. Hunter, A. E. Childress, Removal of natural steroid hormones from wastewater using membrane contactor processes, *Environmental Science & Technology* 40 (2006) 7381–7386
- [51] R. J. York, R. S. Thiel, E. G. Beaudry, Full-scale experience of direct osmosis concentration applied to leachate management, in: Proceedings of the Seventh International Waste Management and Landfill Symposium (Sardinia '99), S. Margherita di Pula, Cagliari, Sardinia, Italy, 1999
- [52] R.A. Khaydarov, R.R. Khaydarov, Solar powered direct osmosis desalination, *Desalination* 217 (2007) 225–232.
- [53] R. N. Johnson, A. G. Farnham, Polyarylene Polyethers, US Patent 4175175, assigned to Union Carbide Corporation, New York, NY, 1979
- [54] E. Staude, L. Breitbach, Polysulfones and their derivatives: Materials for membranes for different separation operations, *Journal of Applied Polymer Science*, vol. 43, 559, 1991
- [55] A. E. Allegrezza, B. S. Parekh, P. L. Parise, E. J. Swiniarski, J. L. White, Chlorine resistant polysulfone reverse osmosis modules, *Desalination*, vol. 64, 285-304, 1987
- [56] J. F. Blanco, Q. T. Nguyen, P. Schaetzel, Sulfonation of Polysulfones: Suitability of the sulfonated materials for Asymmetric Membrane Preparation, *Journal of Applied Membrane Science*, vol. 84, 2461-2473, 2002
- [57] J. F. Blanco, Q. T. Nguyen, P. Schaetzel, Formation and morphology studies of different polysulfones-based membranes made by phase inversion process, *Journal of Membrane Science* vol. 283, 27-37, 2006
- [58] P. S. Machado, A. C. Habert, C. P. Borges, Membrane formation mechanism based on precipitation kinetics and membrane morphology: flat and hollow fibre polysulfone membranes, *Journal of Membrane Science* vol. 155, 171, 1999
- [59] R. M. Boom, I. M. Wienk, T. Van den Boomgaard, C. A. Smolders, Microstructures in phase inversion membranes. Part II. The role of a polymeric additive, *Journal of Membrane Science*, vol. 83, 277, 1999
- [60] M. Ulbricht, M. Riedel, U. Marx, Novel photochemical surface functionalization of polysulfone ultrafiltration membranes for covalent immobilization of biomolecules, *Journal of Membrane Science*, vol. 120, 239, 1996
- [61] J. P. Quentin, Sulfonated Polyarylether Sulfones, US Patent 3709841, 1973
- [62] S. H. Chen; R. M. Lion, Y. Y. Lin, C. L. Lai, J. Y. Lai, Preparation and Characterization of asymmetric sulfonated polysulfones membranes by wet phase inversion method, *European Polymer Journal*, vol.45, issue. 4, 1293-1301, 2009
- [63] K. N. Jacob, S. S. Kumar, A. Thanigaivelan, M. Tarun, D. Mohan, Sulfonated polyethersulfone-based membranes for metal ion removal via a hybrid process, *Journal of Materials Science*, vol. 49, issue.1, 114-122, 2014
- [64] J. F. Blanco, Q. T. Nguyen, P. Schaetzel, Novel hydrophilic membrane materials: sulfonated polyethersulfone Cardo, *Journal of Membrane Science*, vol. 186, issue. 2, 267-279, 2001
- [65] Y. Dai, X. G. Jian, X. M. Liu, M. D. Guiver, Synthesis and characterization of Sulfonated poly(phthalazinoneethersulfoneketone) for ultrafiltration and nanofiltration

- membranes, *Journal of Applied Polymer Science*, vol. 79, issue. 9, 1685-1692, 2001
- [66] B. C. Johnson, I. Yilgor, C. Tran, M. Iqbal, J. P. Wightman, D. R. Lloyd, J. E. McGrath, Synthesis and characterization of sulfonated poly(acrylene ether sulfones), *J. Polym. Sci. Polym. Chem.* (1984), 22, 721–737
- [67] F. Lufrano, G. Squadrito, A. Patti, E. Passalacqua, Sulfonated Polysulfone as Promising Membranes for Polymer Electrolyte Fuel Cells, *Journal of Applied Polymer Science*, Vol. 77, 1250–1257 (2000)
- [68] M. Mulder, *Basic Principles of membrane technology*, Kluwer, Dordrecht, 1996
- [69] M. Sangermano, M. M. Farrukh, A. Tiraferri, C. Dizman, Y. Yagci, Synthesis, preparation and characterization of UV-cured methacrylated polysulfone-based membranes, *Materials Today Communications*, vol. 5, 64-69, 2015
- [70] M. M. Farrukh, P. Bosch, M. Giagnorio, A. Tiraferri, M. Sangermano, Solvent-stable UV-cured acrylic polysulfone membranes, *Polym. Int.*, vol. 66, 64-69, 2017
- [71] C. H. Lee, D. VanHouten, O. Lane, J. E. McGrath, J. Hou, L. A. Madsen, J. Spano, S. Wi, J. Cook, W. Xie, H. J. Oh, G. M. Geise, B. D. Freeman, Disulfonated Poly(arylene ether sulfone) Random Copolymer Blends Tuned for Rapid Water Permeation via Cation Complexation with Poly(ethylene glycol) Oligomers, *Chem. Mater.*, vol. 23, 1039–1049, 2011
- [72] X. Zhang, J. Tian, Z. Ren, W. Shi, Z. Zhang, Y. Xu, S. Gao, F. Cui, High performance thin-film composite(TFC)forward osmosis (FO) membrane fabricated on novel hydrophilic disulfonated poly(arylene ether sulfone) multiblock copolymer/polysulfone substrate, *Journal of Membrane Science* vol. 520, 529–539, 2016
- [73] I. Struzynska-Piron, J. Loccufier, L. Vanmaele, I. F. J. Vankelecom, Parameter Study on the Preparation of UV Depth-Cured Chemically Resistant Polysulfone-Based Membranes, *Macromol. Chem. Phys.* 2014, 215, 614–623
- [74] I. Strużyńska-Piron, M. R. Bilad, J. Loccufier, L. Vanmaele, I. F. J. Vankelecom, Influence of UV curing on morphology and performance of polysulfone membranes containing acrylates, *Journal of Membrane Science* 462 (2014) 17–27
- [75] A. Tiraferri, N. Y. Yip, W. A. Phillip, J. D. Schiffman, M. Elimelech, Relating Performance of Thin-Film Composite Forward Osmosis Membranes to Support Layer Formation and Structure, *Journal of Membrane Science*, 2010
- [76] M. Di Vincenzo, M. Barboiua, A. Tiraferri, Y.M. Legrand, Polyol-functionalized thin-film composite membranes with improved transport properties and boron removal in reverse osmosis, *Journal of Membrane Science* 540 (2017) 71–77
- [77] J. E. Cadotte, (FilmTec Corporation, USA), *Eur Patent Appl* 0,015,149, March 9, 1980
- [78] J. E. Cadotte, (FilmTec Corporation, Minnetonka, MN), *U.S. Patent* 4,277,344, July 7, 1981
- [79] G. W. H. Höhne, W. F. Hemminger, H. J. Flammershein, *Differential Scanning Calorimetry*, 2nd Edition, Springer
- [80] K. V. Kodre, S. R. Attarde, P. R. Yendhe, R. Y. Patil, V. U. Barrge, *Differential Scanning Calorimetry: A Review, Research and Reviews: Journal of Pharmaceutical Analysis*, vol. 3, issue 3, July-September, 2014
- [81] T. Hatakeyama, F. X. Quinn, *Thermal Analysis Fundamentals Applications to Polymer*

- Science: Thermogravimetry, 45-71, 2nd Ed., John Wiley and Sons Publications, 1999
- [82] R. G. Chatwal, S. K. Anand, Instrumental Methods of Chemical Analysis: Thermal Methods, 2703, 5 th Ed., Himalaya Publishing House, 2002
- [83] H. Dhillon, H. De Wit, J. Dodson, Spectroscopy: CVD diamond attenuated-total-reflection prisms benefit FTIR spectroscopy, Laser Focus World, 10/13/2016
- [84] FT-IR Spectroscopy Attenuated Total Reflectance (ATR), <http://www.perkinelmer.com>, 18/11/2017
- [85] B. D. Coday, N. Almaraz, T. Y. Cath, Forward osmosis desalination of oil and gas wastewater: Impacts of membrane selection and operating conditions on process performance, Journal of Membrane Science 488 (2015) 40–55
- [86] M. A. Yam-Cervantes, J. L. Santiago-Garcia, M. I. Loria-Bastarrachea, S. Duarte-Aranda, F. Alberto Ruiz-Trevino, M. Aguilar-Vega, Sulfonated polyphenylsulfone asymmetric membranes: Effect of coagulation bath (acetic acid-NaHCO₃/isopropanol) on morphology and antifouling properties, J. Appl. Polym. Sci., 2017
- [87] J. Jansen, M. Macchione, E. Drioli, High flux asymmetric gas separation membranes of modified poly(ether ether ketone) prepared by the dry phase inversion technique, Journal of Membrane Science, 2005, Vol. 255, pp. 167-180
- [88] R. M. Boom, A. van den Boomgaard, J. W. A. van den Berg, C. A. Smolders, Linearized cloudpoint curve correlation for ternary systems consisting of one polymer, one solvent and one non-solvent, Polymer (Guildf) 1993, 34, 2348
- [89] J. G. Wijmans, J. Kant, M. H. V. Mulder, C. A. Smolders, Phase separation phenomena in solutions of polysulfone in mixtures of a solvent and a nonsolvent: relationship with membrane formation, Polymer 26 (10) (1985) 1539-1545
- [90] I. S. Byun, I. C. Kim, J. W. Seo, Pervaporation Behavior of Asymmetric Sulfonated Polysulfones and Sulfonated Poly(ether sulfone) Membranes, Journal of Applied Polymer Science, Vol. 76, 787–798, 2000
- [91] N. Arahman, T. Maimun, Mukramah, Syawaliah, The Study of Membrane Formation via Phase Inversion Method by Cloud Point and Light Scattering Experiment, International Conference on Engineering, Science and Nanotechnology 2016 (Icesnano 2016)
- [92] T. Young, Philos. Trans. R. Soc. Lond. 95, 65 (1805)
- [93] G. Bracco, B. Holst, Surface Science Techniques, Springer Series in Surface Sciences 51, Springer-Verlag Berlin Heidelberg 2013
- [94] P. H. H. Duong, Tai-Shung Chung, Application of thin film composite membranes with forward osmosis technology for the separation of emulsified oil–water, Journal of Membrane Science 452 (2014) 117–126
- [95] Y. Wang, T. Xu, Anchoring hydrophilic polymer in substrate: An easy approach for improving the performance of TFC FO membrane, Journal of Membrane Science 476 (2015) 330–339
- [96] Stirred Ultra ltration Cells Models 8003, 8010, 8050, 8200, 8400, User Guide, https://www.nist.gov/sites/default/files/documents/ncnr/StirredUltrafiltrationCell_Millipore.pdf, 18/11/2017
- [97] H. B. Park, B. D. Freeman, Z. B. Zhang, M. Sankir, J. E. McGrath, Highly Chlorine-Tolerant Polymers for Desalination, Angew. Chem. Int. Ed. 2008, 47, 6019 –6024

- [98] T. Owen, *Fundamentals of UV-visible Spectroscopy*, Hewlett-Packard Company, 1996
- [99] A. Tiraferri, N. G. Yip, A. P. Straub, S. Romero-Vargas Castrillon, M. Elimelech, A method for the simultaneous determination of transport and structural parameters of forward osmosis membranes, *Journal of Membrane Science* 444 (2013) 523–538
- [100] F. Lufrano, G. Squadrito, A. Piatti, E. Passalacqua, Sulfonated Polysulfone as promising membranes for polymer electrolyte fuel cells, *Journal of Applied Polymer Science*, Vol. 77, 1250-1257 (2000)
- [101] H. Tang, P. N. Pintauro, Q. Guo, S. O' Connor, Polyphosphazene membranes. III. Solid-state characterization and properties of sulfonated poly[bis(3-methylphenoxy)phosphazene], *Journal of Applied Polymer Science*, Vol.71, Issue 3, 387–399 (1999)
- [102] L. J. Mathias, C. M Lewis, K. N. Wiegel, *Macromolecules* vol. 30, 5970 (1997)
- [103] N. Sivashinsky, G.B Tanny, Ionic heterogeneities in sulfonated polysulfone films, *J. Appl. Polym. Sci.* 28 (1983) 3235-3245
- [104] S. H. Chen, R. M. Liou, Y. Y. Lin, C. L. Lai, J. Y. Lai, Preparation and characterizations of asymmetric sulfonated polysulfone membranes by wet phase inversion method, *European Polymer Journal*, 45 (4), 1293-1301 (2009)
- [105] S. A. McKelvey, W. J. Koros, Phase separation, vitrification, and the manifestation of macrovoids in polymeric asymmetric membranes, *Journal of Membrane Science* 112 (1996) 29–39
- [106] R. Naim, A. F. Ismail, H. Saidi, E. Saion, Development of sulfonated polysulfone membrane as a material for Proton Exchange Membrane (PEM), in: *Proceedings of Regional Symposium on Membrane Science and Technology 2004*, 21-25 April 2004, Johor Bharu, Malaysia.
- [107] A. K. Ghosh, E. M.V. Hoek, Impacts of support membrane structure and chemistry on polyamide–polysulfone interfacial composite membranes, *Journal of Membrane Science* 336 (2009) 140–148

Acknowledgments

First and foremost, I am deeply grateful to Dr. Daria Grinic for her extraordinary support in this thesis work.

I would like to express my gratitude and sincere appreciation to my Professors Alberto Tiraferri, for his valuable suggestions and kind supervision, and Marco Sangermano, for his long-lasting support and guidance.

Finally, I would like to extend my acknowledgements to all the members of the *en.sur.e water lab* for their kindness and utmost helpfulness.

